JET PROPULSION

Journal of the
AMERICAN ROCKET SOCIETY

Rocketry . . . . . Jet Propulsion Sciences . . . . . Astronautics

VOLUME 25 OCTOBER 1955 **NUMBER 10**

ARS 25th ANNIVERSARY ANNUAL CONVENTION CHICAGO, ILL. NOV. 13–18

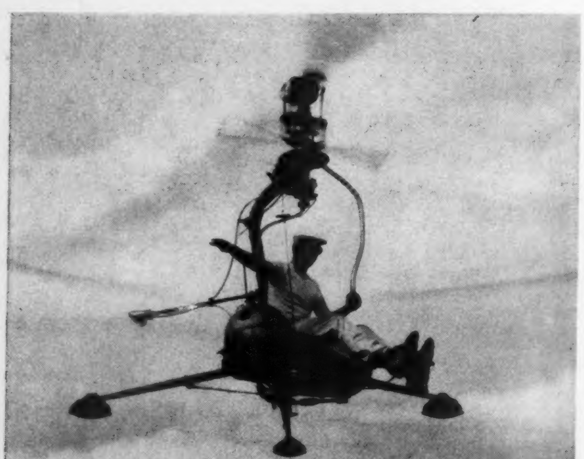

Scope of JET PROPULSION

JET PROPULSION, the Journal of the American Rocket Society, is devoted to the advancement of the field of jet propulsion through the publication of original papers disclosing new knowledge and new developments. The term "jet propulsion" as used herein is understood to embrace all engines that develop thrust by rearward discharge of a jet through a nozzle or duct; and thus it includes systems utilizing atmospheric air and underwater systems, as well as rocket engines. JET PROPULSION is open to contributions, either fundamental or applied, dealing with specialized aspects of jet and rocket propulsion, such as fuels and propellants, combustion, heat transfer, high temperature materials, mechanical design analyses, flight mechanics of jet-propelled vehicles, astronautics, and so forth. JET PROPULSION endeavors, also, to keep its subscribers informed of the affairs of the Society and of outstanding events in the rocket and jet propulsion field.

Limitation of Responsibility

Statements and opinions expressed in JET PROPULSION are to be understood as the individual expressions of the authors and do not necessarily reflect the views of the Editors or the Society.

Subscription Rates

One year (twelve monthly issues)	$10.00
Foreign countries, additional postage . . . add	.50
Single copies	1.75
Special issues, single copies	2.50
Back numbers	2.00

Change of Address

Notices of change of address should be sent to the Secretary of the Society at least 30 days prior to the date of publication.

Information for Authors

Preparation of Manuscripts

Manuscripts must be double spaced on one side of paper only with wide margins to allow for instructions to printer. Submit two copies: original and first carbon. Include a 100–200 word abstract of paper. The title of the paper should be brief to simplify indexing. The author's name should be given without title, degree, or honor. A footnote on the first page should indicate the author's position and affiliation. Include only essential illustrations, tables, and mathematics. References should be grouped at the end of the manuscript; footnotes are reserved for comments on the text. Use American Standard symbols and abbreviations published by the American Standards Association. Greek letters should be identified clearly for the printer. References should be given as follows: For Journal Articles: Title, Authors, Journal, Volume, Year, Page Numbers. For Books: Title, Author, Publisher, City, Edition, Year, Page Numbers. Line drawings must be made with India ink on white paper or tracing cloth. Lettering on drawings should be large enough to permit reduction to standard one-column width, except for unusually complex drawings where such reduction would be prohibitive. Photographs should be clear, glossy prints. Legends must accompany each illustration submitted and should be listed in order on a separate sheet of paper.

Security Clearance

Manuscripts must be accompanied by written assurance as to security clearance in the event the subject matter of the manuscript is considered to lie in a classified area. Alternatively, written assurance that clearance is unnecessary should be submitted. Full responsibility for obtaining authoritative clearance rests with the author.

Submission of Manuscripts

Manuscripts should be submitted in duplicate to the Editor-in-Chief, Martin Summerfield, Professor of Aeronautical Engineering, Princeton University, Princeton, N. J.

Manuscripts Presented at ARS Meetings

A manuscript submitted to the ARS Program Chairman and accepted for presentation at a national meeting will automatically be referred to the Editors for consideration for publication in JET PROPULSION, unless a contrary request is made by the author.

To Order Reprints

Prices for reprints will be sent to the author with the galley proof, and orders should accompany the corrected galley when it is returned to the Assistant Editor.

JET PROPULSION
Journal of the
AMERICAN ROCKET SOCIETY

JET PROPULSION, the Journal of the American Rocket Society, published monthly by the American Rocket Society at 20th and Northampton Streets, Easton, Pa., U.S.A. The Editorial Office is located at 500 5th Ave., New York 36, N. Y. Price $1.75 per copy, $10.00 per year: Entered as second-class matter at the Post Office at Easton, Pa., under the Act of March 3, 1879.

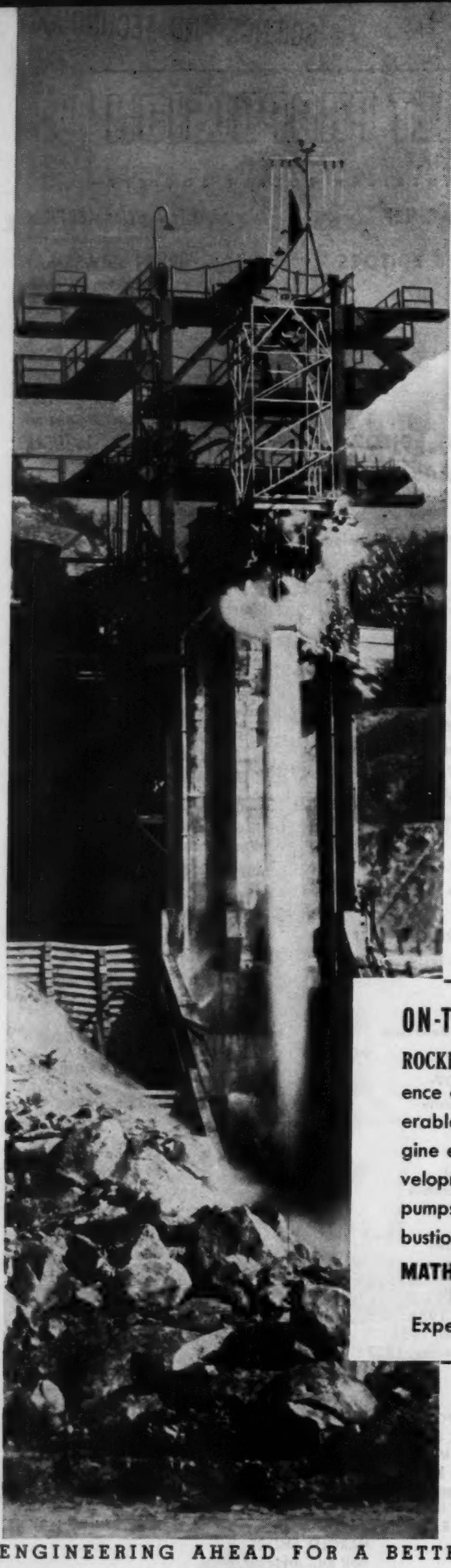


POWER
4555
E

STRATOPOWER

HYDRAULIC PUMPS for the AIRCRAFT INDUSTRY

SERIES 66W
**VARIABLE DELIVERY
PRESSURE COMPENSATED
TYPE REGULATOR**

Designed to operate at service altitudes without reservoir pressurization. These pumps meet or surpass the requirements of Specification MIL-P-7740A. They are self-priming and accommodate inlet pressures to 80 psia. Nominal deliveries of 0.25 to 10 gpm. Speeds to 10,000 rpm on smaller sizes. Continuous pressures to 3000 psi.

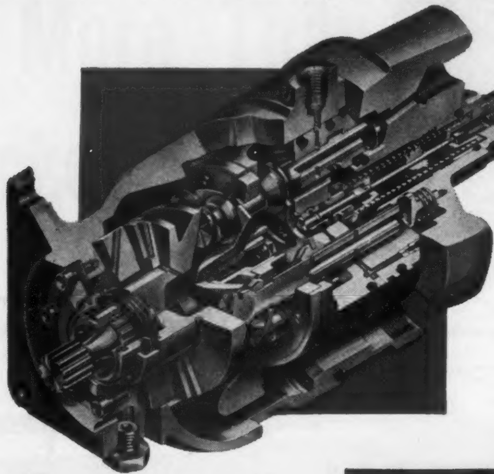

SERIES 65F
**FIXED
DISPLACEMENT**

For use at higher service altitudes without reservoir pressurization. Inlet pressures to 80 psia. Nominal deliveries of 0.5, 1, 2 and 3 gpm.

SERIES 67V
**VARIABLE DELIVERY
INLET FLOW REGULATOR**

The most direct known method of integral maximum pressure regulation. Capacities range from 0.85 to 3 gpm, over two dozen different models.

SERIES 67MW
**VARIABLE DELIVERY
DUAL PRESSURE
SERVO CONTROL**

Selective operation in either of two pressure ranges. Hydraulic or electrical pilot control. Adaptable to 66W or 67W Series Pumps.

SERIES 67
**FIXED
DISPLACEMENT**

Over thirty models include nominal deliveries of from 0.25 to 3 gpm. Pumps of the 0.5, 1, 2 and 3 gpm sizes have AN approval under MIL-P-7850.

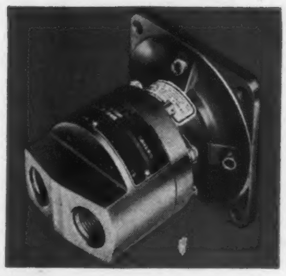

SERIES 67W
**VARIABLE DELIVERY
PRESSURE COMPENSATED
TYPE REGULATOR**

Fluid delivery instantly varied in response to system demands. Five sizes from 2 to 10 gpm, forty different models.

SERIES 167
**ELECTRIC
MOTOR DRIVEN UNITS**

For use in boost, utility or emergency circuits. AC or DC electric motors for both continuous and intermittent duty operation. Any combination of electric motor and STRATOPOWER Pump.

**CAPACITIES: Rated at 1500 rpm.
MAXIMUM CONTINUOUS SPEEDS: 3750 rpm.
MAXIMUM INTERMITTENT SPEEDS: 4500 rpm.
OPERATING PRESSURES: Continuous duty to 3000 psi.**

WATERTOWN DIVISION
THE NEW YORK AIR BRAKE COMPANY
STARBUCK AVENUE • WATERTOWN • N. Y.

WATERTOWN DIVISION
The New York Air Brake Company
730 Starbuck Avenue, Watertown, New York
Please send me full particulars on your STRATOPOWER Hydraulic Pumps.

Name ____________________
Company ____________________
Address ____________________
City __________ Zone ______ State ______

Test vehicle, containing advanced G-E development rocket engine, is swung into pit at U.S. Army's Malta Test Station, N. Y. Complete instrumentation at pit's control building will record hundreds of facts in less than a minute. G-E rocket engine designers have an extensive background in the direct application of engines to complete missile systems.

ROCKET ENGINE PROGRESS AT GENERAL ELECTRIC

Weight Cut More Than 50% In NEW G-E Rocket Thrust Chamber

General Electric has tested an advanced rocket thrust chamber which weighs 50% less per pound of thrust than previous chambers of similar design. This marks another step in General Electric's continuing progress in developing better engines for the aviation industry. The significant weight reduction was achieved without compromising performance and reliability characteristics typical of G-E engines.

General Electric has been cutting rocket engine weight ever since G-E engineers ran the first U.S. tests on German V-2 engines in 1947. For example, the use of lighter materials and the transfer of start-up components from missile to ground are two weight reduction methods G.E. has pioneered. Experiments with new materials and new means of fabrication promise even more improvements on future engines.

Advanced Facilities Speed New Rocket Engine Development

Today, General Electric is able to undertake a wide variety of rocket engine development work. The Company's rocket team, as an integral part of the Aircraft Gas Turbine Development Department, has access to the nation's most advanced privately-owned aircraft engine development facilities, as well as support from other G-E labs.

These facilities spell more and faster development progress for rocket engine programs and they underline G.E.'s increased capability for developing a wide range of rocket systems, subassemblies and components. To find out how General Electric can meet your specific rocket engine needs, contact a G-E Aircraft Specialist through your nearest G-E Apparatus Sales Office. 234-2

Progress Is Our Most Important Product

GENERAL ELECTRIC

ADVANCED ROCKET ENGINE DEVELOPMENT ACTIVITIES AT G.E.

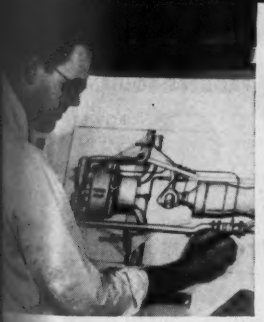

OVER EIGHT YEARS' EXPERIENCE PER MAN is the record of G-E rocket engineers. This experience is now paying off in advanced powerplant designs under development.

STRONGER, LIGHTER ALLOYS being developed at G.E. will give rocket engines greater reliability, higher performance. A technician at the Company's Materials Laboratory checks a new alloy for tensile strength.

PREDICTING ADVANCED G-E ENGINE PERFORMANCE with electronic computer cuts development time, enables G-E engineers to ascertain optimum design characteristics of engines still on the drawing board.

G-E Facilities Available to Support Rocket Engine Programs:

- Component Development Laboratory
- Materials Laboratory
- Research Laboratory
- General Engineering Laboratory
- Combustion Laboratory
- Metals and Ceramics Laboratory

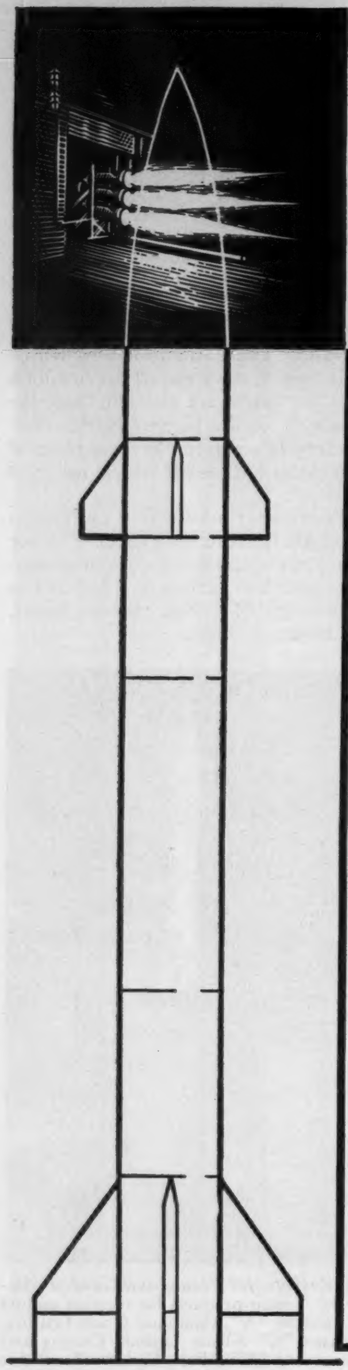

In today's new era of high temperatures . . .

HOW LONG IS A LIFETIME?

Courtesy U. S. Army

The designer of guided missiles measures it in seconds . . .

The designer of industrial equipment measures it in weeks . . . months . . . even years.

But whether design life is 30 seconds or 30 months, the problem is the same: a careful screening of the many super refractories now available to find exactly the right one.

For example, CARBORUNDUM's line includes silicon carbide, fused aluminum oxide, electric furnace mullite and stabilized zirconia.

To these add:

- **boron nitride**
- **silicon nitride**
- **boron carbide**
- **zirconium boride**
- **titanium boride**
- **chromium boride**
- **molybdenum boride**
- **nickel aluminide**

Continuing research is expected to add other new nitrides, carbides, borides and silicides to meet practically the whole gamut of destructive effects that accompany high heat.

It sounds like a big inventory to choose from, and it is. That's why it pays to have CARBORUNDUM's refractory engineers help you pick *the* right materials . . . whether you need linings for rockets or industrial furnaces.

The coupon below offers you an easy way to detailed information. Why not mail it right now?

CARBORUNDUM
Registered Trade Mark

Dept. T-105, Refractories Division
The Carborundum Co., Perth Amboy, N. J.

☐ Please send complimentary descriptive booklet.

☐ I'd like to talk with one of your engineers.

Name____________ Position________

Company____________

Address____________

OCTOBER 1955
VOLUME 25 NUMBER 10

JET PROPULSION
Journal of the
AMERICAN ROCKET SOCIETY

Editor-in-Chief
MARTIN SUMMERFIELD

Rocket Motor Instability Studies

K. BERMAN[1] and S. H. CHENEY, JR.[2]

General Electric Company, Schenectady, N. Y.

Additional experimental data are presented, bearing on the problem of instability. Tests were conducted with a window nozzle, Plexiglas insert motors, conventional and throatless motors. Based on the data, an explanation is presented for the initiation and occurrence of certain types of low and high frequency instability.

Introduction

IN two previous papers (1, 2),[3] experimental data relating to the problems of combustion instability in 3-in. diam rocket motors were presented. Two types of axial oscillations were identified: (a) A low frequency type of instability (220–360 cps) which is distinguished by abrupt and severe variations in radiation intensity. (b) A high frequency type of instability (600–1500 cps) which corresponds to the propagation of waves longitudinally along the motor. In extreme cases these pressure pulses were transformed into shock waves.

In the present paper, additional experimental evidence will be presented relating to these phenomena. All motors were 3-in. ID. Two different injector heads were used: a conventional impinging and a modified impinging (like-on-like type) injector. As described in (1), each injector head uses an injector plate consisting of a series of concentric rings containing drilled injector holes; alternate rings being for fuel and oxidizer. Pairs of liquid jets impinge approximately one inch downstream of the injector plate in the case of the conventional impinging injector, while for the modified impinging head, the impingement point is in the plane of the plate. Table 1 lists details of the injectors. The reactants used in all tests were ethyl alcohol and liquid oxygen.

Table 1 Injector Heads

Type→	Modified impinging	Conventional impinging
Oxygen		
No. of rings	2	2
No. of holes	72	62
Pressure drop, psi (at W_0 = 3.1 lb sec)	39	17
Alcohol		
No. of rings	3	3
No. of holes	96	62
Pressure drop, psi (at W_f = 2.2 lb sec)	20	20

Presented at the ARS Ninth Annual Convention, New York, N. Y., November 30–December 3, 1954.

[1] Rocket Research Engineer, Development Dept., Aircraft Gas Turbine Div., Schenectady, N. Y. Mem. ARS.

[2] Engineer, Development Dept., Aircraft Gas Turbine Div., Evendale, Ohio.

[3] Numbers in parentheses indicate References at end of paper.

[4] Manufactured by Photocon Research Products, Pasadena, Calif.

Experimental Work

A. Length Study With a Conventional Impinging Head

In (1), it was reported that with an assembly consisting of the 10-in. long window motor, a 41 degree convergent nozzle, and a conventional impinging head, intermittent low frequency instability had been obtained. On the other hand, operation with longer chamber assemblies (17 in. or greater) had been characterized by sinusoidal and shock-type high frequency oscillations. To investigate this behavior more thoroughly, a length study was conducted with motor assemblies consisting of the same injector, 3-in.-diam water-cooled chambers of various lengths ($5^3/_4$, $9^3/_4$, $15^3/_4$, and $21^3/_4$ in.) and a 41 degree convergent angle (1.75-in. throat diam) nozzle. Dynagage[4] pressure pickups were mounted on the chamber and the alcohol line to measure chamber pressure and fuel line oscillations. Instability, which started slightly before full-stage operation and lasted only several seconds, was experienced with the $5^3/_4$-in. length assembly during operation at chamber pressures of 300 psig or lower. The chamber pressure record was unsteady. Starting at frequencies of 550 to 650 cps, the frequency changed intermittently to half frequencies of 260 to 330 cps. Although identical oscillation frequencies were observed in the alcohol and chamber pressure traces, no consistent amplitude correlation could be observed. Thus, at times the magnitude of the alcohol line pressure oscillations might be large, while the chamber pressure record for the same interval indicated only small oscillations, or vice versa. The amplitude of the chamber pressure oscillations was never greater than about 50 psi peak to peak.

Fig. 1 is a section of a typical Dynagage pressure record. These characteristics of the $5^3/_4$-in. long assembly were also observed with the $9^3/_4$-in. long assembly. However, in the latter case the oscillation frequencies ranged from about 220 to 500 cps.

Operation with a $15^3/_4$-in. long assembly at a chamber pressure of 330 psig was unstable for a brief period at the

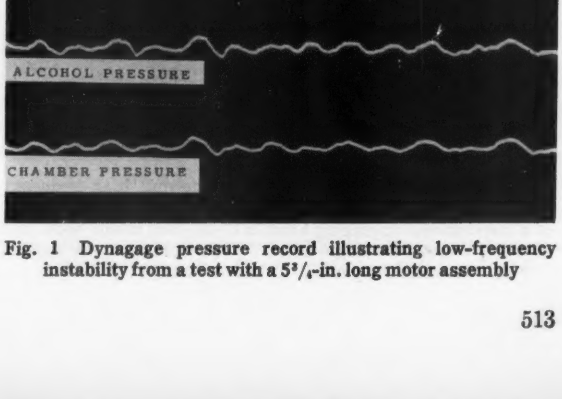

Fig. 1 Dynagage pressure record illustrating low-frequency instability from a test with a $5^3/_4$-in. long motor assembly

start of the run. Sinusoidal-type oscillations at a frequency of 900 cps were observed. When the chamber pressure was lowered to 275 psig, continuous shock-type oscillations of about 1200 cps frequency were obtained.

With a $21^3/_4$-in. long chamber assembly, unstable operation occurred even at chamber pressures as high as 360 psig.

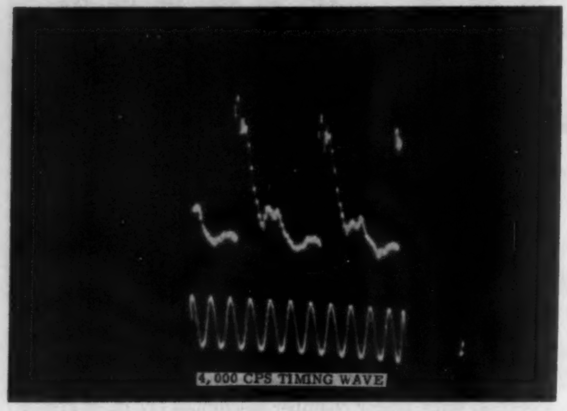

Fig. 2 Dynagage pressure record illustrating high-frequency instability from a test with a $21^3/_4$-in. long motor assembly. Frequency, 1000 cps

Pictures were taken at a rate of 10 per sec with the film traveling at approximately 15 in. per sec. The internal-driven sweep of the oscilloscope was used. The sweep time was about 3 millisec.

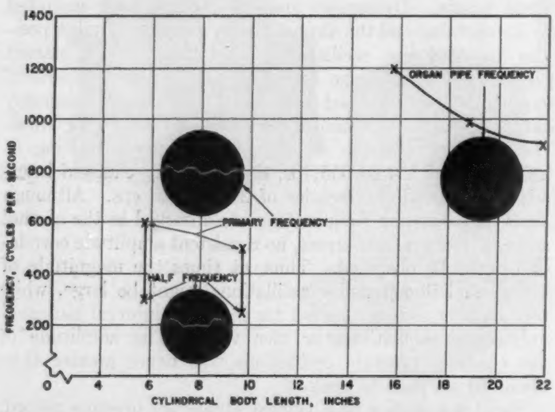

Fig. 3 Frequency of oscillation vs. cylindrical chamber length for 3-in.-diam motors and conventional impinging head

Fig. 4 Radiation streak photograph showing low-frequency type instability with an assembly consisting of a conventional impinging head, a 10-in.-long motor body, and a 41-deg convergent angle nozzle. (300 cps)

Fig. 5 Radiation streak photograph showing high-frequency sinusoidal type instability obtained with an assembly consisting of a conventional impinging head, a 17-in.-long motor body, and a 41-deg convergent angle nozzle. The window motor formed the downstream portion of the assembly. (900 cps)

High frequency (900 cps) shock-type instability was obtained. Fig. 2 is a sample of a Dynagage pressure record of such a run.

These test results seem to indicate that with conventional impinging head assemblies there is a transition from random low-frequency type of instability to the high-frequency type instability as the chamber length is increased. In Fig. 3 the experimental frequencies are plotted as a function of the chamber length. For purposes of comparison and later discussion, a radiation streak photograph of a period of low-frequency type instability obtained with a 10-in. long motor and conventional impinging head is shown in Fig. 4, while a streak photograph of sinusoidal oscillations with a 17-in. long motor and the same injector head is shown in Fig. 5.

B. "Throatless" Motors

In (2), two test runs with a "stove-pipe" assembly were reported. In order to investigate the combustion characteristics of "throatless" motors (throat area/chamber area = 1) in greater detail, the window motor was attached to conventional 3-in.-diam water-cooled bodies and a diverging nozzle having an expansion ratio of 5.4. Since the slit window extended only along the window motor portion of the composite chamber, the flow field along the entire length of the cylindrical motor section was photographed by exchanging the chamber sections so that the window motor would at alternate times form either the upstream or downstream portion of the chamber. Tests were conducted with the modified impinging and the conventional impinging injector heads at composite chamber lengths of 12 and 20 in., respectively. Chamber pressures were varied in an attempt to observe the effect of chamber pressure and head pressure drops on the system stability. Pressure variations in the alcohol line and chamber were measured with Dynagages. Radiation from the chamber was photographed in identical fashion as reported in (1) and (2).

(1) Modified Impinging Head Tests

All runs at both the 12-in. length and the 20-in. length were smooth. The chamber pressure, measured at the injector, was lowered from 240 to 95 psig in the 12-in. length, and from 187 to 115 psig in the 20-in. length. An example of a strip photograph is shown in Fig. 6. It may be noticed that the greatest acceleration occurs within a few inches from the injector. Slit photographs of the downstream portion of the 20-in. motor show the gas to be traveling at almost constant velocity in the last 12 inches of the rocket motor. The gas velocity at a distance $^1/_2$ in. upstream of the nozzle entrance for a smooth running 20-in. motor was found to be 2500 ± 250 ft per sec.

Fig. 6 Radiation streak photograph of a stable test run made with an assembly consisting of a modified impinging head, a 12-in.-long motor body, and a throatless (i.e., no convergent section) nozzle

(2) Conventional Impinging Head Tests

Three runs were made with a 12-in. long assembly at chamber pressure of 165, 126, and 109 psig, respectively. At 165 psig, operation was unstable for about 1.3 seconds after the start of full stage. The chamber pressure oscillation frequency during this period decreased continuously from 1080 to 880 cps. Subsequent combustion was smooth for the remainder of the run. At the lower chamber pressures, however, operation was rough throughout full stage operation.

Similar behavior was observed with the 20-in. cylindrical length body. At chamber pressures of 190 and 175 psig, operation was unstable for the first two seconds of full stage operation and then smoothed out. During the unstable period a continuous decrease in chamber pressure oscillation frequency was recorded. The lower chamber pressure runs were unstable throughout full stage operation. The frequency of the chamber pressure oscillations decreased until a final steady value was reached. Initial instability frequency in the 20-in. motors was about 1000 cps; the final frequency was about 660 cps. A typical strip photographs of an unstable run is shown in Fig. 7. The general appearance of the radiation pattern is very similar to that obtained during low frequency oscillations; i.e., it consists of alternate regions of high and low radiation and shows very little sign of wave propagation, as evidenced by the fact that the streaks undergo no sudden acceleration or deceleration. It is noteworthy that the ratio of dark area to light area is much larger. At a frequency of 1080 cps, the ratio of the periods of moderate radiation to high radiation at the nozzle end of the slit is about 0.7, while for a frequency of 660 cps, this ratio becomes 1.5. That is, the darker part of the cycle becomes greater as the frequency of oscillation decreases.

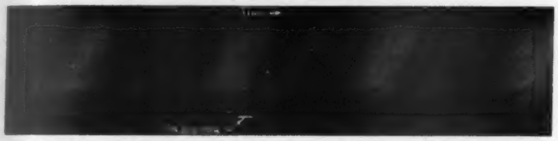

Fig. 7 Radiation streak photograph showing unstable operation of a 20-in.-long throatless motor. The injector used was a conventional impinging type. The window motor formed the upstream portion of the assembly

C. Window Nozzle

In order to observe the flow in a rocket nozzle, a nozzle having an observation window $^1/_4$ in. wide and about 3 in. long was built. This nozzle, having no divergent section, was machined from a copper billet. The window assembly whose primary components are two quartz plates separated by a spacer, extends along the convergent section of the nozzle to a distance within $^1/_2$ in. of the throat and is parallel to the inside surface. The slit extends toward the throat from a point even with the end of the cylindrical chamber. No gas leakage is permitted past the inner quartz plate as is the case in the window motor. Instead, a water passage on each side of the slit serves to keep the window assembly cool. The convergent section of the nozzle is a conical frustum having a convergent half-angle of 10 degrees and a throat diameter of 1.75 in. Slit photographs were made using the General Radio Company Type 651 Camera. The optical axis of the camera was perpendicular to the face of the window and the surface of the frustum. A photograph of the window nozzle assembly is shown in Fig. 8. All test runs with the window nozzle were made with a $23^1/_2$-in. long cylindrical chamber, using both the conventional impinging and the modified impinging injector heads.

Fig. 8 Window nozzle assembled for test with a $23^1/_2$-in.-long, 3-in.-diam water-cooled combustion chamber

The interpretation of the photographic data derived through the nozzle slit must be treated with considerable caution, especially under unstable operation conditions. Under these circumstances the flow can probably not be considered as one-dimensional. Data will be discussed separately for stable and unstable operation.

(1) Stable Operation

An example of a strip record film obtained under stable operation is shown in Fig. 9. This portion is typical of the radiation patterns obtained with either the modified impinging or conventional impinging injector head. The slope of nineteen streaks showing the best definition was measured at half-inch intervals along the $3^1/_4$-in. long slit and the average local velocities were calculated. Since the slit does not extend up to the throat, it was of course impossible to determine an experimental throat velocity. In order to correlate the experimental velocities with isentropic nozzle flow theory, it was necessary to assume that the real and isentropic expansion matched at an arbitrary selected point along the nozzle. This is equivalent to using the isentropic relationship to calculate the throat velocity from the measured velocity at the arbitrary selected station.

In Fig. 10, the isentropic relationship and the experimental

Fig. 9 Radiation streak photograph obtained with the window nozzle during a smooth test run

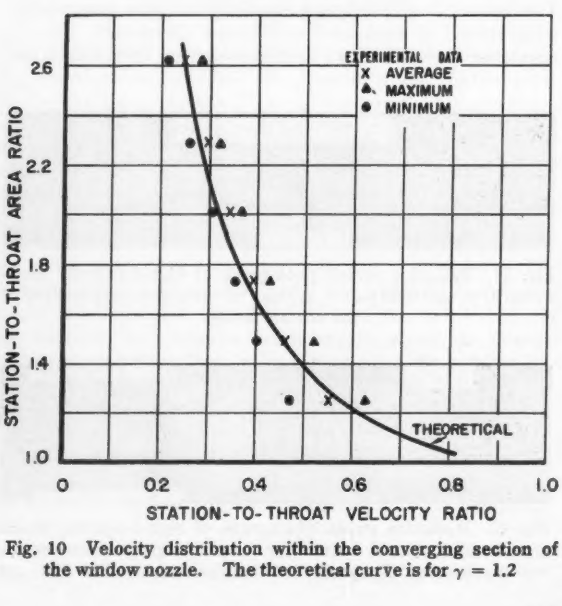

Fig. 10 Velocity distribution within the converging section of the window nozzle. The theoretical curve is for $\gamma = 1.2$

values are plotted, using the ratio of station area to throat area and the ratio of station velocity to throat velocity as coordinates. At a point 1/2 in. downstream from the chamber end of the slit (station area/throat area = 2.6) the expansions were matched. Using the velocity at this point, a throat velocity was calculated by means of the isentropic relationship and all velocities obtained from the strip photographs were divided by it to give values of station to throat velocity. Table 2 is a summary of the average velocities measured at various stations along the nozzle. An extrapolated throat velocity is obtained for each station by dividing this velocity by the station to-throat velocity ratio corresponding to the station-to-throat area at the given location. The average of these extrapolated throat velocities was 3100 fps.

The rather consistent values of throat velocities seem to indicate that the agreement between actual velocity measurement and isentropic flow theory is fairly good.

Table 2

Distance from chamber end of slit, in.	Average velocity, fps	Theoretical station-to-throat velocity	Throat velocity, fps
1/2	743	0.245	3035
1	894	0.275	3250
1 1/2	1040	0.315	3300
2	1185	0.380	3120
2 1/2	1400	0.460	3045
3	1675	0.580	2890
		Average	3105

(2) Unstable Operation

A typical nozzle slit photograph of sinusoidal oscillations is shown in Fig. 11. The frequency is about 800 cps. This may be compared with the slit photograph of the chamber radiation pattern under sinusoidal oscillations in a 17-in. long assembly (the window motor formed the downstream section) shown in Fig. 5. As pointed out in (2), only intermittent shock-type oscillations could be obtained with 21-in. long, 10 degree convergent nozzle angle assemblies, while with a 41 degree convergent angle nozzle, continuous shock-type operation could be established. A streak photograph of the nozzle radiation under intermittent shock-type oscillation is shown in Fig. 12. A region of high intensity is visible at the chamber end of the nozzle slit once each cycle. The front of this disturbance moves downstream very rapidly while its tail is decelerated as it moves downward. On the negatives, the path of an upstream-moving disturbance can be traced behind the initial downstream-moving pulse. For comparison, a window-motor photograph of intermittent shock-type operation in a 21-in. long assembly is shown in Fig. 13.

Fig. 11 Radiation streak photograph of high-frequency sinusoidal type instability as it appears in the converging section of the window nozzle

Fig. 12 Radiation streak photograph of high-frequency shock type instability as it appears in the converging section of the window nozzle. Frequency of oscillation was 820–850 cps

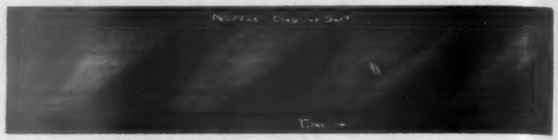

Fig. 13 Radiation streak photograph of high-frequency intermittent shock type instability obtained with an assembly consisting of a conventional impinging head, 21 3/4-in.-long motor body, and a 10-deg convergent angle nozzle. The window motor formed the downstream section of the motor assembly

D. Plexiglas[5] Insert Window Motor

Data obtained from the window motor must be treated with considerable caution. As was pointed out in (1), the radiation appearing in the photographs is a local projection of a three-dimensional phenomenon. To evaluate the reliability of the window motor results, 3-in.-diam rocket motors, composed of conventional water-cooled bodies and nozzles, with a 2 1/2-in. long transparent Plexiglas section inserted between the injector and the body, have been run. The radiation emanating through the Plexiglas section was photographed by means of a Fastax camera with speeds up to 7000 frames per sec. The results obtained appear to agree with the data derived from the slit photographs. The bright gas stream, downstream of the injector, was interspersed with dark streaks which moves axially down the motor. The instantaneous distribution across any cross section appeared to be rather random, indicating that the instantaneous mixture distribution across any cross section is not homogeneous in either space or in time. The inhomogeneities apparently account for the streaks of varying intensity found in the streak photographs. As was pointed out in (1), these streaks appear to indicate the propagation of discrete radiation sources, existing due to random variations of pressure, temperature, and gas composition. The fluctuations do not indicate any one frequency or repetitive frequency spectrum.

When such a Plexiglas assembly was operated under shock-type instability, the Fastax pictures indicated that during each cycle of oscillation, the radiation from the motor disappears momentarily. This agrees with the information obtained from the slit photographs in (2), indicating that after each shock wave reflection from the injector, a nonluminous region moves downstream. A sequence of frames is shown in Fig. 14. The pictures were taken on 16-mm Kodachrome film at 6000 frames per sec.

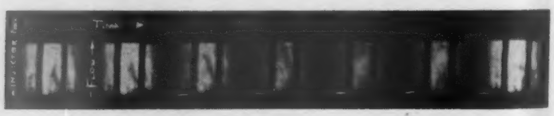

Fig. 14 One cycle of high-frequency shock type instability as photographed through a 2 1/2-in.-long Plexiglas insert with a Fastax camera. Picture speed 6000 frames per sec

Discussion and Interpretation

In this paper, as well as in (1) and (2), photographic and other experimental evidence, bearing on the combustion inside a 3-in. ID. rocket motor, has been presented. Before an attempt is made to establish a physical picture of the encountered combustion instability phenomenon, it will be helpful to summarize some of the pertinent data.

[5] Manufactured by Rohm and Haas Co., Philadelphia, Pa.

Stable operation is characterized by a radiation pattern consisting of streaks of varying intensity. These streaks, randomly distributed throughout the gas volume, represent local inhomogeneities in temperature and gas composition. The propagation velocity along the motor axis is a function of the type of injector head used. In any case, though, there is a region near the injector where the maximum acceleration occurs, which probably corresponds also to the maximum reaction zone. In the case of an assembly consisting of a 10-in. long chamber, a 1.75-in. throat diameter nozzle, and a modified impinging head, this region is approximately three in. long. The average stay time of the gases within a 10-in.-long chamber—i.e., the average time from the point where they enter the slit field until they leave—is approximately 0.003 sec, most of which is spent in the low-velocity region near the injector, since the gas velocity at the entrance to the nozzle was approximately 800 fps. The flow through a 10-degree convergent angle nozzle, attached to a 23-in.-long chamber, follows isentropic expansion theory very closely. This leads to the belief that no abnormal amount of combustion was occurring in the nozzle.

As stated previously, two general types of instability were encountered:

(a) Low-Frequency Instability

Low-frequency oscillation occurred randomly and intermittently. This instability was encountered only at short chamber lengths and only with the conventional impinging head and nonimpinging head assemblies which, as was shown in (1), have much longer low velocity regions near the injector than does the modified impinging head assembly. At longer chamber lengths, the instability was transformed to the high-frequency type. The frequency of the low-frequency oscillation is not steady but varies within a restricted range, usually decreasing during a period of oscillations. On the Dynagage record, the chamber pressure trace appears quite asymmetrical and of small amplitude, usually not much larger than 50 psi peak to peak. The corresponding alcohol line Dynagage record, although agreeing with the chamber pressure frequency, showed no amplitude correlation with same. A typical cycle of 300 cps low-frequency oscillation is shown in the streak photograph of Fig. 4. The cycle consists of a period of high radiation followed by a short interval when all visible luminosity disappears. No wave propagation is apparent except for one upstream moving pressure pulse commencing as the front of the dark streak reaches the nozzle. This is evidenced by the deceleration which subsequent streaks undergo.

(b) High-Frequency Instability

The high-frequency type of instability could be arbitrarily subdivided into two general types: a sinusoidal and a shock-type. This type of instability is distinguished from the low-frequency type by three characteristics: It persists throughout the run; it is of high amplitude; and it exhibits a definite fundamental frequency for a given motor assembly. The sinusoidal oscillation amplitude was of the order of 100 psi peak to peak while the shock-type was 300–500 psi. For a fixed assembly, the sinusoidal type frequency was somewhat lower than the shock-type. High frequency instability can be induced in a given assembly by lowering the pressure drop through the injector. In addition, the assembly becomes more unstable as the chamber length and the nozzle convergence angle are increased. At chamber lengths below 10 in. it is very difficult to obtain high-frequency instability. In Fig. 5 is shown a streak photograph of sinusoidal oscillation. Photographs of shock-type oscillation were presented in (2). In analyzing the photograph (Fig. 5), it is apparent that the cycle corresponds to a period of radiation followed by a short period of no luminosity. In contrast to the low-frequency instability, however, a definite pattern of wave propagation is in evidence throughout the cycle, as evidenced by the local deceleration and acceleration which the flow undergoes. In general, the same pattern of radiation is also in evidence in the nozzle split pictures. However, much less wave propagation can be observed. The slit photograph of the shock-type instability, as it appears in the convergent section of the nozzle, is rather interesting. The front of a high radiation region moves downstream at very great velocity. Since the slope of the angle is very close to 90 degrees, no accurate velocity can be established. The decelerations which the gas particles behind the front undergo, make it appear that a pressure wave moves upstream from the vicinity of the throat. In any case, the tail of the high radiation zone is decelerated as it moves through the convergent nozzle section.

Before a fuller interpretation of all of these results is attempted, it is necessary to establish the nature of the "dark streaks" or period of no luminosity. In (2), it was stated that it consisted of an off-ratio, or temperature gas mixture which covered all or most of the volume. In effect, it represents a region enclosed by two temperature (or entropy) discontinuities or contact surfaces. Two additional pieces of information seem to confirm this conclusion: (a) As was stated in (2), the shock wave, after passing through the dark region, always has a higher velocity than it had entering it. The work of Bitondo and associates (3) seems to indicate that such behavior can be expected from the interaction of a shock wave and a temperature or internal energy discontinuity. (b) The 6000 frames per sec Kodachrome pictures taken of the Plexiglas insert motor under shock-type operation confirm the disappearance of all luminosity momentarily during each cycle.

Consider now the qualitative effect of this temperature discontinuity on the flow through the nozzle. Since, as was stated in (2), no pressure or velocity discontinuity exists at the boundaries of the dark streak, the local mass flow rate represented by the dark streak is

$$\rho A V = \frac{P}{T/M} \frac{V}{R} A$$

where

P = local average static pressure
ρ = local average density
A = local area
V = local average particle velocity
T = local average temperature
M = local average molecular weight

The steady-state isentropic flow through a nozzle, however, is proportional to $P/\sqrt{RT/M}$. In other words, the flow rate in the chamber is inversely proportional to the temperature, while through the nozzle it is inversely proportional to the square root of the temperature. On the basis of these admittedly quasi-steady-state relationships, either a pressure or an expansion wave, depending on whether the temperature continuity is positive or negative, will travel upstream from the nozzle. As mentioned previously, the photographs show an upstream-moving pulse subsequent to the entrance of the discontinuity front into the nozzle. In addition, if one calculates the local velocity distribution at the nozzle end of the window slit, (approx. $^1/_2$ in. upstream of the nozzle entrance), one finds that, a little time after the passage of the dark streak, the velocity initially decreases and then increases fairly rapidly. This could be interpreted as the successive upstream passage of a pressure wave and a rarefaction, produced as the two discontinuity surfaces enter the nozzle.

The length study experience with the conventional impinging injector, reported under Experimental Work, indicates that the low and high-frequency instability are not two separate and distinct phenomena, but rather are different manifestations of the same cause. The hypothesis we wish to

propose is that the interaction of a disturbance with the various phenomena occurring in reaction zone is this cause. Qualitatively, we visualize the mechanism in the following manner: an initial disturbance in the motor reaches the main reaction zone and disturbs the injection pattern. Although the effect of oscillating back pressure on small jets is not too well understood, the Plexiglas insert motor pictures and water tests seem to indicate that the jets are bent backward and undergo many kinds of gyrations under the influence of a disturbance. This effect, apparently, is much more pronounced with conventional impinging and nonimpinging injectors, which, as pointed out, have a much longer main reaction zone. Also, the lower the pressure drop through the injector, the greater is the tendency toward instability. In any case, this interaction produces a momentary off-ratio or off-temperature gas mixture. As already discussed, the passage of this region into the nozzle sends disturbances upstream.

Comparatively little is known about the dissipative forces acting on disturbances moving in incompletely burned, heterogeneous gas mixtures. The effect of chamber length on the severity of instability provides perhaps a clue that a pressure wave is able to maintain itself by obtaining additional energy from further combustion occurring in the wake of the disturbance. The shock-wave photographs presented in (2) seem to indicate that the particle paths, after passing through the downstream moving pulse, are almost straight lines, indicating very little heat addition. This generates the impression that most of the combustion occurs directly behind and as a result of the impulsive action of the shock. This is perhaps the explanation for the claim of other investigators that the combustion efficiency increases during unstable operation.

In any case, the pressure disturbance in short motors remains small and usually very little of the wave is reflected after the interaction within the reaction zone. Thus a cycle of low-frequency instability consists of the passage of the off-ratio region downstream to the nozzle and the return of a disturbance. Hence the period of the oscillation would be

$$T = \frac{l}{a - V} + T'$$

l = length of chamber
a = sonic velocity of gas
T' = time of stay of "off-ratio" region in chamber
T = period of oscillation
V = average particle velocity

The average time of stay of gas particles in the chamber, as was pointed out before, is approximately 0.003 sec. Taking $l = 1$ ft and $a = 3000$ fps, $V = 800$ fps, $T = 0.00046 + 0.003 = 0.00346$ sec, corresponding to a frequency of about 290 cps. This is within the range of the experimentally encountered frequency spectrum. The observation of double frequencies on the Dynagage chamber pressure record at the beginning of the period of oscillation can be explained as the result of weak wave reflection after interaction within the reaction zone. This wave probably decays on its downstream passage and no further noticeable reflection of it occurs. It may be noticed that according to this theory, low-frequency instability is not very sensitive to chamber length since the time of stay increases very slowly with length, as pointed out previously. If, for example, $l = 2$ ft and it is assumed that the gas stay time increases by an amount equal to the additional length divided by the average gas velocity (downstream of the main reaction zone), i.e., $T' = 0.003 + (1/800) = 0.00425$ sec, then $T = (l/a - V + T') = (2/2200) + 0.00425 = 0.00091 + 0.00425 = 0.00516$ sec, corresponding to a frequency of about 194 cps. Thus the theoretical effect of increasing the chamber length from one foot to two feet in our assumed assemblies (chamber area/throat area = 2.94) would be to decrease the oscillation frequency from about 290 to 194 cps.

As the chamber length is increased, the same mechanism just described for low-frequency instability still persists, with the exception that the disturbances apparently grow much stronger and, as a result, reflection of the wave occurs after interaction with the reaction zone. Depending on the steepness of the nozzle convergence angle, a considerable portion of the downstream moving pulse is reflected. The primary oscillation frequency of such a motor is determined by the wave propagation axially along the motor. This was confirmed by the results presented in (2).

One important point should be emphasized in reference to frequency analysis. It has become more or less standard practice to attempt to assign to every major frequency found in the spectrum of the chamber pressure oscillation a mode which is directly related to a geometrical dimension of the motor. This study has brought out the possibility that disturbances can be generated by the reaction of the temperature discontinuity surface with the nozzle and the reflection and refraction occasioned by the interaction of strong waves and contact surfaces. The frequency of such disturbances bear no simple relation to any geometrical dimension of the motor. Hence extreme caution is advisable in any effort to assign a mode of oscillation to every frequency encountered.

Finally, it is necessary to discuss the "throatless" motor experiments. The interesting point about the unstable operation, as shown on the strip photographs, is that instead of having regions of no luminosity there are short periods of extremely high radiation. It may be noticed that the Mach number at the end of the cylindrical section is fixed at a value of one. According to the theory of diabatic flow (4), any fluctuation in the heat release from the combustion will produce disturbances which will change the entrance Mach number. It is conceivable that unstable operation consists of the interaction of a disturbance with the phenomena in the reaction zone which changes the reactant ratio sufficiently to affect the heat release. This in turn would create another disturbance.

Summary

It has been found that in some cases low and high-frequency instability are related phenomena. It is hypothesized that any upstream traveling disturbance interacts within the reaction zone and creates an off-ratio region or temperature discontinuity. The latter, in turn, upon passing into the nozzle, sends another disturbance upstream. Depending upon the strength of the disturbance, the frequencies are governed by the travel of the waves axially along the motor (high-frequency instability) or the upstream travel of a wave and the downstream travel of the temperature discontinuity (low-frequency instability).

Acknowledgments

This work was performed as a part of Project Hermes under Contract No. Da-30-115-ORD-23. We wish to thank Army Ordnance for permission to publish the results. In addition, we acknowledge the assistance and advice of numerous individuals at the Malta Test Station of Project Hermes which made these experiments feasible. Special thanks are due to T. C. Carnavos, who designed the window nozzle, and to E. H. Hull.

References

1 "Combustion Studies with a Rocket Motor Having a Full-Length Observation Window," by K. Berman and S. E. Logan, *Journal of the American Rocket Society*, vol. 22, March-April 1952.

2 "Combustion Studies in Rocket Motors," by K. Berman and S. H. Cheney, Jr., *Journal of the American Rocket Society*, vol. 23, March-April 1953, pp. 89–96.

3 "One-Dimensional Theory of Absorption and Amplification of a Plane Shock Wave by a Gaseous Layer," by Bitondo, Glass, and Patterson, University of Toronto UTIA Rep. no. 5.

4 "On the Addition of Heat to a Gas Flowing in a Pipe at Subsonic Speed," by J. C. Foa and G. Rudinger, *Journal of the Aeronautics Society*, vol. 16, February 1949, p. 84.

Heat Transfer Through Sweat Cooled Porous Tubes

H. L. WHEELER, JR.,[1] and POL DUWEZ[2]

Jet Propulsion Laboratory, California Institute of Technology, Pasadena, Calif.

Several studies of various factors involved in the process of sweat cooling are described in this paper. The heat transfer problem was investigated and the results were interpreted on the basis of a simplified Rannie equation. It was found that the experimental results agree relatively well with this equation. However, for both hydrogen and nitrogen cooling gases, the experimental values of the characteristic temperature ratio were systematically lower than those deduced from the equation. The reasons for this discrepancy are discussed in the paper. In the sweat cooling process the most important property of the cooling gas is its specific heat. The thermal conductivity and the viscosity of the coolant seem to be of secondary importance. The physical properties of the porous wall do not enter into the analytical study, and it has been found experimentally that the thermal conductivity of the porous metal has only a minor effect on the heat transfer in a sweat cooled tube. The results have been interpreted also by considering a conventional heat transfer coefficient. It is shown experimentally that the heat transfer between the main stream and the wall is independent of the rate of coolant flow. A study of the pressure drop in an isothermal porous wall cylinder is discussed, and the experimental results are shown to agree with a theoretically deduced curve.

Nomenclature

C_f = coefficient of friction
C_{pg} = specific heat of main gas stream (Btu/lb °F)
C_{pw} = specific heat of coolant (Btu/lb °F)
d = diameter of tube (in.)
f = friction factor in conventional pipes
g = acceleration of gravity (in./sec²)
h = heat transfer coefficient
l = total length of sweat cooled tube (in.)
$\Delta(P)$ = pressure difference (lb/in.²)
q = heat transferred to wall of specimen (Btu/in.² sec)
Q = coolant flow rate (lb/in.² sec)
Q/W = flow ratio
R = gas constant (in.²/sec² °F)
Re = Reynolds number
T_a = average temperature (°F)
T_g = temperature of main gas stream (°F)
T_w = temperature of gas at porous wall (°F)
T_0 = temperature of gas in coolant reservior (°F)
u_g = velocity of main gas stream (ft/sec)
u_δ = velocity of main gas stream at edge of laminar layer (ft/sec)
v_w = velocity of cooling gas emerging from wall (ft/sec)
W = flow rate of main gas stream (lb/in.² sec)
y^* = constant = 5.6
δ = thickness of laminar layer (in.)
θ_w = characteristic temperature ratio
μ = viscosity coefficient
ρ_δ = density of coolant (lb/in.³)
σ = Prandtl number
P_1 = pressure at upstream end of sweat cooled specimen (lb/in.²)
P_2 = pressure at downstream end of sweat cooled specimen (lb/in.²)
ρ_c = density of coolant (lb/in.³)
ρ_s = density of stream (lb/in.³)

Introduction

THE results of experimental and theoretical studies of gaseous sweat cooling described previously (1, 2)[3] have indicated the existence of a relationship between a characteristic temperature ratio θ and the flow ratio Q/W (see Nomenclature). The agreement between the experimental results and the theoretically deduced relation was qualitative only. In addition, the measurements showed a marked dependency upon the thermal conductivity of the porous material of which the test specimen was made. This behavior was not predicted by the theory, in which the nature of the porous material is not considered. It was believed that the experimental results were influenced by the fact that the test specimen was too short. In the experiments described in the present paper the sweat cooled section was relatively longer and was thermally insulated as completely as possible.

The problem of pressure drop through a sweat cooled porous tube was also investigated. In an effort to reduce the complexity of the problem, the gas injected through the porous tube was at the same temperature as the main stream and no actual cooling was involved.

Simplified Rannie's Equation

As a result of an analytical study of the process of sweat cooling, W. D. Rannie established the following relation (2).

$$\frac{T_w - T_0}{T_g - T_0} = \frac{\exp\left(-\frac{\sigma \rho_w v_w \delta}{\mu}\right)}{1 + \frac{C_{pw}}{C_{pg}}\left(\frac{u_g}{u_\delta} - 1\right)\left[1 - \exp\left(-\frac{\rho_w v_w \delta}{\mu}\right)\right]} \quad \ldots [1]$$

If, instead of the temperature ratio $(T_w - T_0)/(T_g - T_0)$, the ratio $\theta_w = (T_g - T_w)/(T_w - T_0)$ is used, Equation [1] may be rewritten

$$\theta_w = \frac{T_g - T_w}{T_w - T_0} = \left[\exp\left(\frac{\sigma Q \delta}{\mu}\right) - 1\right] + \exp\left[\frac{Q\delta(\sigma - 1)}{\mu}\right] \times \left\{\left[\exp\left(\frac{Q\delta}{\mu}\right) - 1\right]\frac{C_{pw}}{C_{pg}}\left(\frac{u_g}{u_\delta} - 1\right)\right\} \quad \ldots [2]$$

Since the Reynolds analogy was used in establishing Equation [1], the assumption may be made that it will be valid only for fluids whose Prandtl numbers are close to 1. Hence the quotient $\left(\exp\left(\frac{Q\delta}{\mu}\right) - 1\right)\Big/\left(\exp\left(\frac{\sigma Q\delta}{\mu}\right) - 1\right)$ may be dropped without introducing a significant error in the final result. Thus Equation [2] becomes

[3] Numbers in parentheses indicate References at end of paper.

Received December 24, 1952.
Text of paper presented at the Eighth International Congress for Theoretical and Applied Mechanics, Istanbul, Turkey, August 18–28, 1952.
This work was done at the Jet Propulsion Laboratory, California Institute of Technology, under Contract No. W-04-200-ORD-455 with the Army Ordnance Department, Washington, D. C. The authors wish to thank this agency for permission to present the results of this investigation.

[1] Formerly Research Engineer. Now President of Poroloy Equipment, Inc., Pacoima, Calif.
[2] Professor of Mechanical Engineering and formerly Chief of the Materials Section.

$$\theta_w = \left[\exp\left(\frac{\sigma Q \delta}{\mu}\right) - 1\right]\left[1 + \frac{C_{pw}}{C_{pg}}\left(\frac{u_g}{u_\delta} - 1\right)\right] \quad \ldots . [3]$$

The quantities $(\sigma\delta/\mu)$ and (u_g/u_δ) may be evaluated using the assumptions given by Rannie (2). Taking $\delta = (\mu/w)\sqrt{(2/C_f)}y^*$ and assuming that $y^* = 5.6$, $C_f = 0.046/Re^{0.2}$, and $Re \cong 10^5$, then $\frac{\sigma\delta}{\mu} = 117\left(\frac{\sigma}{w}\right)$. Similarly, if $\mu_\delta = \mu_g\sqrt{(C_f/2)}y^*$ then $(u_g/u_\delta) = 1/y^*\sqrt{(C_f/2)} = 3.73$. Hence Equation [3] becomes

$$\theta_w = \left[\exp\left(\frac{117\sigma Q}{W}\right) - 1\right]\left(1 + 2.73\frac{C_{pw}}{C_{pg}}\right) \quad \ldots \ldots [4]$$

As a first approximation consistent with experimental accuracy at small values of Q/W, the exponential may be approximated by the first terms of its expansion, and Equation [4] becomes

$$\theta_w = 117\frac{\sigma Q}{W}\left(1 + 2.73\frac{C_{pw}}{C_{pg}}\right) \quad \ldots \ldots \ldots \ldots [5]$$

This simplified equation will be used for interpreting the experimental results discussed in the present paper.

Experimental Technique

The sweat cooling experiments discussed in this paper were performed with a gasoline-air burner shown in Fig. 1. The test specimen consists of a porous metal cylinder 1 in. in diameter and 8 in. long. The specimen holder is shown in Fig. 2. The coolant annulus, which is 2 in. larger in diameter than the specimen in order to minimize radial heat loss is

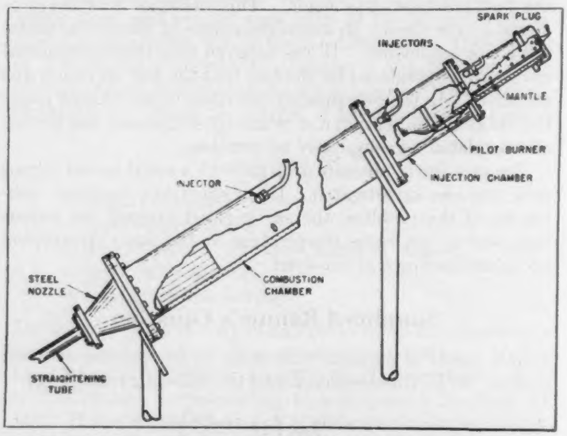

Fig. 1 Combustion chamber for sweat-cooling tests

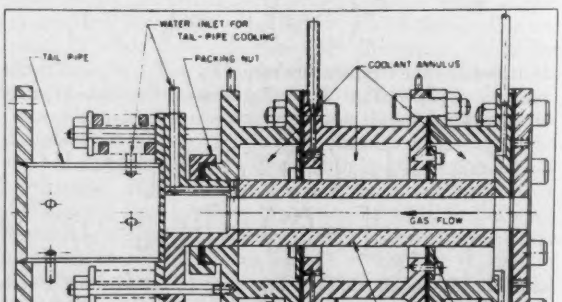

Fig. 2 Test section for sweat-cooling tests

divided into three parts. The coolant entering the center jacket, which is approximately 4 in. long, was metered, and all wall temperature measurements were made in this region. Coolant entering the two outer jackets was not metered, but the pressure in these jackets was maintained equal to that of the center section so that the coolant flow per unit area was the same over the entire specimen. At the downstream end of the holder, provision was made to allow for thermal expansion of the specimen by appropriate spring-loading. This spring-loaded section was protected from the hot gas by water-film cooling.

The joints between the various parts of the holder were sealed with asbestos gaskets impregnated with General Electric Glyptal. This technique formed a gas-tight seal which could withstand pressures of at least 100 lb/in.[2]

The combustion chamber (Fig. 1) was approximately 5 ft long and 6 in. in diameter. The downstream end was terminated in a steel nozzle having an outlet 1 in. in diameter. The nozzle and specimen holder were connected by a 20-in. straightening tube. A pilot burner approximately 2 ft long and 3 in. in diameter, complete with a 1-in. nozzle and one tangential air-fuel injector, was located at the upstream end of the combustion chamber. Air and fuel, which are injected into the pilot, whirl upstream between the mantle and the outside casing and come into the burner through the holes in the mantle, which in this position acts as a flameholder. The addition of the pilot burner to the original assembly extended the operating range of the burner so that the minimum stable operating temperature was about 500 F. Additional fuel and air were brought into the combustion chamber through tangential fuel-air injectors.

For measuring the wall temperature in the sweat cooled section, the following method of thermocouple installation was used. A flat-bottomed hole $^1/_8$ in. in diameter was drilled to the desired depth in the specimen. The two wires of the thermocouple were arc-welded separately to the bottom of the hole by the condenser-discharge method. After the wires were welded in place, a small piece of two-hole ceramic tubing, equal in length to the depth of the hole, was slipped over the wires and cemented in place with a cement composed of magnesium oxide and sodium silicate. This type of installation provided a maximum of strength and thermal contact with the wall and a minimum, though not negligible, amount of interference with the normal pattern of coolant flow through the specimen. Since it was not possible to spot-weld to copper, thermocouples installed in copper specimens were first beaded, then forced into the flat-bottom holes and cemented in place. For all experiments No. 28 chromel-alumel wires were used.

Twelve thermocouples were installed in each specimen, four along the inner wall, four in the center of the specimen radially, and four along the outer surface. All leads were brought out through the gaskets between the segments of the holder.

The measurements of the temperatures in the main gas stream posed a difficult problem. Rigid thermocouple supports or shielded thermocouples could not be used in the straightening tube 1 in. in diameter without seriously disturbing the velocity profile of the gas stream. After several types of thermocouple installations were tried, it was found that the most satisfactory method consisted of a beaded thermocouple supported in two-hole ceramic tubes and introduced radially into the stream of gas. It was not feasible to extend the bead more than $^1/_8$ in. into the stream because the ceramic support would be broken off, either by thermal stresses or by the mechanical shock of solid particles in the products of combustion. The experimental errors inherent in the use of an exposed beaded thermocouple are discussed in the next section.

The porous metal specimens were prepared in this laboratory by methods previously described (3). Difficulties were first encountered in machining the porous shapes without smearing the surface. The method which was finally adopted

consisted in immersing the metal in a bath of molten salt until the pores were filled. The machining was then carried on and the salt subsequently removed by treatment in boiling water.

Discussion of Accuracy of Measurements

The measurement of the temperature of the main gas stream was subject to several sources of error. The error which results from the loss of heat by radiation from the thermocouple to the cooler straightening tube wall was difficult to assess accurately. However, a careful analysis indicated that this error was of the order of 10 F.

The recovery factor of a bead introduced radially into the stream was determined from comparison with a Pratt and Whitney type of stagnation probe. In the range of gas velocities used in these experiments, the correction of stagnation temperature to true temperature is not sensitive to the recovery factor. Hence a value of 0.7 was assumed to apply to all gas temperature data. Another source of error was connected to the location of the thermocouple in the gas stream. The temperature profile of the gas stream was determined for several combinations of gas temperature and velocity and it was found that the rate of temperature change with respect to tube radius was approximately 400 F/in. The uncertainty in locating the thermocouple bead being of the order of $^1/_{32}$ in. an error of 13 F could therefore occur in the indicated gas temperature based on the assumed location of the thermocouple. Since thermocouples were changed frequently (approximately every other test), this error must be assumed to be a major source of data scatter.

In the measurement of wall temperature, the disturbance introduced by the presence of the thermocouple into the coolant flow pattern within the wall is an important source of error. When a thermocouple is installed in a porous wall, it necessarily disturbs the flow pattern and tends to block off the flow of coolant. Thus the thermocouple indicates temperatures which are higher than those that would actually exist on the surface of an undisturbed wall. The magnitude of this error is very difficult to assess and varied with every thermocouple installation.

Although the effects of axial heat exchange between the specimen and the holder are minimized by the presence of the segments, there is unquestionably some radial heat loss from the back of the specimen to the holder. The effect of these losses cannot be accurately determined, but their effect is to decrease the temperature of the sweat cooled porous specimen, and consequently the measured value of the coefficient θ is somewhat larger than its true value.

Experimental Results

The tests described in the present paper were carried out using a copper cylinder having a porosity of approximately 40 per cent. Nitrogen and hydrogen were used as cooling fluids. Tests were also made with propane, but this gas was found unsatisfactory because it undergoes a dissociation.

The interpretation of the results was based on Equation [5]. By inserting numerical values for the parameters[4] of Equation [5], individual expressions for the θ_w vs. Q/W relation may be reached for each of the cooling gases involved. Thus, for hydrogen and nitrogen sweat cooling, Equation [5] becomes $\theta_w = 4050\ Q/W$ and $\theta_w = 348\ Q/W$, respectively. These two expressions have been graphed in Figs. 3 and 4. Also shown in these figures are the results of experiments using copper tubes cooled with nitrogen and hydrogen.

For both hydrogen and nitrogen cooling, the values of θ_w determined by the theoretical curves are higher than the experimentally determined values. It was pointed out above that the measured surface temperature of a sweat cooled tube

[4] Since temperature variations of these parameters are within experimental accuracy, 100 F values have been used.

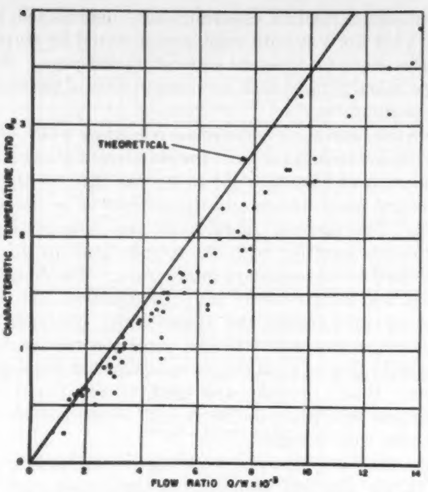

Fig. 3 Curves for sweat-cooling experiments using copper specimen and nitrogen as coolant

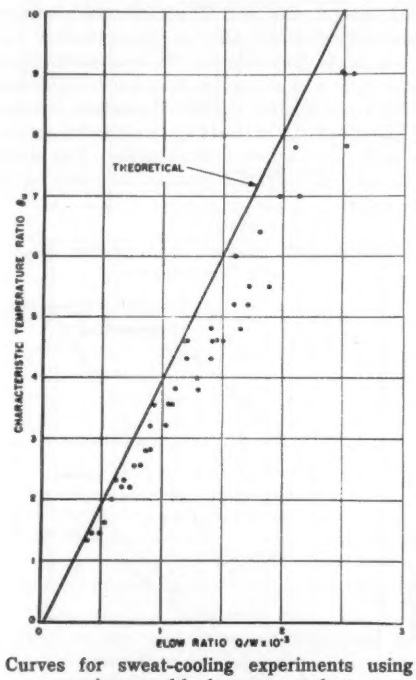

Fig. 4 Curves for sweat-cooling experiments using copper specimen and hydrogen as coolant

would always be higher than the true surface temperature because of the blocking effect of the thermocouple which depressed the value of θ_w. Another possible source of deviation between experiment and theory is Rannie's assumption that the coolant would be perfectly distributed over the surface of the specimen. It has actually been found that the coolant leaves the surface in the form of a number of isolated jets. Thus the sweat cooling process will be less efficient than has been assumed and the values of θ_w will be correspondingly lower. In this regard, it should be noted that Rannie's assumed value for y^* was based on the empirically determined expression for laminar layer thickness in a smooth pipe; that is

$$\frac{\delta u_\tau}{v} = y^*$$

where $u_\tau = \tau_0/\rho$ (τ_0 is the shearing stress at the wall). Quite obviously, the flow near the wall of a sweat cooled pipe and the flow near the wall of a smooth pipe may be quite different.

Furthermore, Prandtl's experimentally determined value of 5.6 for y^* is for a smooth pipe, and it would be surprising if this value were to apply to a sweat cooled pipe. However, these parameters have been accepted in view of the lack of any better assumption.

There has been some speculation regarding which of the gas properties are important from the standpoint of sweat cooling. Examination of Equation [5] shows the ratio of the specific heats of the main stream and the coolant to be the most important. The thermal conductivity and viscosity enter into the equation, together with the specific heat, in the Prandtl number and are of secondary importance. The density of the gas does not enter directly into the equation. It would be interesting to compare the theoretically predicted cooling curve for another gas with the experimental results. Unfortunately, the only other gas available for these tests was propane. When propane was used, it was found that decomposition took place in the vicinity of the porous wall and the results were erratic.

In the analysis of the sweat cooling process leading to Equation [1], the physical properties of the porous wall material are not considered. A series of experiments were performed with a porous cylinder made of an alloy containing 60 per cent nickel, 20 per cent iron, and 20 per cent molybdenum. The heat conductivity of this alloy is approximately $^1/_{35}$ that of copper. A comparison between the results obtained with the alloy and copper is shown in Fig. 5, in which both experimental curves may be compared with the theoretical relation of θ vs. Q/W. The proximity of the two experimental curves leads to conclusion that, as a first approximation, the nature of the wall material has only a secondary influence on the sweat cooling process.

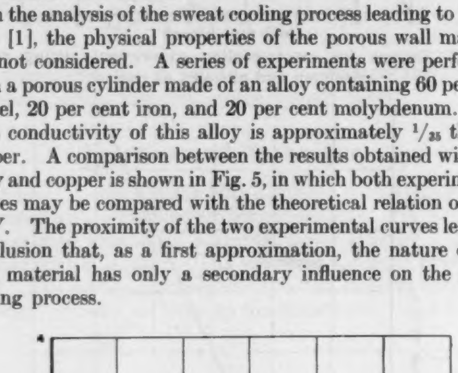

Fig. 5 Theoretical curve and curves of θ vs. $Q/W \times 10^{-3}$ for 8-in. copper and alloy specimens

Heat Transfer Coefficient in Sweat Cooled Tubes

Although the relation between the characteristic temperature ratio and the flow ratio is of theoretical interest, it may be more convenient from the engineering standpoint to deal with the problem in terms of heat transfer coefficients. That such a procedure is possible may be easily demonstrated and some interesting conclusions may be drawn from the analysis.

The usual heat transfer coefficient, h, defined by the relation $q = h\,(T_g - T_w)$, may be introduced in the interpretation of sweat cooling data. Since the process is thermally conservative, the enthalpy increase of the coolant will be equal to the heat absorbed by the wall; that is, $q = QC_{pw}\,(T_w - T_0)$. Hence the heat transfer coefficient takes the form

$$h = \frac{QC_{pw}}{\theta_w} \quad \text{[6]}$$

Replacing θ_w by the expression of Equation [5], the heat transfer coefficient h becomes

$$h = \frac{WC_{pw}}{117\sigma\left(1 - 2.73\,\dfrac{C_{pw}}{C_{pg}}\right)} \quad \text{[7]}$$

This expression is interesting because it shows that h is independent of Q. If numerical values of the constants are inserted into Equation [7], it is observed that the value of the coefficient h is very nearly the same for both hydrogen and nitrogen, namely, $8.9 \times 10^{-4}\,W$ for hydrogen and 7.2×10^{-4} W for nitrogen. This is a difference of only 20 per cent for gases whose cooling properties differ widely.

Experimentally obtained values of h have been computed from Equation [7]. Here again, 100 F values have been used since the temperature fluctuations are within experimental accuracy. The results indicate that h varies somewhat with Q, but this variation is not systematic. The deviation from the theory is attributed to the uncertainties in the determination of T_g and T_w and to the difference between theoretically assumed conditions and actual conditions. Of greater importance, perhaps, is the fact that the theoretical and experimental values of h lie surprisingly close to the values which would be predicted for a conventional pipe where a gas flow rate of 0.2 lb/sec and a temperature of 1500 F would yield a value of h of the order of 1×10^{-4} Btu/sq in. sec °F.

Pressure Drop in a Sweat Cooled Tube

In an effort to reduce the complexity of the problem of fluid flow through a porous tube, a study was made in which the gas passing through the porous tube was at the same temperature as the stream. Although no actual cooling was involved, the injected gas will be referred to as "coolant."

The equipment used for these experiments is shown diagrammatically in Fig. 6. It consisted of a 60-in. length of pipe 1.1 in. in diameter, divided into three segments. The porous copper segment 5.5 in. long was preceded by a 20-in. approach section to stabilize the velocity profile and was followed by a 35-in. tailpipe to allow a study of the stream downward from the porous section. The porous copper segment, which had an outside diameter of 2 in., was contained in the holder, also shown in Fig. 6. Gas under pressure was injected through the porous walls from the small annular space between the holder and the specimen. The entire assembly was aligned on a close fitting mandrel to insure accurate joints. All interior pipe surfaces were ground, but the surface of the specimen was machined.

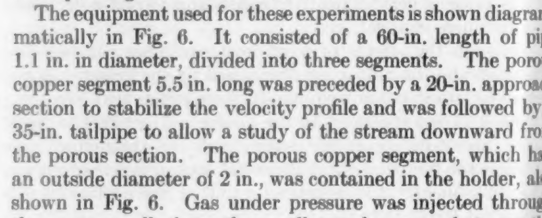

Fig. 6 Apparatus used for isothermal flow tests

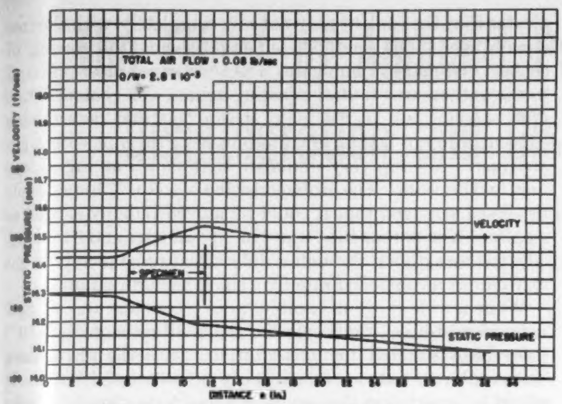

Fig. 7 **Axial velocity and pressure distribution in nitrogen sweat-cooled tube**

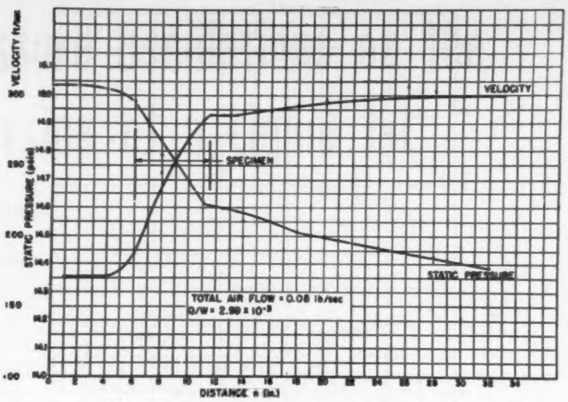

Fig. 8 **Axial velocity and pressure distribution in hydrogen sweat-cooled tube**

The movable probe support consisted of a single piece of $^1/_8$-in. stainless steel tubing located along the axis of the test section. The pitot probe was a hypodermic needle (No. 22) silver-soldered to the probe support and bent parallel to it midway between the support and the wall. The tip of the head tube was braced by a piece of shim stock. A small hole in the probe support directly underneath the tip of the pitot tube constituted the static pressure tap. The probe support was blocked midway between the static pressure opening and the point where the pitot tube entered the probe support. Thus static pressure was transmitted to one end of the probe support and total pressure to the other. The end of the probe support was indexed so that the pitot static openings could be located at any desired position along the pipe. Because of the flexibility of the probe support, it was necessary to provide a movable guide immediately behind the dynamic head tube. The entire assembly was lagged with asbestos to assure isothermal conditions.

Experiments were conducted to determine the velocity and pressure distribution along the axis of the porous tube. These studies were carried out with four different coolant gases: nitrogen, hydrogen, helium, and carbon dioxide. Although the coolant flow rates were varied over a wide range, the main stream air flow rates were confined to the narrow range of values between 0.05 and 0.11 lb/sec.

Typical results of the axial velocity and pressure distribution experiments are shown in Figs. 7 through 10. Similar distribution curves were obtained for many tests under different conditions.

Referring to the axial pressure and velocity distribution curves in Figs. 7 and 8, the most evident features are that in the sweat cooled segment the pressure drop is (a) linear with length, (b) dependent on the rate of coolant flow, and (c) more rapid for the less dense gases for equal values of the flow ratio Q/W. That this experimentally observed behavior follows theoretically predicted behavior is demonstrated below.

It might also be well to point out at this time the slight tendency toward pressure recovery which occurs immediately downstream of the porous specimen and the high velocity values which persist in the exhaust pipe. Both of these phenomena might be interpreted in terms of an extremely distorted velocity profile induced by introduction of the coolant gas.

Analysis of Pressure Drop Data

Both Summerfield and Tsien (4, 5) have suggested that the problem of pressure drop in sweat cooled pipes may be approached from a purely theoretical standpoint using the momentum equation which may be written as

$$d_p + \frac{f}{Z}\,\rho u^2\,dx + d(\rho u^2) = 0 \quad [8]$$

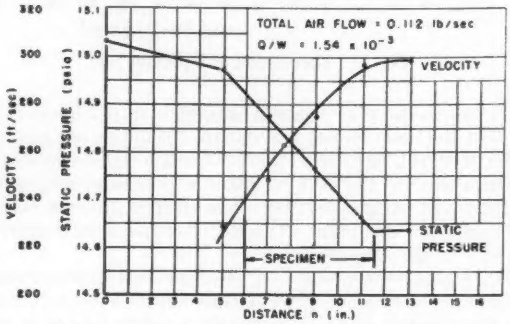

Fig. 9 **Axial velocity and pressure distribution in helium sweat-cooled tube**

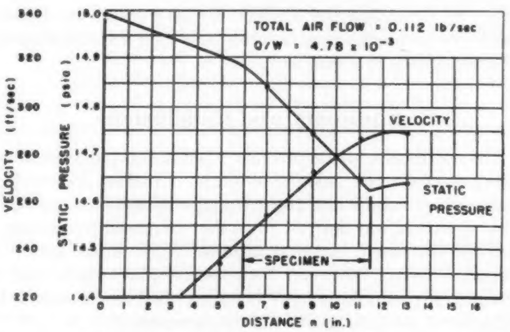

Fig. 10 **Axial velocity and pressure distribution in carbon dioxide sweat-cooled tube**

where Z is the tube diameter,

$$\rho u = W + Q\frac{4x}{Z} \quad [9]$$

and

$$u = \frac{W}{\rho_s} + \frac{Q\frac{4x}{Z}}{\rho_c} \quad [10]$$

A direct integration is possible. For small values of Q/W, higher order terms may be neglected leading to the approximate solution

$$\frac{\rho_s \Delta_p}{W^2 h} = \frac{f}{Z} + \frac{4}{Z}\left(1 + \frac{\rho_s}{\rho_c}\right)\frac{Q}{W} \quad [11]$$

Verification of this relation is demonstrated in Fig. 11 where $\Delta P/W^2L$has been plotted against the term $1/2(1+\rho_s/\rho_c)Q/W$. The small scatter of the points on this plot, with the exception of data for high rates of hydrogen flow, would seem to bear out the correctness of assigning the head losses in a sweat cooled tube purely to the sum of frictional losses and momentum exchange.

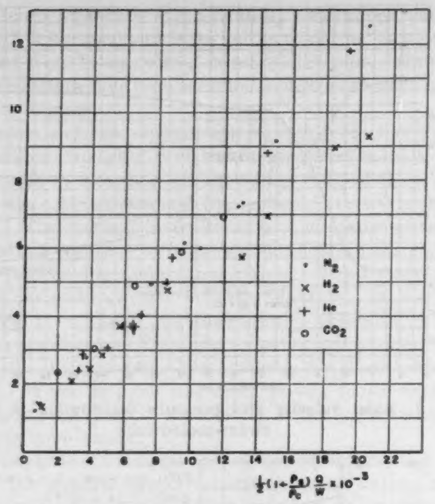

Fig. 11 Correlation of Equation [13]

A basic assumption made in the derivation of Equation [11] is that the main stream gas and the coolant do not mix, and that their volumes are additive. Certain experimental work carried out by the authors into the process of mixing and diffusion in sweat cooled pipes has substantiated the validity of this basic assumption. This corroborative work is described briefly in the Appendix.

In general, the problem of pressure drop in sweat cooled pipes may be summed up by stating that the effects of friction and momentum exchange are additive and that pressure drops will be proportional to the ratio of coolant and stream densities and to the coolant flow ratio. Numerical calculation will show—as demonstrated in Figs. 7 and 8—that the pressure drops due to momentum may be very high if the coolant flow ratio exceeds a few per cent.

Summary and Conclusions

The results of experiments described in this paper have been interpreted on the basis of a simple equation in which the temperature ratio θ is a linear function of the flow ratio Q/W. This equation was derived from that proposed by Rannie by making additional approximations. The rather small discrepancies found between the experimental results and the theoretical predictions have been ascribed to various factors influencing the accuracy of the measurements.

On the basis of the simplified Rannie equation, it has been deduced that the gas property having the greatest effect is the specific heat. Furthermore, the nature of the porous material does not appear to influence the heat transfer process in sweat cooling. This result is in agreement with the theoretical analysis.

The present study has also shown that the heat transfer in a sweat cooled tube may be handled in terms of a conventional type of heat transfer coefficient h and that this coefficient is independent of the coolant flow rate. Experimentally obtained values of this coefficient h do not depart greatly from those pertaining to conventional flow under similar conditions.

The pressure drop in sweat cooled pipes has also been investigated. The pressure difference per unit length in excess of that found in conventional pipes is determined by the flow rate of the main gas stream, the density of the coolant, and the ratio of the flows of main gas stream and coolant.

APPENDIX

The work which is reported in the discussion concerning the velocity and pressure distribution in sweat cooled pipes indicates that the coolant may not mix completely with the free stream gas. The method of investigating the mixing of coolant and main stream gases which appeared most practical to the authors was that of injecting helium as a coolant into a pipe carrying air as the main stream gas and determining concentration of helium in various parts of the pipe with a gas analyzer. A setup very similar to that shown in Fig. 6 was used for this work. The probe consisted of a No. 27 hypodermic needle so arranged that it could be moved radially as well as axially. The porous tube was 2 in. in diameter and 6 in. long. The gas was drawn through a differential resistance type gas analyzer at a controlled rate by a small vacuum pump.

While a wide range of combinations of coolant and air flow rates were studied, the results for the Q/W ratio of 21×10^{-3} have been selected for presentation, since the phenomena observed in all tests are most clearly demonstrated there. It might be noted that the results of these tests were extremely reproducible.

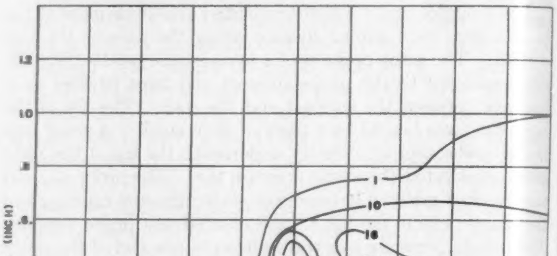

Fig. 12 Concentration field in porous pipe showing per cent helium by volume for $Q/W = 21.7 \times 10^{-4}$

The distribution of helium in the 2-in. diameter sweat cooled pipe is shown in Fig. 12. Helium concentration figures in per cent are given thereon. Starting with the leading edge of the porous section, the concentration increases for approximately one and one-half pipe diameters forcing the undisturbed flow gradually away from the wall. After this interval, the amount of helium in the boundary layer appears to exceed certain stability requirements, and the flow apparently separates from the wall with the creation of three separate concentration centers in the central flow region and several other centers of high concentration near the wall. The position of the inception of separation has been related to the flow ratio Q/W. Exploration further downstream indicated that the flow gradually returned to normal, but many pipe diameters are required before complete mixing has been attained.

The general conclusion to be drawn from this work is that the coolant and main stream mix very slowly, so that their volumes may be assumed to be additive.

References

1 "Experimental Study of Cooling by Injection of a Fluid Through a Porous Material," by Pol Duwez and H. L. Wheeler, Jr., *Journal of the Aeronautical Sciences*, vol. 15, 1948, pp. 509-521.

2 "A Simplified Theory of Porous Wall Cooling," Progress Report no. 4-50, Pasadena, Calif., Jet Propulsion Laboratory.

3 "The Powder Metallurgy of Porous Metals and Alloys Having a Controlled Porosity," by Pol Duwez and Howard Martens, AIME Technical Publication no. 2343, 1948.

4 M. Summerfield, Private communication.

5 H. S. Tsien, Private communication.

The Effect of Ambient Pressure Oscillations on the Disintegration and Dispersion of a Liquid Jet[1]

C. C. MIESSE[2]

Aerojet-General Corporation, Azusa, Calif.

The effect of ambient pressure oscillations on the disintegration and dispersion of a liquid jet was investigated by imposing a high-intensity acoustic field on the jet. The effect of a localized sound source, directed perpendicular to the stream, was to disperse the droplets in a diverging sinusoidal configuration, and the effect of an axial cavity resonance directed parallel to the stream was to coalesce the droplets as a result of the velocity variation of successive fluid particles. Each of these effects was analyzed theoretically, and it was found that the magnitude of each effect decreased with an increase either in the velocity of the stream or in the frequency of the imposed oscillation. The analysis of the droplet coalescence, which occurred for the case of axial cavity resonance, led to a possible criterion for combustion stability.

Nomenclature

a = radius of jet
b = distance from new origin to tank outlet
C_p = profile drag coefficient
D = diameter of jet
D_0 = diameter of orifice
d = diameter of droplet
d^* = diameter of coalescent droplet
F = force of surface tension
f = variation of steady-state velocity
G = $\int_0^L f\,dx$
g = variation of oscillatory component of velocity
h = variation of oscillatory pressure component
K = amplitude of velocity variation
k, k', k'' = proportionality coefficients
L = length of fluid lines
M = total mass of liquid in coalescent droplet
$\dot{M}_0$ = mass flow rate
n = number
P = variable pressure in fluid lines
P_0 = steady-state chamber pressure
P_s = constant supply pressure
p_0 = oscillatory component of chamber pressure
q = variation of line pressure
R = radius of curvature of sinuous jet
s = transverse displacement of droplets
s' = distance between jets
T_i = $t - t_i$
t = time
t_i = time at which droplet was injected
t_0 = time at which droplet was exposed to transverse wave
U = steady-state velocity
V = variable velocity
v = oscillatory component of velocity
w = transverse displacement of jet
x = axial coordinate
y = transverse coordinate
z = axial coordinate
Z = distance from injector to flame front
α = $\lambda\sqrt{\bar{V}}/D_0$
ΔP = steady-state pressure drop
λ = wavelength of jet disturbance
θ = dispersion angle
ρ = density
σ = surface tension coefficient
ϕ = phase angle
ω = angular frequency
γ = weight density

Received November 20, 1954.

[1] The work reported in this paper was performed under the sponsorship of the Air Research and Development Command, U. S. Air Force.

[2] Physicist, Liquid Engine Division.

[3] Numbers in parentheses indicate References at end of paper.

Introduction

EXPERIMENTAL evidence (1)[3] on oscillatory combustion in liquid-propellant combustion reveals that the amplitude of pressure oscillations in the combustion chamber frequently exceeds 50 per cent of the steady-state chamber pressure. Since pressure oscillations of this amplitude will undoubtedly affect the disintegration of the liquid jets, the purpose of the present experimental and theoretical analysis is to determine both the nature and extent of these effects. Although the effects of acoustical disturbances on the liquid supply system have been investigated by Savart, Plateau, Magnus, and Rayleigh (2), neither this effect nor the effect of ambient-pressure oscillations has been analyzed previously. Accordingly, experiments were designed to determine the effect of localized transverse oscillations on a free jet, and to determine the effect of each of the three modes of cylindrical-cavity oscillations on a stream injected into a cylindrical chamber.

Dispersion of a Free Jet

The experimental apparatus for the study of the effect of localized high-intensity sound sources directed normal to a free liquid jet is shown in Figs. 1, 2, and 3. From these figures it is seen that pressurized liquid (water) was forced through an orifice, the length of which was approximately 0.550 in., and the diameter of which varied from 0.014 in. to 0.055 in. The three-orifice injector (orifice diameter of 0.020 in. spaced $^1/_4$ in. apart) was used to study the interaction and

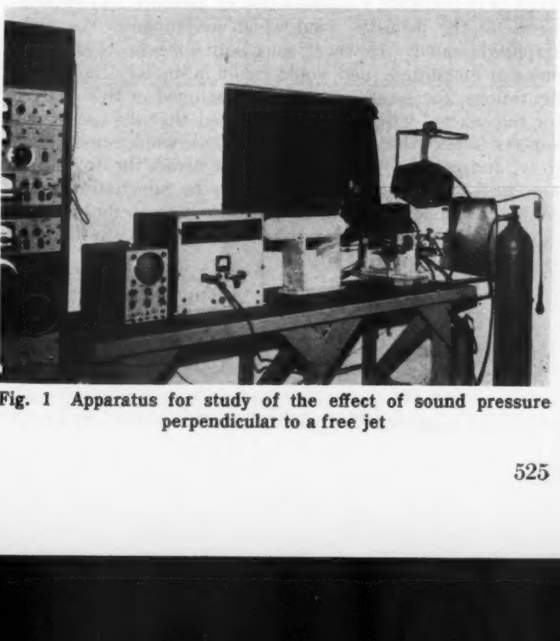

Fig. 1 Apparatus for study of the effect of sound pressure perpendicular to a free jet

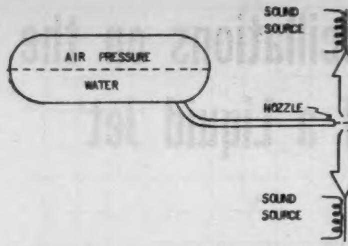

Fig. 2 Schematic diagram of apparatus for the study of high intensity sound on a liquid jet

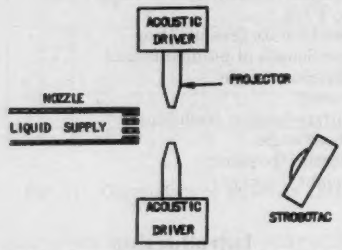

Fig. 3 Schematic diagram of apparatus for study of the effect of free field transverse sound pressure on multiple jets

mixing of three collinear jets. The acoustic field, normal to the jets, was provided by a pair of Western Electric drivers, Model 720-A, which were fitted with special adapters for concentrating the sound field. The sound intensity was measured by placing a microphone midway between the adapters and about $^1/_4$ in. from their common axis. The instantaneous droplet configurations were observed by using stroboscopic light, and photographs of the phenomena were taken with a Speed Graphic camera using Eastman Super XX film with light supplied by two General Electric T-125 microflash bulbs for a duration of approximately 2 microsec.

Fig. 4 shows a series of tests made with the single jet at various frequencies and at various values of the pressure drop across the nozzle. The two sound sources were adjusted so that the sound pulses were 180 degrees out of phase, thus giving the maximum push-pull effect. From this series of pictures, it is seen that the amplitude of dispersion decreased with increases both in the frequency of the imposed oscillation and in the pressure drop across the injector. It was noted also that the sound field produced a considerable decrease in the length of the solid stream.

The diverging oscillatory pattern observed in this figure can be derived theoretically by considering the force which is exerted on the individual droplets by the oscillating pressure difference across the droplets. Actually, the force on the droplets is probably a combination of pressure and entrainment by the acoustic wind which accompanies the high-amplitude sound. However, since both forces are of the same order of magnitude, and would result in similar droplet configurations, the pressure concept is assumed in this analysis for the sake of simplicity. It is noted that the use of this concept implies that the effects of acoustic wind, aerodynamic drag, and ratio of pressure difference across the droplets to amplitude of the pressure wave can be adequately represented by proper choice of the pressure drag coefficient. By equating the pressure forces to the inertia forces, the following equation is obtained

$$C_p \frac{\pi d^2}{4} p_0 \sin \omega t = \frac{\pi d^3}{6g}\,\gamma\,\frac{d^2 s}{dt^2} \quad [1]$$

and

$$s = -\frac{1.5 C_p g}{d\gamma\omega^2} p_0 \left[\sin \omega t - \sin \omega t_0 - \omega(t - t_0)\cos \omega t_0\right] \quad [2]$$

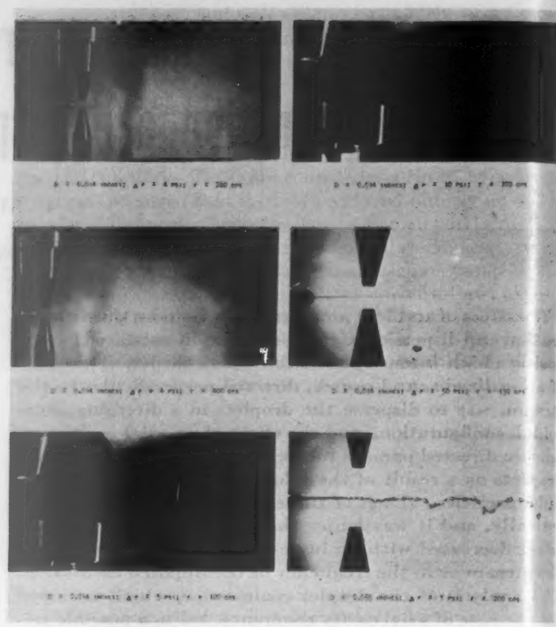

Fig. 4 Typical droplet configurations produced by the effect of a transverse sound field on a free liquid jet

where

d = diameter of droplets (ft)
C_p = pressure drag coefficient of sphere
p_0 = amplitude of acoustic wave (lb/ft^2)
ω = frequency (rad/sec)
γ = weight density of liquid (lb/ft^3)
g = acceleration of gravity (ft/sec^2)
s = distance in which droplet is displaced (ft)
t = time (sec)
t_0 = time at which droplet is initially subjected to oscillating pressure (sec)

Since the dominant term in the brackets of Equation [2] is $\omega(t - t_0)\cos \omega t_0$, it can be shown that the tangent of the dispersion angle θ can be approximated by

$$\tan\theta = \frac{s}{x} = \frac{1.5 g\, p_0 \cos \omega t_0}{d\gamma\omega U} \quad [3]$$

where x is the axial displacement of a droplet in time $(t - t_0)$ and U is the linear velocity of the jet. It is noted that Equation [3] predicts the decrease in dispersion angle both with frequency and with jet velocity as observed in Fig. 4.

Fig. 5 shows a series of tests made with the collinear jets, from which it is apparent that the incidence of a localized transverse wave on a series of jets can establish intimate mixing of the jets in a much shorter distance than would otherwise occur because of random jet dispersion. This phenomenon may well explain the burning out of injector plates which has been observed in combustion chambers in which a tangential mode of oscillation is present. From Equation [2] it is readily seen that the mixing of two adjacent streams, with displacements $s_1(t)$ and $s_2(t)$, respectively, occurs when

$$s_1(t) + s' = s_2(t) \quad [4]$$

for sound sources 180 degrees out of phase, where s' is the distance between orifices.

Fig. 6 shows the instantaneous droplet configuration for three collinear jets in a bipropellant combustor, as determined by Equation [2]. The values of the parameters used in this computation were as follows: p_0 = 120 psi; ω = 11,300 rad/sec; γd = 0.00343 psi and U = 70 fps for the oxidizer droplets; γd = 0.00119 psi and U = 160 fps for the fuel droplets. The

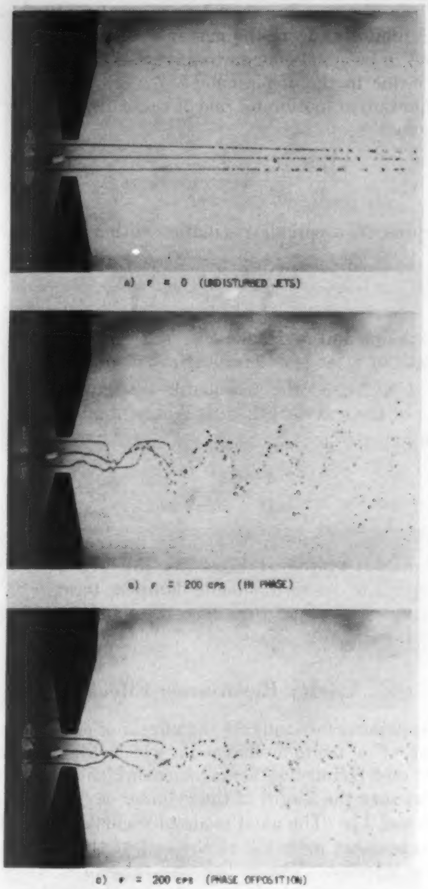

Fig. 5 Typical droplet configurations for three collinear free jets

$D = 0.02$ in.; $\Delta p = 5$ psi.

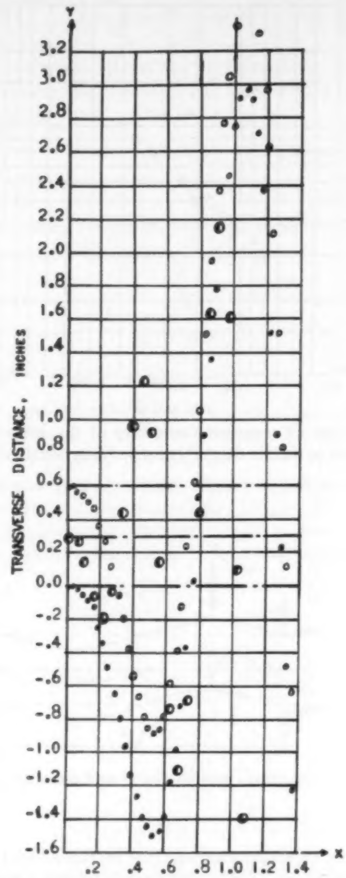

Fig. 6 Positions of droplets from two fuel and one oxidizer orifices for a typical bipropellant liquid combustor

○ ● = fuel droplets; ◐ = oxidizer droplets

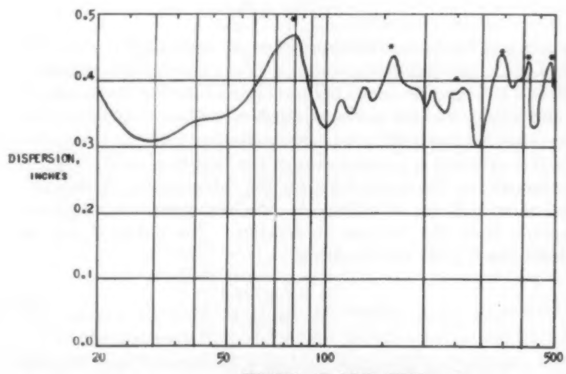

Fig. 7 Variation of jet dispersion (at 6 in. from sound source) with frequency of sound source

$D = 0.014$ in.; $\Delta p = 7$ psi; * points of maximum dispersion.

similarity between this figure and the photographs of Fig. 5 is immediately apparent.

Natural Frequency of a Liquid Jet

When it was noted that, for a given jet and for a constant sound intensity, certain frequencies produced greater dispersions than others, a study of this variation of dispersion with frequency was made by passing a sheet of blotting paper through the jet at a constant distance from the injector. A typical plot of this variation is shown in Fig. 7, from which it is apparent that the maxima of the dispersion occurred at fairly constant intervals on the frequency scale. This constant frequency interval, which was denoted as the natural frequency of the jet (ω_j), appeared to vary directly as the velocity of the jet and inversely as the orifice diameter. Fig. 8 is a logarithmic plot of the natural frequency vs. the ratio of jet velocity to orifice diameter for several velocity-diameter combinations, from which it is seen that the variation is approximately linear:

$$\omega_j = kU/D \qquad [5]$$

It is interesting to note that Savart (2) observed the same type of variation for the frequency of the note produced by the impact of a jet on a plate normal to its axis.

Equation [5] can be derived theoretically by consideration of a cylindrical jet of radius a, which has been displaced sinusoidally by some atmospheric disturbance. The configuration is shown in Fig. 9, from which it is seen that the wavelength of the sinusoidal displacement is designated by λ, and the amplitude of its displacement by w. The equation for the generators of the sinuous cylinder can thus be written

$$y = w(t) \sin \frac{2\pi x}{\lambda} \qquad [6]$$

where the amplitude w is permitted to vary with time.

Since the outboard surface (farthest from original jet axis) is

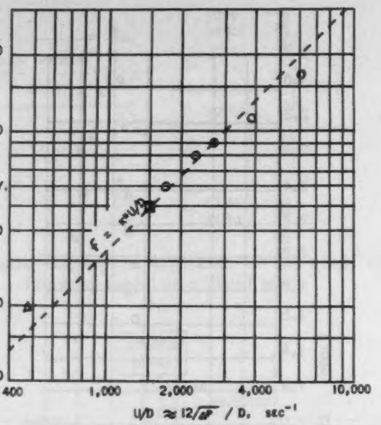

Fig. 8 Variation of resonant frequency of the jet with ratio of jet velocity to nozzle diameter for various nozzle diameters

○ $D = 0.014$ in.; □ $D = 0.028$ in.; △ $D = 0.055$ in.

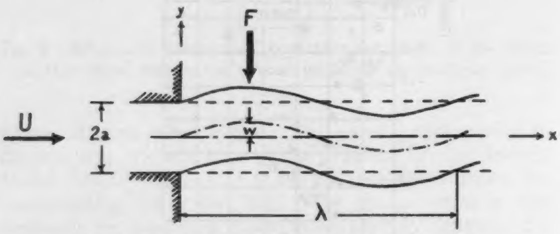

Fig. 9 Original (undisturbed) and sinuous jets

"stretched" by this displacement, the increased surface tension which thus occurs will act as a restoring force to return the jet to its original undisturbed position. The force due to this surface tension is given in differential form by

$$dF = \sigma\left(\frac{1}{R_1} + \frac{1}{R_2}\right) dS \qquad [7]$$

where σ is the surface tension (force per unit length), R_1 is the first principal radius of curvature (the radius of the cylinder), R_2 is the second principal radius of curvature (for the displaced generators), and dS is the element of surface over which the incremental force dF acts. Since the force due to the radius of the cylinder is present also in the undisturbed jet (and is balanced by the same force on the inboard side of the jet), the term $1/R_1$ can be deleted in considering the restoring force arising from the increase in tension. The radius R_2 can be determined from the equation

$$R_2 = \frac{[1 + (dy/dx)^2]^{3/2}}{d^2y/dx^2} \qquad [8]$$

By substituting Equation [6] into Equations [7] and [8], and by letting the value for $x = \lambda/4$ (maximum displacement) be a representative value, then

$$R_2 = \lambda^2/4\pi^2 w \qquad [9]$$

and

$$dF = \frac{4\pi^2\sigma}{\lambda^2} w dS \qquad [10]$$

Application of this surface tension to the outboard surface over half a wavelength results in

$$F = \frac{k'4\pi^2\sigma}{\lambda^2} w \cdot \frac{\pi a\lambda}{2} \qquad [11]$$

where k' is a constant less than 1 to account for the fact that the force diminishes from the maximum, and where w/λ was considered to be small enough to disregard the slight increase in surface due to the displacement.

The equation of motion for one of these displaced segments thus becomes

$$\frac{\pi\rho a^2\lambda}{2}\frac{d^2w}{dt^2} + \frac{4\pi^3 k'\sigma a}{2\lambda} w = 0 \qquad [12]$$

which represents a periodic oscillation with a frequency of

$$\omega = \frac{1}{2\pi}\sqrt{\frac{4\pi^2 k'\sigma}{\rho a\lambda^2}} = \frac{1}{\lambda}\sqrt{\frac{k'\sigma}{\rho a}} \qquad [13]$$

Since experimental evidence (3) has indicated that the wavelength of a jet is determined principally by the Weber number $U\sqrt{2\rho a/\sigma}$, the reasonable assumption of inverse variation of the wavelength with Weber number leads to the equation

$$\frac{\lambda}{D} = \frac{k''}{U}\sqrt{\frac{\sigma}{\rho a}} \qquad [14]$$

Substitution of Equation [14] into Equation [13] then leads directly to the empirical Equation [5]. It is noted that consideration of an aerodynamic damping term in Equation [12] would merely tend to reduce the theoretical frequency somewhat.

Cavity Resonance Effects

The apparatus for studying the effects of cavity resonance consisted of a lucite cylinder in which the injector was mounted on a piston-type arrangement which could be moved axially to vary the length of the cylinder cavity, as shown in Figs. 10 and 11. The axial mode of oscillation was induced by a loudspeaker mounted at the end of the cylinder away from the injector. The radial and tangential modes were excited by mounting the loudspeakers with adapters radially and tangentially, respectively, to the walls of the cylinder, close to the injector end.

Fig. 12 shows the droplet configurations which resulted from a cavity resonance in each of the three modes of oscillation. Inspection of this figure reveals immediately that there is little

Fig. 10 Apparatus for continuously varying the axial resonant frequency of a chamber

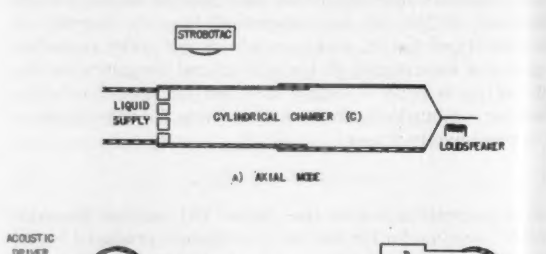

Fig. 11 Schematic diagram of apparatus for studying the effect of cylindrical modes of pressure oscillation on liquid jets

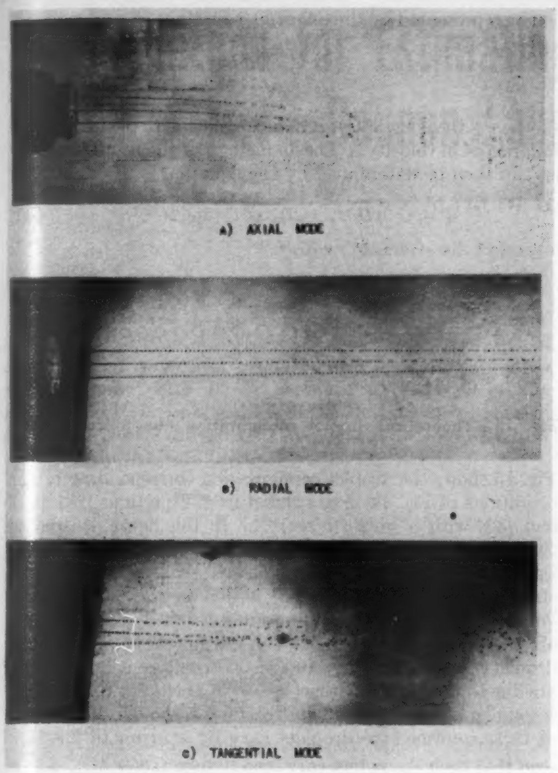

Fig. 12 Deflection of jets due to axial, radial, and tangential modes of oscillation

or no effect brought about by either of the transverse modes at the sound intensities available in the acoustic range, probably due to the previously observed fact that dispersion decreases with frequency (cf. Equation [3]). Excitation of the longitudinal mode, however, had a decided coalescent effect on the droplets, which is due to the sinusoidal velocity variation of successive fluid particles. In each case, the length of the solid stream was decreased by the sound field.

Since, for the imposed first axial mode of oscillation, the amplitude of pressure oscillation is very large compared to its gradient in the vicinity of the closed (injector) end of the chamber, it appears that the observed coalescence is due rather to the oscillating pressure drop across the injector than to the pressure drag considered in Equation [1]. Under this assumption, the coalescence can be predicted theoretically by considering the idealized configuration shown in Fig. 13. From this figure, it is seen that the pressure of the fluid at rest in the supply tank is denoted by P_s and its density by ρ. The length of the supply line is L, the steady-state chamber pressure is P_0, and the distance from the injector to the combustion front is Z.

Consider the equation of motion, in which the viscous forces have been neglected, as applied to the fluid in the supply line

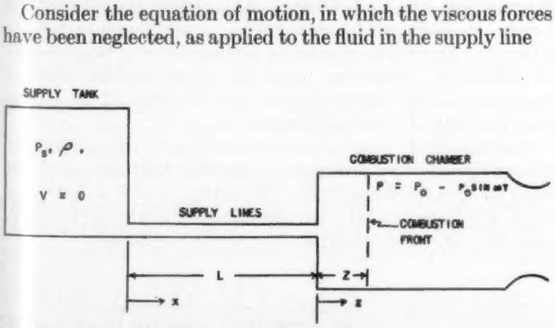

Fig. 13 Schematic diagram of idealized propellant feed system

$$\frac{dV}{dt} + V\frac{dV}{dx} = -\frac{1}{\rho}\frac{dP}{dx} \qquad [15]$$

where V is the velocity of the liquid particle, P is the pressure of the surrounding medium, t is time, and x is the axial distance from the tank. Now let

$$V(x, t) = f(x)U + g(x)v(t), \ (v \ll U) \qquad [16]$$

and

$$P(x, t) = q(x)P_0 - h(x)p_0 \sin \omega t, \ (p_0 \ll P_0) \qquad [17]$$

where

$$f(0) = g(0) = h(0) = 0$$

$$q(0) = P_s/P_0$$

$$f(L) = g(L) = h(L) = q(L) = 1$$

U and P_0 are the steady-state values of the jet velocity and chamber pressure, respectively, and p_0 is the amplitude of the chamber pressure oscillations.

Consideration of the continuity condition reveals that $f = g$, so that substitution of Equations [16] and [17] into Equation [15], with subsequent integration with respect to x, yields the following steady-state and perturbation solutions, respectively

$$U = \sqrt{\frac{2(P_s - P_0)}{\rho}} = \sqrt{\frac{2\Delta P}{\rho}} \qquad [18]$$

and

$$v(L) = v_0 = \frac{p_0 \sin(\omega t - \phi)}{\rho\sqrt{G^2\omega^2 + U^2}} \qquad [19]$$

$$= K \sin(\omega t - \phi)$$

where

$$G = \int_0^L f\, dx \qquad [20]$$

and

$$\phi = \arctan(\omega G/U).$$

Since the continuity condition allows for no velocity gradient for an inviscid fluid in a channel of constant cross section, it is apparent that the acceleration of the fluid particles from zero to U must occur entirely inside the supply tank, thus requiring that the origin ($x = 0$) be shifted to the left in Fig. 13, if continuity of inviscid flow is to be preserved. For hyperbolic streamlines in the tank (which converge to the tank outlet), $G = L + b/3$, where b is the distance from the new origin to the tank outlet. For $b << L$, ϕ is then approximately equal to the product of the frequency and the time required for the fluid to traverse the distance L at the steady-state velocity U.

Having determined the variation of injection velocity due to the oscillating chamber pressure, it is now possible to determine the position z of each element of liquid (e.g., a droplet) at time t

$$z = (t - t_i)\cdot V(L) = (t - t_i)\,[U + K \sin(\omega t_i - \phi)] \qquad [21]$$
$$= T_i[U + K \sin(\omega t - \phi - \omega T_i)]$$

where t_i is the time at which the droplet under consideration was injected from the orifice at a velocity $V(t_i)$, and T_i is the interval of time during which the droplet has traveled.

If it is now assumed that the slowest moving droplets ($V = U - K$) will retain their original velocity, and that the more rapidly moving droplets which follow will coalesce with the slow droplets and continue at the minimum velocity, then the situation at any instant will be quite similar to that shown in Fig. 12(a) with evenly spaced large droplets, each followed by a number of smaller droplets. As one proceeds farther from the injector, the number of intermediate small droplets will decrease and the size of the larger droplets will increase, because more of the faster-moving smaller droplets will have coalesced with the larger droplets.

The quantity of liquid coalesced in any of the larger droplets can be determined as follows: The appropriate value of the

time of injection t_i can be obtained by minimizing the sine function in Equation [21]

$$t_i^* = \frac{1}{\omega}\left(\frac{3\pi}{2} + \phi\right) \ldots\ldots\ldots\ldots\ldots [22]$$

where ϕ is determined from Equations [20] and [18] by using the appropriate values for ΔP, ρ, ω, and G. Having established the position z^* of one of the larger droplets (photographically), the corresponding value of the time of travel T_i^* can be determined from Equations [21] and [22].

$$T_i^* = \frac{z^*}{U - K} \ldots\ldots\ldots\ldots\ldots [23]$$

The minimum time of travel T_i^{**} for a segment of liquid which is included in the large droplet can then be determined as the smallest (of three) values of T_i which satisfies the equation

$$z^* = T_i[U + K \sin(\omega t^* - \phi - \omega T_i)] = T_i V(T_i) \ldots [24]$$

where

$$t^* = T_i^* + t_i^* \ldots\ldots\ldots\ldots\ldots [25]$$

Since it is impossible to solve the transcendental Equation [24] by analytical means, a graphical method appears to be appropriate. By plotting the curves for $V(T_i)$ and z^*/T_i vs. T_i, it is very simple to determine the value of T_i^{**} as the lowest value of T_i at which the two curves intersect. Then all of the liquid which has traveled from T_i^{**} to T_i^* sec can be assumed to have coalesced in the larger droplet at the point z^*. Fig. 14 shows a typical graphical solution, with $\omega = 2000$ rad/sec, $U = 100$, $K = 50$, $\phi = 0.75$, and $z^* = 0.1, 0.25$. The cross-hatched portions represent the larger coalescent droplets.

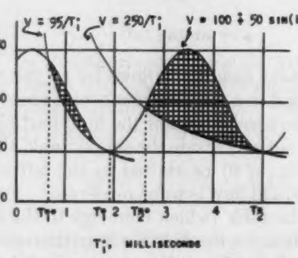

Fig. 14 Graphical solution of Equation [24]

Determination of the actual volume of liquid in this droplet requires an assumption regarding the variable thickness of the stream from which the droplets are formed. By assuming that the mass flow, which begins far back in the supply lines (where the effect of chamber pressure oscillations is negligible), is constant, the appropriate equation becomes

$$\pi\rho V D^2/4 = \text{const} = \dot{M}_0 \ldots\ldots\ldots\ldots\ldots [26]$$

where D is the variable diameter of the stream. The total mass M of liquid in the larger droplet can then be determined from the equation

$$M = \int_{T_i^{**}}^{T_i^*} (\pi\rho V D^2/4)dT = \dot{M}_0(T_i^* - T_i^{**}) \ldots [27]$$

and the diameter d^* of the corresponding spherical droplet can be determined from the equation

$$d^* = \sqrt[3]{6M/\pi\rho} \approx D_0^{2/3}\sqrt[3]{3U(T_i^* - T_i^{**})/2} \ldots [28]$$

where D_0 is the exit diameter of the orifice.

The size of the smaller droplets can be determined from the diameter of the stream D and the wavelength of the disturbance λ. Experimental evidence (3) indicates that the variation of wavelength with stream diameter and stream velocity can be represented by the following equation

$$\frac{\lambda}{D_0} = \frac{\alpha}{\sqrt{V}} \ldots\ldots\ldots\ldots\ldots [29]$$

where α is the constant of proportionality with the units of the square root of velocity. The diameter d of the resultant droplet can then be determined by the equation

$$d = \sqrt[3]{3\lambda D_0^2/2} \approx D_0\sqrt{U}(3\alpha/2U^2)^{1/3} \ldots [30]$$

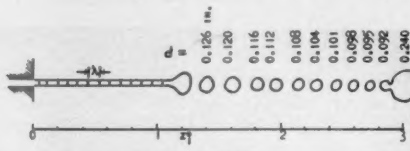

Fig. 15 Theoretical droplet configuration due to coalescence

Fig. 15 shows the droplet configuration corresponding to the conditions of Fig. 14 as calculated from Equations [28], [29], and [30] with $\alpha = 20(\text{ft/sec})^{1/2}$. In this figure, it is noted that the jet was assumed to remain solid until after the formation of the first large droplet. The relatively thin stream upstream of the first coalescence is due to the fact that the velocities to the left of the first cross-hatched area in Fig. 14 are close to the maximum $(U + K)$, while the relatively large droplets between the first and second coalescent fluid masses are due to the low velocities ($\approx U - K$) between the first and second cross-hatched areas in Fig. 14. Although the volumes of these intermediate droplets vary by a factor of 2.5, it is seen that their diameters vary merely by a factor of $\sqrt[3]{2.5} = 1.35$. The similarity between this calculated figure and the photograph of Fig. 12(a) is also noted.

Combustion Stability

Since it has been established by Godsave (4) and others (5, 6) that the mass rate of burning varies directly as the diameter of the droplet, it is apparent from Equation [30] that the rate at which combustible gases are liberated at a combustion front, which is assumed to occur at a constant distance Z from the injector, will vary periodically with a frequency of $\omega/2\pi$. By postulating that an increase in the rate of gas evolution brings about a simultaneous increase both in burning rate and in chamber pressure, it can be deduced that a slight pressure impulse will occur whenever one of the coalescent droplets reaches the combustion front. Instability will occur whenever the times at which these pressure pulses occur coincide with the maxima of the oscillating chamber pressure, i.e., when the burning rate and chamber pressure are in phase.

It is noted that this instability mechanism presupposes the existence of an oscillating chamber pressure, which may well be due either to the cavity type oscillation observed by Berman and Cheney (7) or to the system oscillations analyzed by Summerfield (8) and Crocco (9). Hence the mechanism herein proposed can be regarded as an additional factor, by which the amplitude of existing oscillations will be increased or decreased, depending upon the phase relation between chamber pressure oscillations and the incidence of the coalescent droplets at the flame front.

This instability condition can be expressed by requiring that the jet velocity be a minimum at the time that the coalescent drop reaches the flame front. By setting $z = Z$, $t = t^*$, and $T_i = 0$ in Equation [21], consideration of Equations [21], [23], and [25] yields the following condition for instability

$$U - K = \frac{\omega Z}{2n\pi}, \quad n = 1, 2, 3, \ldots\ldots\ldots\ldots [31]$$

(*Continued on page 534*)

A Method for Estimating Altitude Performance of Balloon Launched Rockets

MALCOLM S. JONES, JR.[1]

Project Matterhorn, Forrestal Research Center, Princeton, N. J.

An approximate method has been developed for estimating the altitude performance of balloon launched rockets which were first proposed and used by Van Allen and Gottlieb. This paper presents an analysis of the preliminary data on 17 rounds of Deacon rockets fired from balloon altitudes during 1952 and 1953, and a comparison with the approximate theory.

Nomenclature

t = time
x = distance, vertical coordinate upward
$\dot{x}$ = velocity
$\ddot{x}$ = acceleration
m = mass of rocket at time specified by subscript

	SUI Rounds	NRL Rounds
m_o =	194#	218#
m_{bo} =	94#	118#

C_D = coefficient of drag
M = Mach no. = velocity divided by local velocity of sound
$\bar{a}$ = local velocity of sound in atmosphere, assumed = 1000 ft sec^{-1}
D = drag
A = cross-sectional area of missile = 0.23 ft^2 for Deacon rocket
ρ = density of the atmosphere = $\rho_0 \exp(-\alpha x)$
ρ_0 = sea level reference density of atmosphere = 0.170 lb ft^{-3}
α = const. = 1/17,400 ft^{-1}
g = acceleration of gravity, assumed constant = 32.2 ft sec^{-2}
T_b = total burning time, sec. $\cong$ 3 sec for Deacon rocket
K = drag factor (see Eq. 2) = $^1/_2 A\rho_0\bar{a}k$
k = drag coefficient normalization factor, Eq. [1]
V_E = effective exhaust velocity of rocket motor $\cong$ 5500′/sec for Deacon rocket
b = $-\dot{m}$ = rate of mass flow through motor nozzle, assumed const., $\cong$ 1.0 for Deacon rocket
Γ = ratio of initial mass to burnout mass = 2.065 SUI rounds
 = ratio of initial mass to burnout mass = 1.848 NRL rounds
γ = specific heat ratio of exhaust gases (see Ref. 5) assumed = 1.20
Ae/A_t = exhaust area ratio (see Ref. 5) assumed = 7.0
p_1/p_3 = pressure ratio (see Ref. 5), assumed $\cong$ 60 @ sea level
C_F = normalized thrust coefficient
L = launching parameter = $Ke^{-\alpha x_0}/b$
J = burnout parameter = $Ke^{-\alpha x_{b_0}}/m_{b_0}$
X = max. vertical distance above burnout altitude

Subscripts

t = at time t
0 = at launching time or altitude
b_0 = at burnout
max = at maximum altitude
b = distance traveled or time elapsed while burning

Introduction

THE balloon launched rocket, proposed and first used by Van Allen and Gottlieb (1)[2] represents a relatively low cost vehicle for the performance of certain types of high altitude experiments. Because of the large number of experiments which can be performed with this vehicle within a short period of time (as many as five flights per day, or 20 flights in a two-week season), it seemed desirable to have some sort of a first order theory which would take into account the many launching and rocket parameters and allow an estimate to be made of the performance of the vehicle based on the limited information available without a complete analysis of the data collected. With the rocket motors used thus far, the Deacon rocket, whose characteristics are outlined in (1), the experimental apparatus has been simple and lightweight, hence limited in the intelligence that could be transmitted. For this reason, such factors as launching altitudes, peak altitudes, etc., are only known or estimated to an accuracy of several thousand feet. In addition, there is a normal dispersion in the internal ballistic performance of rocket motors. Therefore, a more elegant theoretical approach does not seem warranted for the stated purpose. For more accurate work, such as evaluation of experimental data, it may be necessary to resort to step-by-step calculations.

Summary of Theory

In addition to the usual assumptions—such as (a) constant gravitational attraction, (b) that the rocket is fired in a vertical direction, (c) logarithmic density of the atmosphere, (d) that the properties of the atmosphere such as temperature, molecular weight, etc., can be suitably averaged in regions where drag forces are important(2)—it was assumed (e) that the drag forces on the rocket were proportional to the Reynolds number. Assumption (e) can be adapted to conventional notation by expressing a relation for the coefficient of drag as

$$C_D \equiv \frac{k}{M} \qquad [1]$$

where k is a constant, suitably chosen to provide some measure of agreement with drag forces, or drag coefficients, determined by the equation: drag = $^1/_2\, \rho A C_D(\dot{x})^2$, in the region of interest, usually near the end of the burning period where the drag forces are the largest. With the above assumptions the drag on the rocket can then be expressed as

$$\text{drag} = {}^1/_2\, A\rho_0\, \bar{a}k(\dot{x})e^{-\alpha(x_0 + x)} \qquad [2]$$

$$= Ke^{-\alpha x_0}(\dot{x})e^{-\alpha x} \qquad [2a]$$

where $K = {}^1/_2 A\rho_0\bar{a}k$.

By equating the forces acting on the rocket during burning, with the additional assumption of constant burning rate of propellant, it is found that

$$m_t\ddot{x} = \text{thrust} - \text{gravity} - \text{drag}$$

$$= bV_E - m_t\, g - K\dot{x}e^{-\alpha(x_0 + x)} \qquad [3]$$

Assuming that $K \exp\{-\alpha(x_0 + x)\}$ can be regarded as constant during the burning period, a rapid burning motor such as the Deacon rocket will travel only some 6000 ft while burning. Equation [3] can be integrated to obtain a relation for the burnout velocity which for most practical cases can be expressed with sufficient accuracy as

Received September 11, 1954.

[1] Research Associate; formerly Lieutenant (CEC) U. S. Navy, Office of Naval Research, Washington, D. C.

[2] Numbers in parentheses indicate References at end of paper.

$$\dot{x}_{b0} \cong \frac{V_E b \exp(\alpha x_0)}{K}\left[1 - \left(\frac{m_0}{m_{b0}}\right)^{-\frac{K}{b\exp(\alpha x_0)}}\right] + \dot{x}_0\left(\frac{m_0}{m_{b0}}\right)^{-\frac{K}{b\exp(\alpha x_0)}} - gT_b \ldots [3a]$$

This relation has been checked against step-by-step calculations and agrees to within about 2 per cent if (K/b) exp $(-\alpha x_0)$ is less than about 0.2. Calculations using Equation [3a] can be simplified if we call the factor (K/b) exp $(-\alpha x_0)$ the launching parameter L, and define a velocity function $\phi = [1 - \beta^{-L}]$, where $\beta = m_0/m_{b0}$ is the mass ratio; then, if $\dot{x}_0 = 0$, Equation [3a] can be expressed as

$$\dot{x}_{b0} = V_E\phi(\beta, L) - gT_b \ldots\ldots\ldots\ldots\ldots [3b]$$

Fig. 1 is a plot of the velocity function ϕ for a range of values of β and L. Also shown on Fig. 1 as dashed lines are the values of β for use with the Deacon rocket configuration used in later work. The dashed line labeled SUI is for the rounds

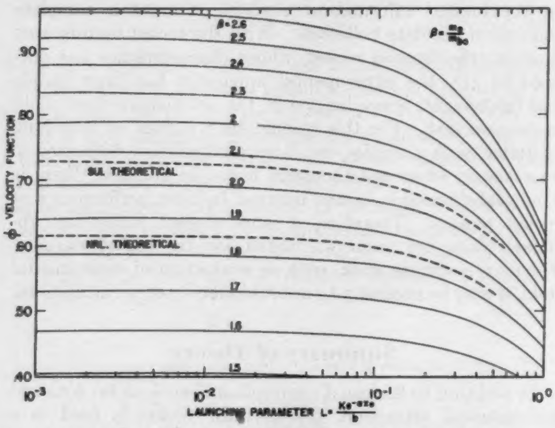

Fig. 1 Variation of velocity function, ϕ, with launching parameter L for various mass ratios

fired by the State University of Iowa, while the dashed line labeled NRL is for the rounds fired by the Naval Research Laboratory.

After burnout, with the above assumptions regarding drag, the maximum vertical distance above burnout altitude can be expressed by the relation

$$X = \frac{1}{2}(K_1)^2 g + \frac{1}{\alpha}\log_e\left[1 + \frac{Ke^{-\alpha x_{b0}}}{m_{b0}B}\left(e^{-(BK_1)^2}\int_0^{BK_1} e^{(BK_1)^2}\, d(BK_1)\right)\right] \ldots [4]$$

where

$$K_1 = \frac{\dot{x}_{b0} - (Ke^{-\alpha x_{b0}}/\alpha m_{b0})}{g}$$

$$B = \left[\frac{\alpha g}{2}\right]^{1/2} \qquad X = x_{max} - x_{b0}$$

The integral on the right side of Equation [4] can be evaluated by reference to tabulated values of the $\int_0^x \exp(x^2)\, dx$ (see Ref. 4).

Thus it is possible to express the maximum altitude performance after burnout in terms of the burnout velocity $\dot{x}_{b0}$, and the burnout parameter $K \exp(-\alpha x_{b0})/m_{b0}$, which we will call J. The variation of X with J for various constant values of $\dot{x}_{b0}$ can then be plotted in graphical form, as is done in Fig. 2. With this chart or nomograph it is possible to find X, if $\dot{x}_{b0}$ and J are known, or $\dot{x}_{b0}$ if X and J are known, etc. This chart also forms a basis for the comparison of the performance of several rounds fired under different conditions,

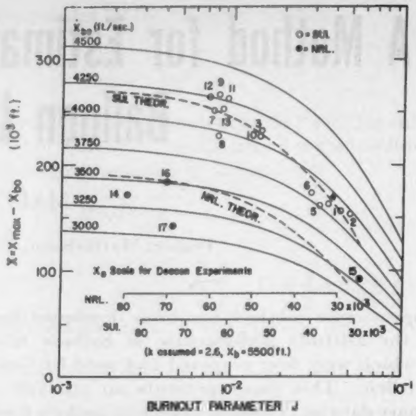

Fig. 2 Variation of maximum vertical distance above burnout altitude with burnout parameter J for various burnout velocities. Experimental points for Deacon rockets fired at balloon altitudes in 1952 and 1953 shown with appropriate reference scales for altitudes at which rounds were launched. Dashed curves show theoretical variation of performance of the different weight rounds

since it allows a determination of $\dot{x}_{b0}$ which can be compared with that predicted by Equation [3].

Experimental Data

Preliminary data (1,7–10) on seventeen Deacon rockets fired from balloon altitudes during 1952 and 1953 are presented in Table 1. Column 1 gives the launching altitude, column 2 the reported or estimated maximum altitude, column 3 the total flight time, and column 4 the value of X as used in Equation [4] (i.e., $x_{max} - x_{b0}$), allowing 5500 ft for x_b. Column 5 gives the type of experiment performed, the reference in which the work was reported, and in parentheses the round

Table 1 Performance of Balloon Launched Deacon Rockets 1952–1953

Col.	1	2	3	4	5
	x_0, ft	x_{max}, ft	Total time of flight, sec	X, ft	Type of flight & reference
1	38,000	200,000	252	156,500	B, 7b(3)
2	36,000	195,000	220	154,500	A, 1(4)
3	57,000	295,000	280	232,500	A, 1(5)
4	41,000	210,000	235	163,500	A, 7(6)
5	43,000	210,000	223	161,500	A, 7(7)
6	45,000	225,000	235	174,500	B, 8(15)
7	68,000	325,000	286	251,500	B, 8(17)
8	67,000	300,000	268	227,500	B, 8(21)
9	67,000	340,000	280	267,500	B, 8(22)
10	57,000	290,000	270	227,500	A, 9(13)
11	65,000	Est. 334,500	277	264,000	A, 10(11)
12	70,000	340,000	285	264,500	A, 9(20)
13	66,000	325,000	255	253,500	A, 9(23)
14	83,000	260,000	242.5	171,500	C, 10(9)
15	29,300	125,000	176	90,200	C, 10(14)
16	75,000	265,000	250	184,500	C, 10(15)
17	73,500	220,000	202	141,000	C, 10(22)

A = SUI single counter flight; B = SUI ion chamber flight; C = NRL meteorological flight.

or flight number used to indicate the flight in that reference. The cosmic ray altimeter method (6) of Gangnes, Jenkins, and Van Allen, was used to estimate the maximum altitude of flights where this information was not available. On the flight reported as round No. 11, the Geiger counter failed soon after firing, near burnout. The maximum altitude of this flight was calculated from the total flight time.

The data from Table 1 are plotted on Fig. 2, using the

numerical values for constants and derived quantities listed in the Nomenclature, together with the assumption that $k = 2.6$, to determine the burnout parameter J. Also shown on Fig. 2 by the dashed lines are the expected burnout velocities determined by Equation [3] for the two different weight rounds, i.e., SUI and NRL, launched under such conditions that they would have that particular J at burnout. For this calculation, the increase in thrust with altitude, using the charts contained in (5) with the values $\gamma = 1.20$ and $A_e/A_t = 7.0$, was included. The sea level effective exhaust velocity, V_E, was derived from the thrust-time characteristics of the Deacon rocket reported by Van Allen and Gottlieb in (1). For easy reference, scales showing x_0 for each of the two types of rounds are given at the bottom of Fig. 2. It should be noted that the positioning of the x_0 scales and the dashed lines for $\dot{x}_{b0}$ is dependent upon the weight, thrust, and drag parameters; therefore those shown are applicable only to rounds of the weight and configuration, using the same motors as are considered herein. For different vehicles, etc., the curves and scales can still be easily plotted on the form of Fig. 2.

Choice of Drag Coefficient k

Fig. 3 shows unpublished data (3) derived by Ray and Van Allen from tracking data for the coefficient of drag, C_D, of a tower-launched Deacon rocket of substantially the same configuration as used in the later work covered in Table 1. Superimposed on this figure are lines representing the assumption expressed in Equation [1], i.e., $C_D \equiv k/M$, for various values of k. It may be noted that in the velocity region $1.7 \leq M \leq 3.0$ a fairly good fit of the data can be obtained by this relation. However, it can be seen from Fig. 2 that the rounds fired at high altitudes achieved velocities

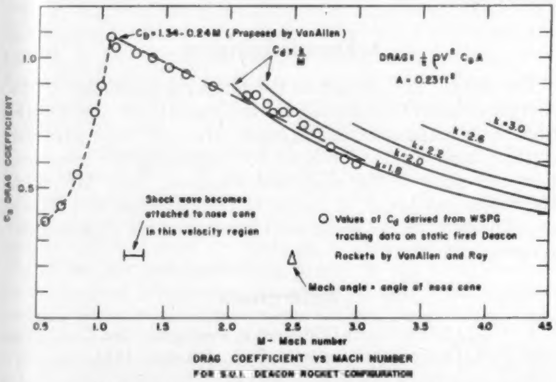

Fig. 3 Variation of drag coefficient C_D, with Mach number of tower-launched Deacon rocket. Derived by Ray and Van Allen from White Sands Proving Ground tracking data

somewhat greater than those covered by Fig. 3. It should also be noted that for the tower-launched round, maximum velocity was achieved at about 8000-ft altitude (Reynolds number approximately 4.9×10^6 at burnout), whereas for more than 50 per cent of the rounds considered in Table 1, burnout was higher than 70,000 ft (Reynolds number = 4.23×10^5). Therefore in addition to the higher velocities, there is a large difference in Reynolds numbers between the data of Ray and Van Allen and those considered herein.

For this reason, and to check the validity of the calculations, an analysis was carried out to determine an appropriate value of k. Values of the burnout parameter J for each round in Table 1 were computed using the values $k = 1.8$, 2.2, 2.6, and 3.0. These values of J were plotted on the J-X curves, as per Fig. 2. Values of $\dot{x}_{b0}$ were then determined for each case. The values of J were then converted to values of L, the launching parameter, and from Fig. 1 the corresponding values of ϕ, the velocity factor, were determined. The burnout velocities plus an allowance for gravity were then

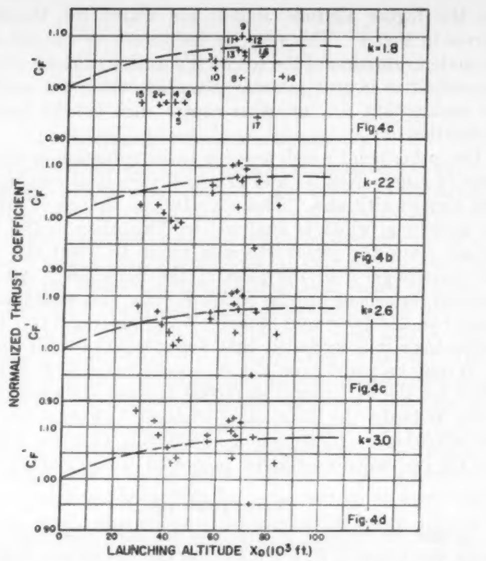

Fig. 4 Comparison of normalized thrust coefficient, C_F', for experimental points, shown numbered in top figure, with theoretical value, shown as dashed line, as a function of launching altitude, x_0, for various values of the drag normalization factor, k. Value $k = 2.6$ chosen as most appropriate

divided by ϕ, to give a value for the effective exhaust velocity V_E, which was then divided by sea level effective exhaust velocity to obtain what is called the normalized thrust coefficient, C_F'. The normalized thrust coefficient can be calculated, using the method in (5), from the known characteristics of the rocket motor and propellant, as a function of altitude. Therefore, since C_F' is practically independent of the velocity, but a function of pressure ratio, it should be an independent measure by which to compare the calculations and experimental data. Fig. 4 presents the calculated values of C_F' for the experimental data on the assumption that $k = 1.8$, 2.0, 2.4, and 2.6. The dashed line in each figure is the theoretical variation of C_F' with altitude.

Comparison with Experimental Data

The effect of changes in k, as shown in Fig. 4, is most marked in the lower altitude region, i.e., 30,000 to 50,000 ft, as would be expected. For this region, the value of $k = 2.6$ is considered the most appropriate choice. While this value is somewhat higher than that which would be predicted by the extrapolation of Van Allen and Ray's data on C_D, it must be remembered that for the experimental data presented on high altitude launchings, the flow pattern is probably in the transition region between turbulent and laminar flow, as compared with the strictly turbulent flow of the static fired round. Unfortunately, wind tunnel data are not available to determine this point. In addition, because of lower aerodynamic restoring forces, more yaw angle is expected for the higher altitude launchings which would lead to larger projected cross-sectional areas, vortex shedding, etc. For these reasons, and because of the uncertainties involved in the basic data and assumptions, including the interior ballistics of the rocket motor, a strict comparison with the values of C_D determined for the static fired round should not be made until either the analysis has included many more rounds, or detailed tracking data from a round launched at moderately high altitudes are available. Such a comparison should then allow an assessment of the amount of error introduced by assumption (e) which made possible the linearization of the equations of motion, and this simplified analysis.

It may also be noted that most of the experimental points

for the higher altitude rounds are above the theoretical curves in Fig. 4. This may be due to any of the following: an underevaluation of the sea level effective exhaust velocity, the reduction in gravitational attraction which was neglected by assumption (b), or other causes such as the improper evaluation of C_F'.

One other point worth noticing is the reduction in performance of rounds Nos. 14 and 17 which were launched at about the highest altitudes. This may be due to lack of stability at launching, which is analyzed by Van Allen in (1), which would allow the jet overturning forces to point the rocket at some angle θ to the path of the launching. Assuming normal performance of the rocket motors, this would indicate that $\theta = 21°$ for round 14 and $\theta = 30°$ for round 17. On the same basis it is indicated that θ may equal 16° for round 8.

It may be noted from Fig. 3, using a value of $J = 1.31 \times 10^{-2}$ for the SUI round at 60,000 ft, that the experimental data indicate the maximum altitudes achieved are some 50,000 ft higher, for launching at 60,000 ft, than was predicted by the preliminary estimates presented in Fig. 1 of (1).

Conclusions

It can be concluded that the method presented herein, with the value of $k = 2.6$ for the Deacon rocket motor and configuration used, gives an agreement of maximum altitude performance within ±10 per cent over the range of launching altitudes from 35,000 to about 75,000 ft. Thus it is felt that this method will be useful for:

(a) The intercomparison of performance of rounds of the same external configuration and internal ballistic characteristics over a wide range of launching parameters.

(b) Making preliminary performance estimates of rounds using motors other than the Deacon for high altitude launchings from either balloons or other multistage vehicles such as aircraft or multistage rockets.

Acknowledgment

The author is greatly indebted to J. A. Van Allen on two accounts. The first, for proposing the expeditions to the northern latitudes where the author acted as Project Officer; and secondly, for the personal encouragement and critical review of the manuscript in its formative stages.

References

1 "The Inexpensive Attainment of High Altitudes with Balloon Launched Rockets," by J. A. Van Allen and M. B. Gottlieb, published in the book, "Rocket Exploration of the Upper Atmosphere"; Pergamon Press, London, 1954, and Interscience Publishers, New York, 1954, pp. 53–64.

2 "Pressures, Densities, and Temperatures in the Upper Atmosphere," The Rocket Panel, *The Physical Review*, vol. 88, December 1, 1952, pp. 1027–1032.

3 Private communication, J. A. Van Allen, April 1954.

4 "Tables of the function $\int_0^h e^{x^2}dx$," Dawson, *Proceedings of the London Mathematical Society*, vol. 29, 1898, p. 521. This table was extended by F. J. Malina in the *Journal of the Franklin Institute*, vol. 230, 1940, pp. 433–454.

5 "Rocket Propulsion Elements," by G. P. Sutton, John Wiley and Sons, New York, 1949, pp. 58 and 59.

6 "The Cosmic Ray Intensity Above the Atmosphere," by A. V. Gangnes, J. F. Jenkins, and J. A. Van Allen, *The Physical Review*, vol. 75, 1949, pp. 57–69.

7 "The Cosmic Ray Intensity Above the Atmosphere Near the Geomagnetic Pole," by J. A. Van Allen, *Il Nuovo Cimento*, vol. 10, 1953, pp. 630–647.

8 "Low-Momentum End of the Spectra of Heavy Primary Cosmic Rays," by R. A. Ellis, Jr., M. B. Gottlieb, and J. A. Van Allen, *The Physical Review*, vol. 95, July 1, 1954, pp. 147–159.

9 "Direct Detection of Soft Radiation above 50 Kilometers in the Auroral Zone," by L. H. Meredith, M. B. Gottlieb, and J. A. Van Allen, submitted to *The Physical Review* for publication in August 1954.

10 "Summary of Project Mushrat," by M. S. Jones, Jr., H. E. LaGow, and M. B. Gottlieb, report submitted to Office of Naval Research, September 1953. (Private Communication.)

Disintegration and Dispersion of a Liquid Jet

(*Continued from page 530*)

which leads to the stability criterion

$$U\left(1 - \frac{p_0}{2\Delta P\sqrt{G^2\omega^2/U^2 + 1}}\right) > \frac{\omega Z}{2\pi} \quad [32]$$

By assuming that $G << U$, Equation [32] can be written

$$U\left(1 - \frac{p_0}{2\Delta P}\right) > \frac{\omega Z}{2\pi} \quad [33]$$

which shows that instability, as evidenced by complete flow reversal in the supply lines, is inevitable if the amplitude of chamber pressure oscillations exceeds twice the steady-state pressure drop across the orifice.

Conclusions

As a result of this investigation, the following conclusions can be drawn:

1. Ambient pressure oscillations, either normal to or parallel to the axis of a liquid jet, tend to decrease the length of the solid stream and have a decided effect on the dispersion pattern of the jet.
2. It can be shown both experimentally and theoretically that the magnitude of this effect decreases as either the pressure drop across the orifice or the frequency of the pressure oscillation is increased.
3. The mixing of parallel streams is aided greatly by transverse pressure waves.
4. The coalescence of droplets, which results from axial pressure oscillations in a chamber, can lead to unstable combustion if the steady-state flow velocity is less than a certain critical value.

Acknowledgments

The author is indebted to the following personnel of the Aerojet-General Corporation for their assistance and suggestions in the preparation of this paper: Mr. C. C. Ross, manager of the Liquid Engine Division, for suggesting the investigation and some of the analytical solutions; and Mr. B. J. Gastineau and Mr. J. A. Orme, of the Electronics and Guidance Division, for designing and carrying out the experimental program.

References

1 "AGARD Selected Combustion Problems," by C. C. Ross and P. P. Datner, Butterworths Ltd., London, 1954, pp. 352–376.

2 "Theory of Sound," vol. II, by Rayleigh, Dover Publications, New York, 1945, p. 362 ff.

3 "Correlation of Experimental Data on the Disintegration of Liquid Jets," by C. C. Miesse, American Rocket Society Paper no. 88-53, July 3, 1953.

4 "The Burning of Single Drops of Fuel," part II, "Experimental Results," by G. A. E. Godsave, London, Ministry of Supply, National Gas Turbine Establishment Report no. R.87, April 1951.

5 "Experiments in the Burning and Extinction of Liquid Fuel Spheres," by D. B. Spalding, *Fuel*, vol. 32, 1953, pp. 169–185.

6 "The Generation and Burning of Uniform-Size Liquid Fuel Drops," by J. A. Bolt, T. A. Doyle, and W. Mirsky, University of Michigan, Engineering Research Institute, May 1953 (for U. S. Air Force, Air Research and Development Command).

7 "Combustion Studies in Rocket Motors," by K. Berman and S. H. Cheney, Jr., *Journal of the American Rocket Society*, vol. 23, 1953, p. 89.

8 "A Theory of Unstable Combustion in Liquid Propellant Rocket Systems," by M. Summerfield, *Journal of the American Rocket Society*, vol. 21, 1951, p. 108.

9 "Aspects of Combustion Stability in Liquid Propellant Rockets," by L. Crocco, *Journal of the American Rocket Society*, vol. 21, 1951, p. 163.

Technical Notes

Studies of the Mechanism of Flame Stabilization by a Spectral Intensity Method[1]

RICHARD R. JOHN,[2] EDWARD S. WILSON,[3] and MARTIN SUMMERFIELD[4]

**The James Forrestal Research Center
Princeton University, Princeton, N. J.**

In research on ramjet-type combustion chambers, it is important to be able to determine the local intensity of combustion and the local fuel-air ratio at various points in the flame zone. The standard method is chemical sampling, but it is usually tedious and difficult. This paper reports a new method for two-dimensional hydrocarbon-air flames based on measurements of radiation intensity from the emitters CH and C_2. The method is applied to the problem of the mechanism of flame holding, particularly to the question of the observed shift of the blow-off curves at Reynolds numbers below 10^4, with the result that a certain aspect of the effect of selective molecular diffusion is clarified.

Introduction

The practical performance characteristics of bluff body flame stabilizers are generally presented as plots of blow-off velocity as a function of the inlet fuel/air ratio, inlet flow conditions, and the flame holder and combustion chamber geometries (1, 2, 3).[5] From the scientific standpoint, however, the flame stabilization mechanism must be treated in terms of the aerodynamic, thermal, and chemical structure of the region in the vicinity of the bluff body. Specifically, an investigation of this region would include such factors as the shape of the recirculation pattern (4), the importance and type of the local transport mechanisms (laminar or turbulent) (5), the distribution of chemical reaction downstream of the stabilizer (6, 7), and the effect of local boundary layer characteristics (8, 9). The techniques described in the preceding references for examining these effects include schlieren and shadowgraph pictures, particle and sodium vapor tracers, gas sampling, and boundary layer removal.

It had been noted previously, in observations of the flameholder region through transparent side walls, that under some flow conditions, e.g., low Reynolds numbers, the region immediately downstream of the stabilizer has a color different from that in the main flame (5, 10). As a part of the current research in this laboratory pertaining to the radiation from laminar and turbulent flames of premixed gases (11), a series of experiments was carried out to determine whether this difference in visible radiation could be used in a quantitative fashion as another tool to obtain additional information on the structure of the flame holding region.

Visible Flame Radiation

The visible radiation in premixed hydrocarbon-air flames and in hydrocarbon-oxygen flames is due for the most part to the emitters CH, C_2, and CO_2*. Of these three sources, CH and C_2 are the strongest and occur mainly in the primary burning zone, whereas CO_2* occurs both in the primary burning zone and in the after-burning zone (interconal region of a bunsen flame) (12). The strongest radiation emitted by the CH radical is concentrated in a group of bands near 4300 A, and the strongest radiation from C_2 occurs near 5100 A. The characteristic blue-violet color of fuel-lean flames and the blue-green of fuel-rich flames are determined by the relative emission strengths of the CH and C_2 radicals.

Paradoxically, despite the prominence of their radiations, the radicals CH and C_2 are present in very small concentrations, e.g., much less than 0.001 mole fraction for an acetylene oxygen flame at 1 atm pressure (13), and do not seem to play an important role in the combustion mechanism (14). However, since their concentrations and the resultant luminosity reach a peak very near to the point of maximum reaction rate in a laminar flame, it is plausible that the spatial distribution of luminosity of CH or C_2 will give a quantitative indication of the spatial distribution of reaction intensity in a complex combustion region. This hypothesis is now being tested.

Another result which could not have been anticipated on theoretical grounds is that the intensity ratio of CH radiation to C_2 radiation (denoted hereafter simply as CH/C_2) in a laminar flame is a unique function of fuel/air ratio. This conclusion was suggested by Gaydon and Wolfhard in their work on the comparison of turbulent and laminar flame spectra (15) and by the work of Clark and Bittker on turbulent flames (16). It has been verified in this Laboratory for premixed propane-air flames. Having established this result, the curve of CH/C_2 vs. fuel/air ratio for a laminar flame can be used (within limits) as a calibration curve to determine the local fuel/air ratio in any section of a flame of nonuniform mixture ratio burning at approximately the same temperature and pressure. This method has been used, as indicated in the following sections, to investigate the degree of selective diffusion in the flame stabilizer region. The possibility of using this technique for flame zones that are highly turbulent is still under investigation and will be discussed in a future paper.

Selective Diffusion Near a Flameholder

The process of selective diffusion in the wake of a flame stabilizer has recently been investigated in some detail by Zukoski at CalTech (5) and Williams and Shipman at M.I.T. (17). Briefly, the effect is the following. The stability curves (blow-off velocity vs. fuel/air ratio) of bluff body flame stabilizers operating at high Reynolds numbers (above 10^4) peak at some point near the stoichiometric fuel/air ratio. However, below this critical Reynolds number, the fuel/air ratio corresponding to the maximum blow-off velocity shifts to the rich or lean side of stoichiometric, depending on whether the gaseous fuel is heavier or lighter than oxygen; e.g., for propane, the fuel/air ratio for the maximum blow-off velocity is greater than stoichiometric.

From these observations, it is concluded that the mechanism of flame stabilization at low Reynolds numbers is in some way influenced by the molecular diffusion of fuel and oxygen into the flameholder region. For a heavy fuel, the oxygen molecules will diffuse more rapidly than the fuel molecules, and as a result, the flameholder region may have a stoichiometric mixture ratio when the over-all fuel/air ratio is on the

Received Sept. 1, 1955.

[1] This Note is based on part of the research performed by the two junior authors in fulfillment of the requirements for advanced degrees.

[2] Graduate Student in Aeronautics; Candidate for the Ph.D. degree.

[3] Guggenheim Jet Propulsion Fellow; Candidate for the M.S.E. degree; Major, USAF.

[4] Professor of Jet Propulsion, Department of Aeronautical Engineering. Mem. ARS.

[5] Numbers in parentheses indicate References at end of paper.

EDITOR'S NOTE: This section of JET PROPULSION is open to short manuscripts describing new developments or offering comments on papers previously published. Such manuscripts are published without editorial review, usually within two months of the date of receipt. Requirements as to style are the same as for regular contributions (see first page of this issue).

rich side. Therefore, associating the maximum blow-off velocity with a stoichiometric fuel/air ratio in the flameholder region, the rich shift for the heavy fuels and the lean shift for light fuels are explained.

To verify this reasoning, both the M.I.T. and CalTech groups measured chemically the fuel/air ratio in the middle of the wake of the flameholder near the rear stagnation point (effective fuel/air ratio based on combustion products). Here it was explicitly assumed that the fuel/air ratio in the wake is the same as that in the region of active combustion at the sides of the holder. In the CalTech experiments it was determined that, at Reynolds numbers less than 4×10^3 for fuels heavier than oxygen, the fuel/air ratio indicated by the products of combustion is less in the flameholder wake than in the main stream. At high Reynolds numbers (above 10^4) it was found by the CalTech group that the fuel/air ratio in the free stream and that in the flameholder wake were the same. These results correspond to the observed shift of the peak of the stability curves toward the stoichiometric fuel/air ratio at high Reynolds numbers.[6]

However, in the intermediate Reynolds number region (4×10^3 to 1×10^4), whereas the fuel/air ratio in the flameholder region appears to be approximately the same as that in the main stream, there is still a shift of the stability curve indicating that, in contradiction to the results of chemical sampling, selective diffusion still appears to be present. The difference is attributed to the fact that the sample taken in the wake region contains the products of combustion recirculated from the flame spreading region downstream of the actual flameholding region. Therefore, these chemical sampling experiments failed to give a correct indication of the influence of diffusion in the intermediate range of Reynolds number where the chemical compositions of the two flame zones are different. However, the spectral intensity technique described in this paper does provide the desired information because it examines directly the mixture ratio in the important flameholding region. (See Ref. 5, particularly Fig. 33, and discussion, p. 14.)

Experimental Program

Combustion in these experiments took place in a $^1/_2$-in. $\times$ 2-in. two-dimensional duct, 12 in. long, with Vycor #790 glass walls. The burner which exhausted to the open atmosphere was connected to an air and propane supply system which permitted operation at burner entrance velocities from approximately 20 to 200 ft/sec. The burner was equipped with a series of shields which permitted the isolation of the visible radiation from individual parts of the flameholding and flame spreading regions.

The CH and C_2 radiations were isolated by interference filters which had a band width of about 100 A and were centered respectively at 4280 A (CH) and at 5080 A (C_2). The radiation intensity was measured by a standard photomultiplier tube, RCA Type 931-A, fitted first with one of the filters, then with the other. The CH/C_2 ratio reported herein is the ratio of the two output signals, and thus involves the spectral sensitivity of the tube and the transmission factors of the filters. These are simply constants. Preliminary tests, which are to be repeated later with greater precision, indicated that self-absorption is negligible in the case of these particular radiations.

Fig. 1 presents a plot of CH/C_2 as a function of fuel equivalence ratio. These measurements were made on a quiescent (nearly laminar) flame segment at a point away from the influence of the flameholder, and constitute the calibration curve for determining local mixture ratio in the zone near the flameholder. In Fig. 2 are presented axial traverses of CH/C_2 in two different runs with the same $^1/_2$-in. diameter flameholder

[6] To clarify the reference to "high Reynolds numbers," it should be noted that there appears to be still another significant range above 10^5, where blow-off velocity is proportional to the first power of flameholder dimension. This range was not accessible for study in our equipment.

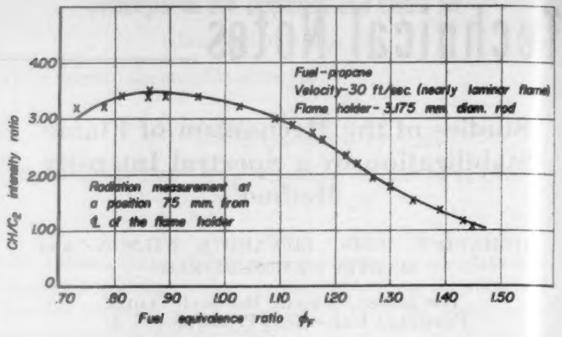

Fig. 1 CH/C_2 vs. fuel equivalence ratio at a station remote from the flameholder (calibration curve)

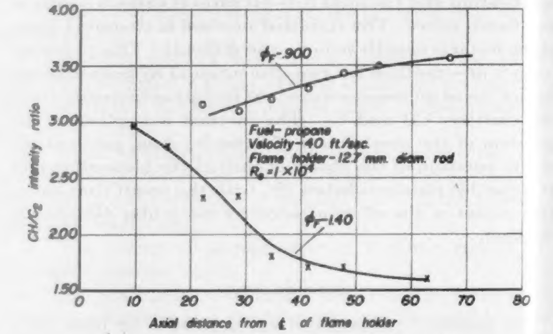

Fig. 2 CH/C_2 vs. axial distance from flameholder (mm). Effect of fuel equivalence ratio

operated at the same stream velocity but at different equivalence ratios. (At each axial position the magnitude of CH/C_2 was recorded at the point of peak luminosity along a cross-stream traverse.) The curve corresponding to the fuel rich equivalence ratio decreases from a maximum as the distance from the flameholder is increased. In the case of the fuel lean equivalence ratio just the opposite is the case. Reference to Fig. 1 shows that in both cases the change in CH/C_2 corresponds approximately to a 20 per cent reduction of the fuel/air ratio at which combustion actually takes place in the flameholding region near the stabilizer. It is to be noted that the process of selective diffusion is not confined to a sharply defined region but rather falls away gradually from a maximum in the immediate proximity of the flame stabilizer. This 20 per cent reduction in fuel concentration at our Reynolds number of 1×10^4 explains the observation of Zukoski (5) that the peak of the blow-off curve was shifted to 20 per cent higher fuel supply concentration when his Reynolds number was 0.9×10^4.[7] This 20 per cent shift was not explained by the measured chemical composition in the holder wake.

In Fig. 3 a comparison is made of two CH/C_2 traverses for the same $^1/_2$ inch flameholder at Reynolds numbers above and below the critical value indicated by Zukoski's tests (5). In the case of the high Reynolds number flow CH/C_2 is approximately constant, while in the low Reynolds number case there is a decrease in CH/C_2 as the holder is approached, corresponding to a progressively leaner fuel concentration. (The fact that the CH/C_2 values in Fig. 3 for Reynolds number 5×10^4 exceed the corresponding value in Fig. 1 by 12 per cent is probably due to an undetected change in the spectral sensitivity of the measuring system. This is being investigated more carefully.) This result appears to corroborate the postulate that, in the flow regions above and below the critical Reynolds number, different types of transport proc-

[7] The difference between the 1.0×10^4 value in our experiments and the 0.9×10^4 of Zukoski may be instrumental error or a real difference due to different operating conditions.

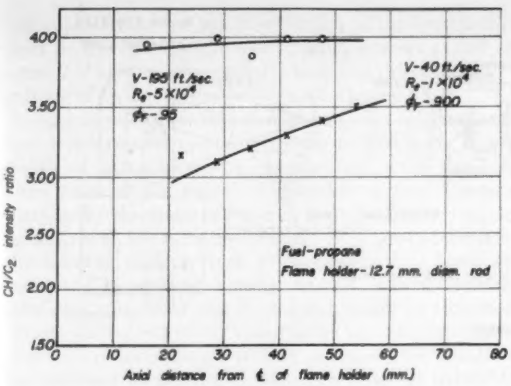

Fig. 3 **CH/C_2 vs. axial distance from flameholder. Effect of inlet Reynolds number**

esses predominate. Above the critical Reynolds number the transport is turbulent, while below it is laminar with resultant selective diffusion.

Conclusions

From the preliminary results presented above and the results currently being obtained at this laboratory, it is apparent that measurements of the visible CH and C_2 radiation in the region immediately downstream of a bluff body flame stabilizer can lead to information on the mechanism of flame stabilization which cannot be easily obtained by other methods.

References

1 "Flame Stabilization and Propagation in High Velocity Gas Streams," by G. C. Williams, H. C. Hottel, and A. C. Scurlock; Third Symposium on Combustion, Flame and Explosion Phenomenon, Williams and Wilkins, Baltimore, 1949, pp. 21–39.

2 "Flame Blow Studies of Cylindrical Flame Holders in Channeled Flow," by G. W. Haddock; Progress Report no. 3–24, Pasadena: Jet Propulsion Laboratory, May 1951.

3 "Stabilisation des Flammes par des Obstacles," by M. Barrere and A. Mestre, AGARD Combustion Colloquium, Cambridge, December 1953. Butterworths, London.

4 "Some Experimental Techniques for the Investigation of the Mechanism of Flame Stabilization in the Wakes of Bluff Bodies," by H. M. Nicholson and J. P. Field, Third Symposium on Combustion (See Ref. 1), pp. 44–68.

5 "Flame Stabilization on Bluff Bodies at Low and Intermediate Reynolds Numbers," by E. Zukoski, Report no. 20–75, Pasadena: Jet Propulsion Laboratory, June 1954.

6 "Flame Stability in Bluff Body Recirculation Zones," by J. P. Longwell, E. E. Frost, and M. A. Weiss, *Industrial and Engineering Chemistry*, vol. 45, August 1953, pp. 1629–1633.

7 "Ignition and Combustion in a Laminar Mixing Zone," by F. E. Marble and A. E. Adamson, JET PROPULSION, vol. 24, 1954, pp. 85–94.

8 Semi-Annual Project Squid Reports, April 1, 1953–April 1, 1955, by G. C. Williams (M.I.T. Combustion Laboratory).

9 "Effects of Boundary Layer Thickness on Flame Stability," by A. A. Putnam, *Fuel*, vol. 33, 1954, pp. 355–360.

10 "Stabilized Flames in High Velocity Streams of Propane and Air," by R. F. Baddour and L. D. Carr, M.S. Thesis, Department of Chemical Engineering, Massachusetts Institute of Technology, 1949.

11 "Physical Structure of Turbulent Flames," by M. Summerfield, S. Reiter, V. Kebely, and R. W. Mascolo, JET PROPULSION, vol. 24, 1954, pp. 254–255.

12 "Spectrophotometric Traverses Through Flame Fronts," by K. Wohl and F. Welty, Project SQUID, Technical Report Del-4-P, September 1954 (Univ. of Delaware).

13 "Spectroscopic Studies of Low-Pressure Flames IV. Measurements of Light Yield for C_2 Bands," by A. C. Gaydon, and H. G. Wolfhard, *Proceedings Royal Society of London*, vol. 201A, 1950, p. 570.

14 "Spectroscopic Studies of Premixed Laminar Flames," by S. S. Penner, AGARD Combustion Colloquium, Cambridge, December 1953.

15 "Comparison of the Spectra of Turbulent and Laminar Flames," by A. C. Gaydon and H. G. Wolfhard, *Fuel*, vol. 33, 1954, p. 286.

16 "A Study of the Radiation from Laminar and Turbulent Open Propane-Air Flame," by T. P. Clark and D. A. Bittker, NACA RM E54 F 29, Cleveland, Ohio, August 1954.

17 "Some Properties of Rod Stabilized Flames of Homogeneous Gas Mixtures," by G. C. Williams and C. W. Shipman, Fourth Symposium on Combustion, Williams and Wilkins, Baltimore, 1953, pp. 733–742.

Experimental Flame Temperatures of an Ammonium Perchlorate Solid Propellant[1]

GEORGE S. SUTHERLAND,[2] DWIGHT A. MAHAFFY,[3] and MARTIN SUMMERFIELD[4]

The James Forrestal Research Center
Princeton University, Princeton, N. J.

A brightness-emissivity method for measuring transient flame temperatures produced by the combustion of solid propellants has been developed and applied to the study of an ammonium perchlorate-polyester resin propellant. The method is capable of a spatial resolution of less than 50 microns for two-dimensional flames and can be used with flames of rapidly varying temperatures or emissivities. Experimental flame temperatures close to the burning surface were found to agree reasonably well with the theoretically calculated values. Systematic effects of particle size, mixture ratio, and pressure are being studied.

IN A study of the mechanism of combustion of solid propellants, it is important to determine the extent and structure of the active reaction zone. The extent of this zone may be deduced from the variation of temperature in the combustion region.

The difficulty of accurately determining the temperature profile in a small zone or combustion wave is well known. Thermocouples have been used to measure the temperature in the solid phase adjacent to the surface for certain double-base propellants (1).[5] However, difficulty in manipulating these small thermocouples, embedding them in the solid, and locating the thermocouple bead in relation to the burning surface, tend to discourage their use.

On the other hand, various electro-optical methods for measuring flame temperatures have been developed (2, 3). A decided advantage of these methods is the ability to measure temperatures in flames that, for various reasons, may be rather inaccessible. Another advantage is the avoidance of any disturbing influence on the combustion process that might be caused by the insertion of immersion-type instruments. Unfortunately, the optical methods are useful only at relatively high temperatures, and are limited generally to measurements of temperature in rather gross zones compared to the resolution obtainable with fine-wire thermocouples.

The development of an instantaneous electro-optical method for exploring microscopic regions is described in this note. Such microscopic exploration is necessary to find the peak flame temperature, since the temperature profile achieves its peak within 100 microns from the solid surface, and then falls away due to heat loss from the flame. Most of the visible flame has a temperature substantially less than the

Received Sept. 1, 1955.

[1] This paper is based on research performed for the Ph.D. and M.S.E. degrees of the two junior authors.

[2] Research Assistant, candidate for Ph.D. degree. Mem. ARS.

[3] Daniel and Florence Guggenheim Fellow in Jet Propulsion, candidate for the M.S.E. degree.

[4] Professor of Jet Propulsion, Department of Aeronautical Engineering. Mem. ARS.

[5] Numbers in parentheses indicate References at end of paper.

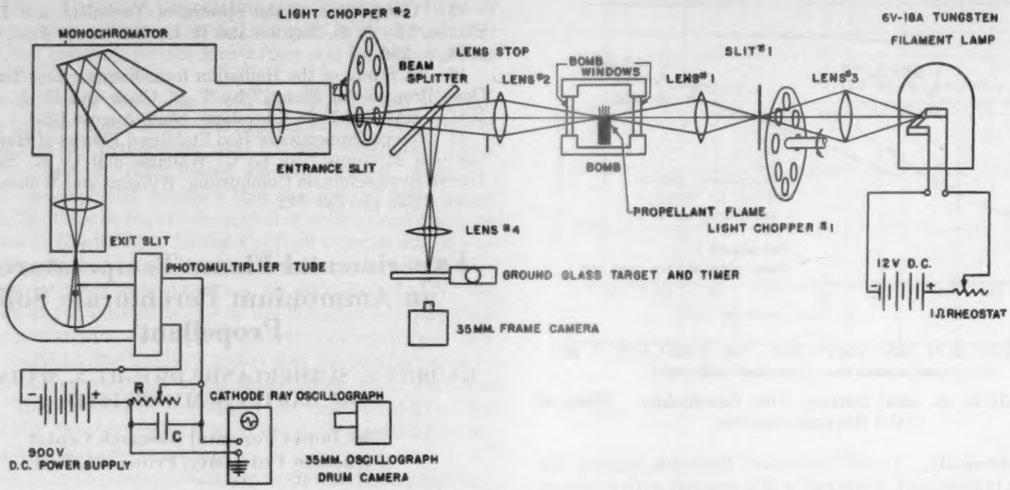

Fig. 1 Apparatus for the determination of flame temperature by the brightness-emissivity method

peak value. According to Lawrence-Dekker (7), the height of the visible flame from a similar ammonium perchlorate propellant ranges from 5 mm at 200 psi down to 2 mm above 1000 psi. Our data show that the active combustion zone occupies only 1/10 mm or less, right near the surface.

Experimental Apparatus

The propellant under study was a composite or heterogeneous type composed of finely ground ammonium perchlorate dispersed in a polymerized matrix of Rohm and Haas P-13 styrene-base polyester resin. The propellant was mixed with 0.1 per cent sodium chloride by weight to produce the desired intensity of Na D line radiation. It was manufactured by a straightforward process in the Princeton Laboratory.

The method used in this investigation is a brightness-emissivity method (4, 5) based on the assumption of thermal equilibrium of the emitter under observation with the combustion gases whose temperature it is desired to measure. The propellant flame displays considerable luminosity even with small amounts of added sodium, particularly at the 75:25 mixture ratio and with coarse oxidizer grinds. This luminosity is due to carbon, which can be assumed to be in reasonably close thermal equilibrium with the gas. The experimental setup (Fig. 1) starts with a tungsten lamp, whose ribbon filament is focused in the plane of the propellant flame by means of lenses 1 and 3. The transmitted radiation from the tungsten filament plus that from the flame is in turn focused on the monochromator entrance slit by means of lens 2. The monochromator exit slit then passes the desired

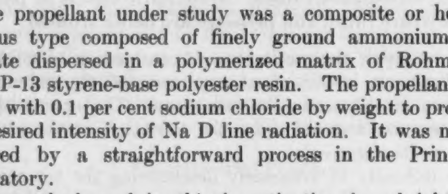

Fig. 2 Idealized oscillograph trace of radiation intensity showing measurements used to calculate flame temperature

(a): Tungsten lamp alone; taken before or after flame test. (b): Flame plus lamp; taken as flame burns past monochromator entrance slit.

portion of the spectrum of both radiation sources to the photosensitive surface of a battery-operated RCA 1P21 photomultiplier tube. The signal from the photomultiplier tube is recorded by a drum camera and d-c. oscillograph combination. A 100K load resistor R allows an adequate frequency response at 300 cps in conjunction with a 0.002 mfd filter condenser across the oscillograph input. The use of light choppers 1 and 2 provides a temperature-time history of the propellant flame. An idealized trace is shown in Fig. 2.

A portion of the flux from the flame and lamp is removed by a beam splitter and focused by lens 4 on a ground-glass screen. This screen contains a reference mark indicating the position of the monochromator entrance slit. Adjacent to the screen, a precision timer is located in the field of view of the 35 mm frame camera. From this film record, displacement-time information can be obtained as well as information concerning the one-dimensionality of the propellant surface as it burns past the monochromator entrance slit reference mark. The tungsten comparison source, with its associated lenses and bomb window, was calibrated with a disappearing-filament type optical pyrometer.

Theoretical Considerations

The calculation of experimental flame temperatures from the data proceeds as follows. The oscilloscope deflections due to the signal from the photomultiplier tube may be written as:

$$D_1 = kI_{bl}(\lambda, T_l')$$
$$D_2 = k\epsilon_f I_{bf}(\lambda, T_f)$$
$$D_3 = k(1 - \alpha_f)I_{bl}(\lambda, T_l')$$

where D_1, D_2, and D_3 are the deflections caused by the flux from the tungsten comparison lamp, the flame, and the comparison lamp shining through the flame, respectively. k is a proportionality constant whose value depends on the response characteristics of the system. I_b is the spectral intensity of black body radiation at the indicated temperature and wavelength λ. ϵ_f and α_f are the emissivity and absorptivity of the flame, respectively. Subscripts l and f refer to lamp and flame, respectively. For hot gases in thermal and radiative equilibrium, $\epsilon_f = \alpha_f$, according to Kirchhoff's law. Using Wien's approximation to Planck's radiation law, the flame temperature may be written in terms of the lamp brightness temperature T_l' as

$$1/T_f - 1/T_l' = \lambda/c_2 \ln (D_1 - D_3)/D_2$$

where c_2 is the second radiation constant (1.438 cm deg K).

It is evident that the space resolution of the system is dependent on the speed of chopper 1, which was set at 300 cps. Chopper 2 is used to give periodic base line references. The magnitude of D_1 is recorded before and after each run.

The spatial resolution in a direction normal to the burning surface is determined primarily by the following six factors: 1—width of monochromator entrance slit when projected into the plane of the flame; 2—location of focal planes of the lenses; 3—thickness of flame in line of sight; 4—numerical aperature of the radiation beams; 5—degree of deviation of the burning surface from a one-dimensional horizontal surface; and 6—optical quality of the lenses. Through detailed study of these effects, it was possible to reduce the effective scanning slit width in the flame to about 50 microns. Some further reduction is possible by increasing the sensitivity of the radiation measuring system. In order to reduce the effect of burning surface tilt, the monochromator entrance slit length was reduced by a mask to a projected length of 200 microns in the flame.

It was also necessary to give some attention to the problem of obtaining the optimum flame absorptivity to achieve the desired accuracy of T_f. The sodium emission line at 5890 A was chosen for temperature measurement. A review of the various factors affecting the spectral width and intensity of this line is given by Bundy and Strong (2, 6). The two factors of most concern in this experiment were broadening of the line due to increasing pressure, and absorption broadening. It was found that, at combustion pressures below 20 atmospheres, the line was sufficiently broad due to absorption that average absorptivities of about 20 per cent were obtained, when the NaCl was added to the extent of 0.1 per cent by weight. At higher pressures, the line width increased enough that the monochromator exit slit had to be opened wider to maintain the optimum balance between lamp and flame emission. The relationship between the measured deflections, sodium concentration, spectral line width, and exit slit width was given detailed study to optimize the accuracy of the temperature measurements.

Consideration was also given to the problems of vignetting of the comparison lamp, refraction of the lamp beam due to the temperature gradient in the flame, and the recurring problem of burning surface tilt. The only practical way to deal with the last problem was to carefully monitor each strand and discard the runs with excessive tilt.

An interesting result obtained by this method was the appearance of nearly maximum temperatures within fifty microns of the surface for the case of the fine oxidizer particle size. However, at least two factors exist that could mask the true temperature profile near the surface. One is the presence of Na atoms in nonequilibrium states in the active reaction zone. The fact that no abnormal temperatures were observed is indirect evidence that this factor is not important. Another is the possibility that, if the propellant flame consists of a mixed zone of fuel-rich and oxygen-rich gas pockets, the sodium chloride added to the propellant does not dissociate sufficiently in the cooler regions between the reacting gaseous interfaces to give a free sodium atom density comparable to that in the hotter zones. This situation would lead to a measured temperature always near the maximum even where the average temperature is considerably lower. Further experiments are in progress to shed more light on this question.

Experimental Results

A comparison between measured and calculated flame temperatures is made in Table 1. In all cases, the experimental temperatures were lower than the theoretical temperatures. In particular, the flame temperatures of the propellants with coarse oxidizer particles (150–200 microns) were consistently lower than those with fine oxidizer particles (5–10 microns). This fact is not unexpected in view of the heterogeneous nature of the flame zone, and indicates that best combustion efficiency is obtained with fine oxidizer particle sizes. Also, the results show that combustion efficiency improves with increasing pressure.

Table 1

Flame temperature, deg K

Combustion pressure psi	Weight mixture ratio, oxidizer:fuel 75:25 Experimental Coarse	Fine	Theoretical	80:20 Experimental Coarse	Fine	Theoretical
5	. .	. .	2400	2350	2500	2700
50	2210	2300	2410	2500	2680	2750
200	2270	2320	2412	2440	2760	2800
400	2350	2310	2415	2590	2800	2810

Note: Coarse grind propellant has an average oxidizer particle size of 150–200 microns. Fine grind propellant has an average oxidizer particle size of 5–10 microns.

Due to the fluctuating behavior of the flame, the temperatures listed in Table 1 are average values taken from the zone of maximum temperature. The estimated uncertainty interval of the temperature measurements is about ±100 deg K. The probable error of the temperature measurements for the propellants with fine oxidizer particles is less than ± 100 deg K as a consequence of a more homogeneous flame zone.

The theoretical temperatures were calculated by the method of successive approximations, allowing for the following combustion products: H_2O, CO_2, CO, H_2, H, OH, HCl, Cl,N_2.

Other work in progress designed to obtain more information on the extent of the active reaction zone of this propellant flame includes the study of the spatial distribution of transient radicals such as CN, CH, and C_2.

Acknowledgments

The authors would like to express their gratitude to the Aerojet-General Corporation for a grant to Princeton University in partial support of this research, and to Dan A. Kimball, President of Aerojet-General Corporation, for his personal interest in the over-all program. The Rohm and Haas Company, the Bakelite Company, and the Hercules Powder Company aided the research by supplying various propellant ingredients.

References

1 "Determination of the Thermal Structure of a Combustion Wave by Fine Thermocouples," by R. Klein, M. Mentser, G. von Elbe, and B. Lewis, *Journ. Phys. and Coll. Chem.*, vol. 54, 1950, pp. 877–884.

2 "Measurements of Flame Temperature, Pressure, and Velocity," by F. P. Bundy and H. M. Strong, "Physical Measurements in Gas Dynamics and Combustion," Vol. IX, High Speed Aerodynamics and Jet Propulsion, Princeton University Press, 1954, pp. 343–386.

3 "Optical Methods for the Determination of Combustion Temperatures," by P. J. Dyne and S. S. Penner, *Journal of the American Rocket Society*, vol. 23, 1953, pp. 165–169.

4 "A Fast, Electro-Optical Hot Gas Pyrometer," by G. H. Millar et al, *Journ. Opt. Soc. Am.*, vol. 43, 1953, p. 609.

5 "A Modified Sodium-line Reversal Technique for the Measurement of Combustion Temperatures in Rocket Engines," by M. Heidmann and R. Priem, *Journal of the American Rocket Society*, July–August 1953, pp. 248–253.

6 "Theoretical Shapes and Intensities of Sodium Lines from Flames of Complex Structures," by F. P. Bundy and H. M. Strong, General Electric Report no. 55275, Schenectady, Sept. 20, 1948.

7 "Structure of Flames from Ammonium Perchlorate Propellant," by R. W. Lawrence and A. O. Dekker, JET PROPULSION, vol. 25, February 1955, p. 81.

Manifolds for Solid-Propellant Rocket Motors

RICHARD D. GECKLER[1]

Aerojet-General Corporation, Azusa, Calif.

A method is given for computing the required size of manifold connecting two similar solid-propellant rockets so that the difference in combustion chamber pressure between them will be reduced to any specified value.

Introduction

THE use of solid-propellant rockets fired simultaneously in clusters for launching missiles imposes stringent tolerances on the thrust developed by each rocket. The individual rockets of the cluster are usually located at a distance from the center line of the missile. Therefore, unless their lines of thrust pass through the center of gravity of the missile-cluster combination, any differences in rocket thrusts will lead to a moment of force about the C.G. Oftentimes it is not possible either to provide the controls necessary to overcome this moment of force or to arrange for the lines of thrust to pass through the C.G.

In these cases it may be possible to reduce the extent of the thrust differences of the individual rockets by interconnecting them with a manifold large enough to nearly equalize their chamber pressures. The approximate theory for a pair of rockets given below permits the appropriate size of manifold to be easily selected once the ballistic properties of the propellant, the known variability in thrust before manifolding, and the desired variability in thrust after manifolding are given.

Derivation of Theory

We consider two rocket motors having the same nozzle throat area A_t (in.^{2}). Mass flow rates of propellant gas are symbolized by w (lbm·sec^{-1}); the subscripts G, N, and M refer to gas generated by combustion, gas flowing through the nozzle, and gas flowing through the manifold, respectively; the subscripts 1 and 2 refer to the chamber numbers; and the subscripts i and f refer to initial conditions (without manifold) and final conditions (with manifold). It is assumed that the chamber pressure p_1 (lbf·in.$^{-2}$) in the first rocket is always higher than the chamber pressure p_2 in the second.

When a manifold is used, the equilibrium rate of gas generation in the first chamber must equal the rate at which gas flows out through the nozzle plus the rate at which gas flows out through the manifold

$$w_{G1f} = w_{N1f} + w_M \quad [1]$$

In the second chamber the rate of gas generation plus the rate at which gas flows in through the manifold must equal the rate at which gas flows out through the nozzle

$$w_{G2f} + w_M = w_{N2f} \quad [2]$$

(These equations neglect the small amount of gas which goes to fill the space left by the solid propellant which has burned.) Subtraction of Equation [2] from Equation [1] gives the fundamental material balance which will furnish the solution to our problem

$$(w_{G1f} - w_{G2f}) = (w_{N1f} - w_{N2f}) + 2w_M \quad [3]$$

It is now necessary to express each of the three terms of this equation as functions of the propellant ballistic properties, the manifold area, the nozzle throat area, and the pressure differences $p_1 - p_2$ with and without a manifold.

Received July 21, 1955.

[1] Manager, Solid Engine and Chemical Div.

The equilibrium mass flow rate through a rocket nozzle is given by

$$w_N = C_w A_t p \quad [4]$$

where the proportionality constant C_w is called the mass flow coefficient. Since the addition of a manifold affects only the chamber pressures, without changing C_w or A_t, it is clear that we can write for the second term of Equation [3]

$$(w_{N1f} - w_{N2f}) = C_w A_t \Delta p_f \quad [5]$$

where $\Delta p_f = p_{1f} - p_{2f}$ is the desired difference in chamber pressures to be achieved by adding a manifold.

To obtain the first term of Equation [3] we note that the rate of gas generation from a burning solid propellant is $rA_p\rho_p$ where r (in.·sec^{-1}) is the linear burning rate, A_p (in.^{2}) is the propellant burning area, and ρ_p (lbm·in.$^{-3}$) is the density of the solid propellant. Furthernore, r can ordinarily be taken as proportional to p^n where n is a constant. Hence, for the rate of gas generation in a chamber without a manifold we can write

$$w_G = kp^n \quad [6]$$

When there is no manifold, the rate of gas generation must equal the rate of gas flow out the nozzle, which is given by Equation [4]. Consequently, it can be seen that the constant k of Equation [6] is given by

$$k = C_w A_t p_i^{1-n} \quad [7]$$

It is important to note that here p_i is a constant, being the equilibrium chamber pressure corresponding to the nozzle throat area A_t. On the other hand, p in Equation [6] is a variable, and by differentiating that equation with respect to p, we can see the effect on the rate of gas generation when a manifold is added, thereby changing p. Thus

$$w_{Gf} - w_{Gi} = \Delta w_G = knp^{n-1}\Delta p \quad [8]$$

where $\Delta p = p_f - p_i$. An equation of this type holds for each chamber, and we can write, therefore, the following two equations

$$w_{G1f} = w_{G1i} + \Delta w_{G1} = C_w A_t (p_{1i} + n\Delta p_1) \quad [9]$$

$$w_{G2f} = w_{G2i} + \Delta w_{G2} = C_w A_t (p_{2i} + n\Delta p_2) \quad [10]$$

In obtaining these equations use has been made of Equation [7]. Subtraction of Equation [10] from Equation [9] gives the desired expression for the first term of Equation [3]

$$(w_{G1f} - w_{G2f}) = C_w A_t (\Delta p_i + n\Delta p_f - n\Delta p_i) \quad [11]$$

where

$$\Delta p_i = p_{1i} - p_{2i} \quad [12]$$

$$\Delta p_f = p_{1f} - p_{2f} \quad [13]$$

There remains the flow through the manifold to consider. The necessary equation is the same as that for the flow of a compressible fluid through an orifice (Ref. 1)

$$w_M = 0.67CYA_M\sqrt{\rho_g \Delta p_f} \quad [14]$$

where

C = empirical discharge coefficient, including the velocity-of-approach factor
Y = net expansion factor, a function of the pressure ratio, the ratio of specific heats, and the velocity-of-approach factor
ρ_g = gas density, lbm·ft^{-3}
A_M = cross-sectional area of manifold, in.^{2}

This equation furnishes the third term of Equation [3].

When Equations [5], [11], and [14] are substituted in Equation [3], we obtain the following expression for the area of the

manifold in relation to the nozzle throat area

$$\frac{A_M}{A_t} = \frac{C_w(1 - n)(\Delta p_i - \Delta p_f)}{1.34CY\sqrt{\rho_g \Delta p_f}} \qquad [15]$$

Some simplification is possible by first expressing Δp_i and Δp_f as percentages of the final pressure in chamber 2

$$100\Delta p_i/p_{2f} = P_i \qquad [16]$$

$$100\Delta p_f/p_{2f} = P_f \qquad [17]$$

With these substitutions Equation [15] becomes

$$\frac{A_M}{A_t} = \frac{C_w(1 - n)}{13.4\ CY}\sqrt{\frac{p_{2f}}{\rho_g}}\left(\frac{P_i - P_f}{\sqrt{P_f}}\right) \qquad [18]$$

Next we note that according to the perfect gas law

$$\frac{p_{2f}}{\rho_g} = \frac{RT_g}{M} \qquad [19]$$

where

R = universal gas constant, 10.73(lbf · in.$^{-2}$)/(lbm-mol · ft^{-3} · °R)
T_g = gas temperature, °R
M = molecular weight

Moreover, the theoretical expression for the mass flow coefficient is (Ref. 2)

$$C_w = \frac{0.473\Gamma}{\sqrt{RT_g/M}} \qquad [20]$$

where

$$\Gamma = \sqrt{\gamma}\left(\frac{2}{\gamma + 1}\right)^{\frac{\gamma+1}{2(\gamma-1)}} \qquad [21]$$

$\gamma = C_p/C_v$, ratio of specific heats

Therefore, we can write

$$\sqrt{\frac{p_{2f}}{\rho_g}} = \frac{0.473\Gamma}{C_w} \qquad [22]$$

With this substitution and taking $CY = 0.59$, $\Gamma = 0.66$ (for $\gamma = 1.26$) we obtain

$$\frac{A_M}{A_t} = 0.04(1 - n)\left(\frac{P_i - P_f}{\sqrt{P_f}}\right) \qquad [23]$$

And finally the expression for the diameter of the manifold in relation to the diameter of the nozzle throat is

$$\frac{D_M}{D_t} = 0.2(1 - n)^{1/2}\left(\frac{P_i - P_f}{\sqrt{P_f}}\right)^{1/2} \qquad [24]$$

A graph of this equation is shown in Fig. 1 for $n = 1$. To use the figure for other values of n, it is only necessary to multiply the diameter ratio D_M/D_t read from it by $(1 - n)^{1/2}$. It is unnecessary to make corrections for values of Γ corresponding to values of γ other than 1.26, since the small effect is outweighed by uncertainties in the value of the discharge coefficient C.

As an example of the use of Fig. 1, we may consider two rockets containing the composite propellant based on potassium perchlorate oxidizer for which ballistic data are given in Ref. (3). The value of n is given as 0.740, and the standard deviation of chamber pressure at a constant nozzle throat area is given as 4.74 per cent. The standard deviation of the difference in chamber pressure between two similar rockets is thus $4.74\sqrt{2}$ or approximately 6.7 per cent. If it is desired to reduce this difference to 1.0 per cent, we read from Fig. 1 at $P_i = 6.7$, $P_f = 1.0$, that $D_M/D_t = 0.47$ for $n = 1$. Multiplication by $(1 - n)^{1/2} = 0.51$ gives $D_M/D_t =$

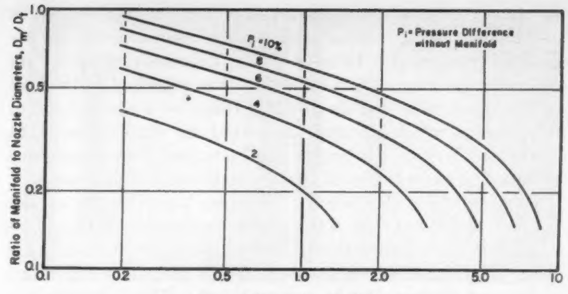

Fig. 1 Ratio of manifold diameter to nozzle throat diameter as a function of desired pressure difference with manifold P_f. Lines are for constant values of the pressure difference without a manifold P_i. Multiply D_M/D_t by $(1 - n)^{1/2}$

0.24. In other words, a manifold only one-quarter the diameter of the nozzle will reduce the pressure and thrust differences almost fivefold.

No experimental tests verifying the validity of Equation [24] are known to the author. However, it is not likely that it is greatly in error, and the merit of relatively small manifolds thus appears worthy of trial.

References

1 "Fluid Meters—Their Theory and Application," part 1, The American Society of Mechanical Engineers, 4th ed., 1937.

2 "Principles of Jet Propulsion and Gas Turbines," by M. J. Zucrow, John Wiley and Sons, Inc., New York, 1948, p. 490.

3 "The Correlation of Interior Ballistic Data for Solid Propellants," by R. D. Geckler and D. F. Sprenger, JET PROPULSION, vol. 24, 1954, pp. 22–26.

A Flow Instability Following Shock Reflection from a Flared End of a Duct[1]

GEORGE RUDINGER[2] and LOWELL M. SOMERS[3]

Cornell Aeronautical Laboratory, Inc., Buffalo, N. Y.

It was observed that violent pressure oscillations may occur in a duct following the reflection of a shock wave from a flared end. These could be qualitatively explained by alternate periods of separation and reattachment of the flow in the flare. This view is supported by high-speed schlieren motion pictures of the flow just outside the exit of the flare which show that a number of vortices are emitted from the duct when pressure oscillations appear. Apparently, the instability occurs only when the flow becomes supersonic in part of the flare. While flow separation in the flare is not surprising, the mechanism of reattachment of the flow is not clear at this time.

THE reflection of shock waves from an end of a duct which is terminated by a short flare is being investigated as part of a general study of nonsteady-flow phenomena. The purpose of this preliminary note is to describe an unexpected flow instability which was found to occur in the flare under certain conditions.

A shock tube of 3.23-in. internal diameter was used to carry

Received Aug. 15, 1955.

[1] This research was conducted under the auspices of Project SQUID, jointly sponsored by the Office of Naval Research (Department of the Navy), the Office of Scientific Research (Department of the Air Force), and the Office of Ordnance Research (Department of the Army).

[2] Principal Physicist, Aerodynamic Research Department. Mem. ARS.

[3] Associate Physicist, Aerodynamic Research Department.

[4] Numbers in parentheses indicate References at end of paper.

out the experiments, and the pressure was recorded by means of a Rutishauser transducer and auxiliary electronic and photographic equipment. Details of this experimental setup are described elsewhere (1).[4] The flare was attached to the end of the shock tube and its profile formed by a circular arc of 5-in. radius which smoothly increased the duct diameter to 7.0 in. at the exit. Its length was 3.5 in. and the pressure was recorded at a point located 18 in. from the exit of the flare.

Consider first the relation between the strength of the incident shock and that of the reflected expansion wave. This can be computed directly without preparation of a complete wave diagram if one assumes that the length of the flared portion of the duct can be neglected (2). The corresponding simplified wave diagram appears then as shown in the inset of Fig. 1, where 0,1,2, and e indicate the flow in the duct before and after passage of the incident shock wave, after passage of the reflected expansion wave, and in the exit section of the flare, respectively. The pressure ratio p_2/p_0 can be computed for various shock pressure ratios p_1/p_0 and expansion ratios of the flare (ratio of the exit area of the flare Ae to the duct area A). Actually the pressure level p_2 is quickly established only at the flare inlet while further inside the duct it is more gradually approached because of the spread of the reflected expansion wave.

Some results of such calculations for a ratio of the specific heats of $\gamma = 1.4$ are shown as the solid lines in Fig. 1. For weak shock waves, p_2 is lower than p_0 and decreases with increasing shock strength or expansion ratio of the flare. At the same time, the flow velocity in region 2 increases until the flow at the inlet of the flare becomes sonic. This determines the largest depression of p_2 below p_0. If the shock strength or the expansion ratio is further increased, the flow at the flare inlet remains sonic while p_2 rises again. The flow in the flare then becomes supersonic at the beginning of the flare and a stationary shock is formed at such location that the subsonic flow in the remainder of the flare produces just the required ambient pressure at the exit. It can be seen that a flare may have a remarkably large effect on the strength of the reflected expansion wave. While a shock pressure ratio of about 1.95 is required to produce sonic outflow from a straight duct, this value is reduced to about 1.64 by a flare with an expansion ratio of only 1.1.

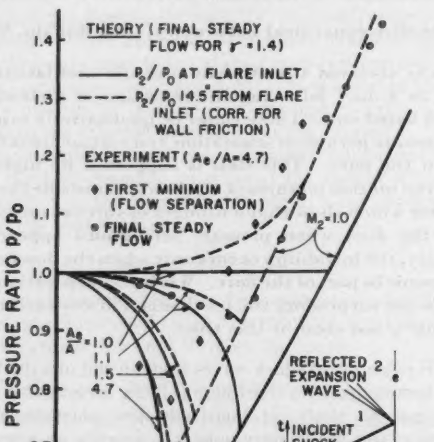

Fig. 1 Theoretical and experimental results for shock reflection from a flared exit

Inset: Simplified wave diagram in which the length of the flared section is neglected.

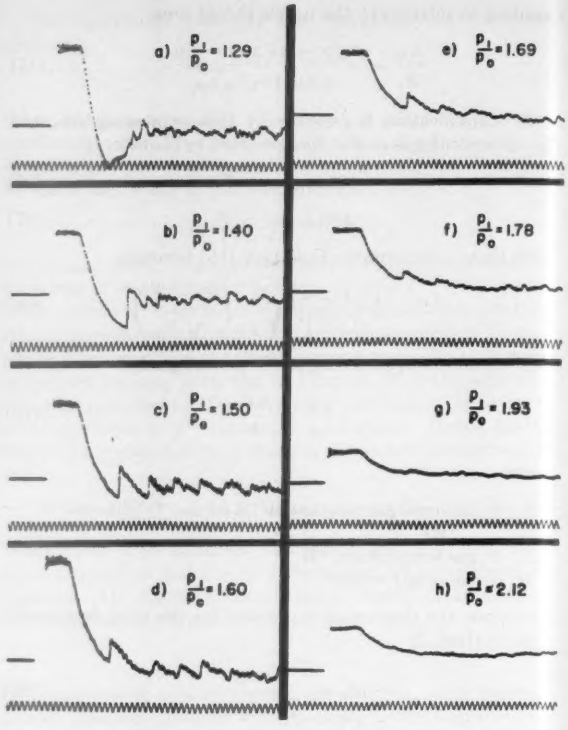

Fig. 2 Pressure records obtained 18 in. from the exit of the flare for various shock pressure ratios

The frequency of the sine wave below each record is 2500 cps.

The effect of wall friction has not been considered in these calculations. Although generally insignificant, it does become important if the finally established steady-flow velocity is sonic or near-sonic. Since the flow at the flare inlet is sonic for a good part of the range of interest here, the calculated pressure at the point of measurement should be corrected for the pressure difference between this point and the flare inlet. Friction effects were neglected in the flare where the flow velocities cannot be sonic. The Reynolds number of the finally established steady flow is always in the neighborhood of 2×10^6; accordingly, the calculations (3) were based on a constant mean friction coefficient for a smooth pipe and the value $f = 0.0031$ was used.[5] The results of the calculations corrected for the pressure drop due to friction between the point of measurement and flare inlet are entered in Fig. 1 as the dashed lines.

A number of typical pressure records obtained with the described flare (expansion ratio of 4.7) are collected in Figs. 2(a)-(h) for shock pressure ratios between 1.29 and 2.08. Most of these records show that the reflected expansion wave is followed by violent damped pressure oscillations, the initial amplitude of which may exceed one half of the pressure rise of the incident shock wave. These oscillations are not accounted for by a wave diagram analysis which predicts a smooth pressure decay. The first minimum, after which the pressure rises again, was determined from the records and the corresponding values are plotted in Fig. 1 (points marked as diamonds). The final pressure level that is established after the oscillations have died out is also indicated in the figure (circled points).

The discrepancy between the anticipated and the recorded

[5] The friction coefficient f is here defined as the ratio of the wall shearing stress to the dynamic head of the stream.

pressure variations can be explained if one assumes a sequence of alternate periods of flow separation and reattachment at the walls of the flare. The local pressure increases every time the flow separates, while reattachment causes it to drop again and the resulting pressure waves travel upstream. The pressure at the first minimum is indicative of the instant at which the flow separates from the wall for the first time. This point lies quite close to the theoretical curve for the flare used if the incident shock wave is weak enough to allow the flow to be subsonic throughout the flare ($p_1/p_0 < 1.4$ for $A_e/A = 4.7$). Thus, separation did not take place until the fully expanded flow had been established. For shock waves that are strong enough to produce supersonic flow in part of the flare, the points indicating flow separation lie well above the theoretical curve. This implies that full expansion of the flow was never reached in these cases. If the flow in the flare is entirely subsonic, the pressure adjustment after flow separation is gradual. If the flow is partly supersonic, the adjustment can take place only through a shock wave since no other signal could travel upstream.

The effects of this flow instability seem to be particularly pronounced when the incident shock wave is just a little stronger than necessary to produce sonic flow at the flare inlet. For weaker waves, the instability, apparently, does not occur. This view is supported by the findings from high-speed schlieren motion pictures which are discussed below. Probably the small residual oscillations, which can be noted on all records, are caused by transversal disturbance waves which originate at any slight irregularity of the duct.

With increasing strength of the incident shock wave, the recorded pressure oscillations decrease in amplitude until they finally become insignificant, as in Figs. 2(g) and (h). This merely means that no disturbances are created in the flare which are strong enough to propagate upstream through the supersonic flow region but nothing can be said at this time about the flow inside the flare.

The pressure that is established in the duct after the oscillations have died out (circled points in Fig. 1) depends on the location of the point of flow separation in the final steady flow. For the particular flare used in these experiments, the effective expansion ratio is seen to be near 1.1 for shock pressure ratios up to about 1.6. Even this small expansion ratio is sufficient for stronger shock waves to produce sonic flow at the flare inlet and the experimental points fall satisfactorily close to the theoretical curve for $M_2 = 1.0$ and with allowance for wall friction.

In order to support the above qualitative explanation of the flow instability, high-speed schlieren motion pictures of the flow just outside the flare exit were taken. In the process of flow separation, a vortex is formed that is then swept downstream, and it was expected that a whole series of vortexes should be emitted by the flare if the aforementioned explanation of the instability is correct. A conventional schlieren system was used in combination with a Fastax high-speed motion picture camera. The frame rate was about 6000 frames per sec and a number of frames from one film are reproduced in Fig. 3. The pressure ratio of the incident shock wave was about 1.7 and the times indicated on the frames are measured from the instant when the shock wave arrives at the exit of the flare. At least ten vortexes can be counted in this case (only eight of them are shown in Fig. 3). On a similar motion picture taken with a shock pressure ratio of about 1.3, only one vortex could be seen. This seems to support the hypothesis that no flow oscillations appear if the flow in the flare is entirely subsonic.

While it is not surprising that flow separation occurs in the flared section, the reasons for reattachment of the flow are not clear at this time. A few experiments were also carried out with other flare configurations and similar observations could be made. The findings reported here are tentative and further work is being planned to obtain a better insight into the phenomena.

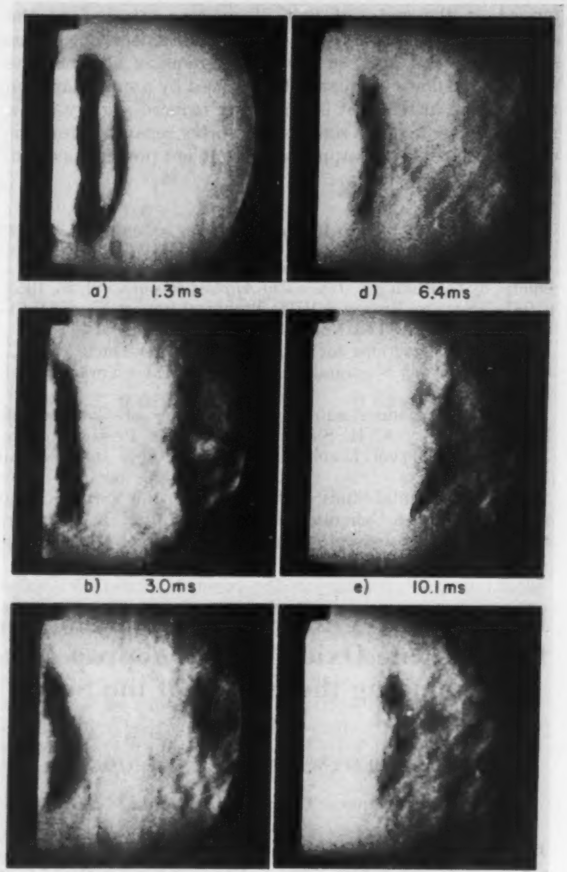

Fig. 3 Selected frames from a high-speed schlieren motion picture (about 6000 frames per sec) for a shock pressure ratio of about 1.7

The time on each frame represents the interval since the arrival of the shock at the exit of the flare. (a), 1st vortex; (b), 2nd and 3rd vortexes; (c), 4th and 5th vortexes; (d), 6th vortex; (e) 8th vortex; (f), 10th vortex.

APPENDIX

In a previous investigation (1), pressure records were taken with a straight open duct and it was noted that the expansion wave was always followed by a weak compression pulse. This can be seen on the record shown in Fig. 4 and may now be explained on the basis of the results presented in this note. When a shock wave emerges from the duct, a vortex ring is

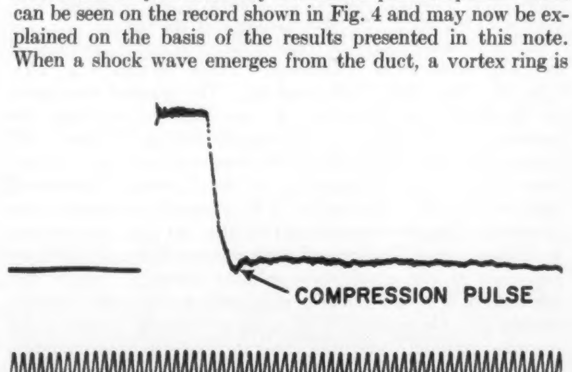

Fig. 4 Pressure record obtained 18 in. from the end of a straight open duct for a shock pressure ratio of about 1.5

The frequency of the sine wave below the record is 2500 cps. Note the short compression pulse that follows the expansion wave.

formed at the exit; at first, it remains attached to the edge of the duct but, after a short time, it is swept downstream (4). As long as the vortex remains attached, its effect on the flow is similar to that caused by a small flare and the pressure in the duct is, therefore, reduced slightly below ambient pressure. As soon as the vortex separates from the edge, the flare effect disappears and ambient pressure is established.

References

1 "On the Reflection of Shock Waves from an Open End of a Duct," by G. Rudinger, *Journal of Applied Physics*, vol. 26, 1955, p. 981. (See also Project SQUID Technical Report No. CAL-61-P, August 1954, ASTIA No. AD52851, Microcard.)

2 "Wave Diagrams for Nonsteady Flow in Ducts," by G. Rudinger, D. Van Nostrand Company, Inc., New York, 1955, p. 173.

3 "The Dynamics and Thermodynamics of Compressible Fluid Flow," by A. H. Shapiro, The Ronald Press Company, New York, 1953 (vol. 1) and 1954 (vol. 2), pp. 162–168, 184, and 1131.

4 "Experimental Study of the Formation of a Vortex Ring at the Open End of a Cylindrical Shock Tube," by F. K. Elder, Jr., and N. de Haas, *Journal of Applied Physics*, vol. 23, 1952, pp. 1065–1069.

Equilibrium Performance Calculations for Ethylene Oxide as a Monopropellant —Including the Effects of the Solid Phase

D. M. MEEHAN[1] AND SEBA ELDRIDGE[2]

Aerojet-General Corporation, Azusa, Calif.

THE theoretical performance of ethylene oxide as a monopropellent has been reported by other investigators (1 2).[3] Preliminary calculations were reported by Robison (1) assuming decomposition of ethylene oxide to form only carbon monoxide and methane, or by subsequent decomposition of all of the methane to yield solid carbon and hydrogen. Recently, a more rigorous treatment of the decomposition process was presented (2), assuming the formation of CO, CH_4, CO_2, O_2, H_2, C_2H_4, and H_2O, and as a result of the calculations, the decomposition reaction of ethylene oxide was postulated as

$$C_2H_4O \rightarrow a\,CO + b\,CH_4 + c\,H_2 + d\,C_2H_4$$

However, complete equilibrium relations involving solid carbon have not as yet been reported, and the presence of this constituent seriously alters the nature of the decomposition products and, hence, the performance characteristics.

In the present study, all possible decomposition products of ethylene oxide were considered. These include $C_{(s)}$, CO, CH_4, H_2, CO_2, H_2O, C_2H_4, and O_2. The method developed by Kandiner and Brinkley (3) was used to establish the presence of solid carbon in the equilibrium gas mixture. All thermodynamic data for liquid ethylene oxide and its products were taken from publications of the National Bureau of Standards (4, 5). The results of the present investigation are shown for chamber pressures of 20 atm, 40 atm, and 60 atm in Tables 1 and 2, where all performance data are based on expansion to one atmosphere exhaust pressure. From this tabulation, it is seen that the solid carbon comprises approximately 29 mole per cent or 26 to 28 per cent by weight of the chamber products, and this value increases to approximately 36 per cent by weight at the exit temperatures under equilibrium conditions. Ethylene and oxygen were found to be absent from both the flame gas and the exit gas compositions.

Received Aug. 9, 1955.

[1] Chemist.

[2] Assistant Senior Engineer.

[3] Numbers in parentheses indicate References at end of paper.

Table 1 Equilibrium decomposition products of ethylene oxide at the adiabatic flame temperature

Product	Mole % (at 3 chamber pressures) 20 atm	40 atm	60 atm
$C_{(s)}$	29.39	29.26	29.08
CO	18.50	18.54	18.71
H_2	37.20	35.06	33.76
CH_4	7.01	8.58	9.56
CO_2	2.11	2.20	2.20
H_2O	5.79	6.36	6.67

Performance values were calculated for both the assumption of shifting equilibrium and frozen composition during expansion. The results are presented in Table 2. For the reactions involved, it is believed that the chamber composition is maintained for reactors of reasonable size, i.e., that the assumption of frozen composition is more applicable. For this reason, more complete results are given for the case of frozen flow.

The decomposition products are a mixture of gases and particles of solid carbon; therefore, the usual compressible hydrodynamic equations do not apply without modification. The performance calculations discussed above were carried out assuming that the solid carbon maintains thermal and velocity equilibrium with the gas. These assumptions should closely approximate experimental conditions because the carbon particles formed are expected to be considerably smaller than 10μ. Consequently, thermal and velocity lags will be insignificant (6). Since heat capacities of the decomposition products change appreciably over the expansion range considered, it was necessary to determine performance values by trial-and-error, that is, by determination of temperatures, enthalpies, etc. at constant entropy. The exact throat conditions ($M = 1$) were found in this way. Subsequently, c^* was computed from the following relationship, which accounts for the presence of a solid phase in the gas stream.

$$c^* = \frac{p_c}{p_t}\frac{a_1}{\bar{M}_1}\frac{gRT_t}{a_t}$$

The values of characteristic velocity so obtained can be compared directly with data calculated from the usual experimental relationship

$$c^* = \frac{p_c A_t g}{\dot{w}}$$

where p_c is chamber pressure, p_t throat pressure, a_1 weight fraction of gas in products, $\bar{M}_1$ mean molecular weight of gas in products, g gravitational acceleration constant, R universal gas constant, T_t throat temperature, a_t throat sonic velocity, A_t throat area, $\dot{w}$ weight flow rate of gas.

The expression given for c^* derives from the continuity relationship, the gas law applied to the gaseous portion of the mixture, and the relation

$$\frac{p}{\rho^{\psi}} = \text{const}$$

The isentropic exponent, ψ, for the solid-gaseous mixture (see Ref. 7) is given by

$$\psi = \left(a_1\frac{R}{\bar{M}_1} + a_1c_v + a_2c_s\right)/(a_1c_v + a_2c_s)$$

where a_2 = weight fraction of solid, c_v = mass specific heat of gas at constant volume, and c_s = mass specific heat of solid. The values of ψ given in the tables at chamber, throat, and exit conditions were calculated using this last equation. Finally, values of the thrust coefficient, C_F, given in Table

Table 2 Theoretical performance of ethylene oxide

Parameter	20 atm Shifting	20 atm Frozen	40 atm Shifting	40 atm Frozen	60 atm Shifting	60 atm Frozen
T_c, °R	2137	2137	2227	2227	2281	2281
T_t, °R	......	1926	......	2020	......	2072
p_t, atm	......	11.1	......	22.6	......	33.8
T_e, °R	1642	1222	1602	1130	1579	1078
p_e, atm	1.0	1.0	1.0	1.0	1.0	1.0
I_{sp}, lb-sec/lb	169.6	162.8	188.0	178.1	196.3	186.0
c^*, ft/sec	......	3780	......	3810	......	3820
C_F (opt. expan.)	......	1.38	......	1.52	......	1.57
$\overline{M}$ (all products)[1], lb/mole	12.40	12.56	12.67	12.90	12.86	13.13
$\overline{M}$ (gases only)[1], lb/mole	12.58	12.79	12.99	13.27	13.27	13.58
ψ chamber	1.21	1.21	1.20	1.20	1.20	1.20
ψ throat	......	1.22	......	1.21	......	1.20
ψ exit	......	1.25	......	1.25	......	1.26
$\bar{c}_p$ (all products), chamber, Btu/lb°R	0.641	0.641	0.647	0.647	0.649	0.649
$\bar{c}_p$ (all products), throat	......	0.624	......	0.630	......	0.633
$\bar{c}_p$ (all products), exit	......	0.556	....	0.539	......	0.528

[1] Averaged between chamber and exit for shifting equilibrium, constant for frozen composition.

2 were determined from $C_F = V_e/c^*$, where the exhaust velocity, V_e, was computed directly from the root of the enthalpy drop.

The equations used to calculate the performance parameters, c^*, C_F, and ψ are outlined herein because the conventional expressions for their determination are based on a single gaseous phase and do not apply to a heterogeneous system. Therefore, revision of the standard equations to the forms cited above was necessary to complete the present study.

Consideration of complete equilibrium relationships among all decomposition products of ethylene oxide has resulted in flame temperatures of from 80 to 180°R lower than those obtained by Glassman and Scott (2) for the same pressure range; the specific-impulse values presented herein for frozen composition are approximately 3 to 4 per cent higher than those reported by these same investigators. A comparison of the results of this study with those of the earlier work of Robison (1) reveals that flame temperatures resulting from the formation of only CO and CH_4 are approximately 400°R too high, and that if all of the CH_4 is assumed to decompose to $C_{(s)}$ and H_2, the resultant temperature is 1000°R too low. The corresponding specific-impulse values determined from these two decomposition reactions are 1 per cent and 29 per cent, respectively, lower than the new frozen composition values. Even more startling is the low value of mean molecular weight (Table 2) determined in the present study; this is due to the large volume fraction of hydrogen present in the decomposition products.

The authors recognize the fact that the largest difference between the results of these equilibrium calculations and those obtained by Glassman and Scott (2) lies in the product compositions and, hence, average molecular weight, and comparatively smaller discrepancies were found for theoretical flame temperature and specific-impulse data. Nonetheless, solid carbon must be considered as a constituent of the equilibrium decomposition products of ethylene oxide; therefore, the data presented herein represent a soundly established theoretical yardstick with which experimental data can be compared.

References

1 "Ethylene Oxide as a Monopropellant," by W. C. Robison, Jet Propulsion, vol. 24, March-April 1954, pp. 111–112.

2 "Performance of Ethylene Oxide as a Monopropellant," by I. Glassman and J. E. Scott, Jr., Jet Propulsion, vol. 24, November-December 1954, p. 386.

3 "Calculation of Complex Equilibrium Relations," by H. J. Kandiner and S. R. Brinkley, Jr., *Ind. Eng. Chem.*, vol. 42, May 1950, pp. 850–855.

4 "Selected Values of Chemical Thermodynamic Properties," Circular no. 500, National Bureau of Standards, February 1, 1952.

5 "Selected Values of Chemical Thermodynamic Properties," Series III, National Bureau of Standards, March 1954.

6 "Velocity Lags of Particles in Linearly Accelerated Combustion Gases," by M. Gilbert, L. Davis, and D. Altman, Jet Propulsion, vol. 25, January 1955, pp. 26–30.

7 "Adiabatic Expansion of a Gas Stream Containing Solid Particles," by W. R. Maxwell, W. Dickinson, and E. F. Caldin, *Aircraft Eng.*, vol. 18, October 1946, pp. 350–351.

Jet Propulsion News

Alfred J. Zaehringer, American Rocket Company, *Associate Editor*

Jet Aircraft, Engines

A NEW version of the Super Sabre, the F-100C, was delivered to the Air Force. The new North American craft can be fueled in flight and carries extra bombs and tanks under its wings. The Super Sabre, with new electronic fire control system, is armed with four M-39 20-mm cannon. F-100C is 47 ft long, 15 ft high, and has a 45-deg swept wing with a span of 38 ft. (Photo.)

● First production model of the Convair F-102A was delivered to Edwards AFB. The delta-wing craft features new upswept tips with cambered leading edges. The fuselage is 68 ft long, height is 18 ft, span is 38 ft. In the F-102A, a new version of the J-57 will deliver 17,200 lb thrust and eventual power will be from the J-75 turbojet. The Ford Motor Co., Dearborn, Mich., is to produce three versions of the J-57. Production of 763 engines costs $195,572,897. The TF-102 is to be a training model and is slated for tests in October. Featuring side-by-side seating, the craft will have the same rocket fire control system as the F-102 and can carry a full complement of rockets. The regular version of the interceptor will carry FALCON missiles in missile bays adjacent to fuel tanks aft of the cockpit.

● Two other fighters—the McDonnell F-101 and the Lockheed F-104—are now in an accelerated production program. A GE J-79 turbojet is to power the fighter-bomber model of the F-104, giving it a range of 1800 miles and a speed of Mach 2.

● The Republic F-105 is a new swept-wing attack bomber powered by two Allison J-71 turbojets. Rollout is expected to take place early this fall. Now powered by the J-57 turbojet, eventual use of the J-71 or J-75 will give it a design speed of Mach 2 and a range of about 2000 miles. Because of the extremely thin wings, all fuel is stowed in the fuselage.

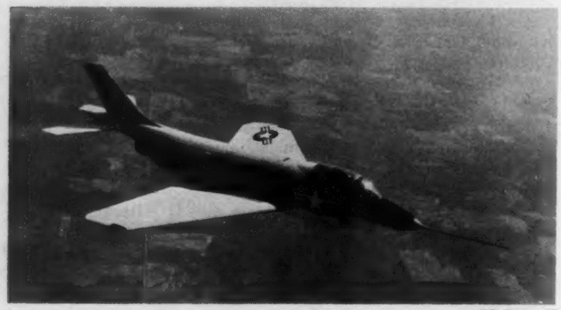

McDonnell

New Demon

Boeing

B-52 sports new cross-wind landing gear

North American

Long-range Super Sabre

Chance Vought

XF8U-1, Navy fighter

● A new transcontinental speed record was set by Air National Guard Lt. John Conroy when he flew his F-86 Sabrejet from California to New York and back again in 11$^1/_2$ hours. It was the first transcontinental round trip to be made between sunrise and sunset.

● XF8U-1 is the Navy's new carrier-based supersonic fighter. Chance-Vought is building the new plane which is powered by an afterburner-equipped J-57-P-4 turbojet. Performance data are still classified. Specifications call for a high rate of climb, high combat ceiling, and sonic speed in level flight. (Photo.)

● Deliveries of the new F3F-2N Demon are being made to the Navy by McDonnell Aircraft. The carrier-based fighter is powered by an Allison J-71 turbojet in the 10,000 lb thrust class. Thin wings and tail surfaces are of sharp sweepback provide a speed of 600 mph. Demon carries 20-mm cannon, rockets, and electronic equipment to put it into the all-weather class. (Photo.)

● Under an accelerated program, the Boeing B-52 is to be produced at a rate of 10 to 20 planes per month. Present production cost is about $10 million per plane; annual operation of a B-52 wing of 30 planes costs nearly $40 million. The 650 mph, 8 jet bomber is now equipped with a novel cross-wind landing gear which will enable the 350,000 lb B-52 to take off or land in a crabbing attitude. (Photo.)

● Three new transport aircraft have made the news. Douglas is now working on the DC-8 jet transport which is to fly in December 1957. The swept-wing craft (photo) is powered by four J-57 turbojets of 10,000 lb thrust each.

Editor's Note: The information reported in this Section has been selected from approved news releases originating with the Department of Defense, private manufacturers, universities, etc., and from published news accounts in journals and newspapers. The reports are considered generally reliable, although no attempt has been made to verify them in detail.

Specifications: gross weight, 211,000 to 257,000 lb; span, 134.5 ft; length, 140 ft; cruising speed over 550 mph at above 35,000 ft; cruising range, 3,700 miles; capacity, 80–125 passengers. Lockheed has received orders for its Electra turboprop liners. (Photo.) Probable power by four Allison T56 turboprops of 3750 eshp each, the Electra is slated for delivery in late 1958. Specifications: gross weight, 98,500 lb; span, 95 ft; length 101 ft; cruising speed, over 400 mph at up to 30,000 ft; cruising range, 2,000 miles; capacity, 70 passengers. Meanwhile, the Boeing 707 jet transport has logged about 200 hours of flight since its first flight in July 1954. The model is to be delivered to the Air Force as a jet tanker, the KC-135. Another version of the 707 is to be made available as a commercial jet liner with deliveries in 1959 to airlines.

● The Canadian CF-100 is to be fitted with afterburner to give an increase of 15 per cent power. Also to be used is a Marquardt Aircraft variable area (iris type) nozzle. Meanwhile, the CF-105 is a new delta-wing long-range jet interceptor by Avro, Canada. Present thrust rating of this Orenda engine powered craft is 18,000 lb, but this is expected to be boosted to 25,000 lb thrust with afterburner.

● In a recent flight over Europe, the British RAF jet bombers, Victor and Vulcan, attained a speed of nearly 600 mph at an altitude of 59,000 ft.

● The French Super Mystere interceptor Dassault IV B.1, powered by an Avon RA7 turbojet engine, has made supersonic flights and reached an altitude of 52,000 ft. Another French craft has made searing speed runs. The French SNCASO SO-9000 Trident is to get two Armstrong-Siddeley Viper turbojets. The main powerplant, which has pushed the craft to speeds of 800–930 mph in recent tests, are three rocket motors. Meanwhile, the jet transport, Caravelle S.E. 210 has begun ground tests at the SNCASE plant at Blagnac. Flight tests of the craft, powered by two Rolls-Royce Avon RA 16 turbojets are soon scheduled. The S.E. 210 cruises at 500 mph and carries a payload of 21,000 lb, equivalent to about 70 passengers.

Douglas

Turbojets power new DC-8

Lockheed

Turboprops become Electra

Boeing

Navy's jet boat

● Heavy jet bombers were recently seen in large formations in the USSR. Among these were a sweptwing bomber, the Il-38, powered by four turboprop engines of about 5000 hp each; the Type 39 (Badger) twin jet bomber similar in size to our B-47; and the Type 37 (Bison) four jet bomber. Also seen for the first time were a new supersonic fighter, a new all-weather fighter, and the Il-20, a four-jet transport.

● The first Swiss jet—the FFA P-16 ground support fighter—has made its initial flight. The P-16 is powered by an Armstrong-Siddeley Sapphire turbojet and is built by Flug & Fahrzeugwerke, A.G. The craft features thin, straight wings, tip tanks, dorsal fin and spine, and swept variable incidence tail. The plane is armed with two 30-mm cannon and external rockets.

● Gas turbine engines have been installed in Navy LCVP landing craft by Boeing. (Photo.) Installation is the Navy's first attempt to utilize gas turbines as the main propulsion units of seagoing vessels. Other gas turbines have been used by the Navy for fire pumps, deicers, and generators.

● The first US jet engine to be licensed for foreign use is the GE J-47. The Fiat works of Turin, Italy, is to build the engines under an NATO agreement.

● CAA approval for commercial use has been given to the Allison 501 (T56) turboprop engine. The T56 is now being used on the Lockheed C-130 transport and figures in the design of two commercial turboprop airline designs.

● Five versions of the Boeing 502 gas turbine are in use as auxiliary power sources for starting jet engines. All models operate at 36,500 rpm and 53 psia, and have air hp ratings of 140–210. The delivered air temperature is 410–425 F, and 90–120 lb of air can be delivered per minute.

● The new Bristol turbojet, Orpheus, delivers 3285 lb thrust with an engine weight of 746 lb. Orpheus has recently completed its 150 hr test. Another Bristol engine delivers 4800–4900 lb thrust with an engine weight of less than 850 lb.

New Developments

THE Armour Research Foundation, Chicago, Ill., has developed a flame spray method of coating aluminum oxide-zirconium oxide ceramics on metals. The coat, up to 10 mils thick, is harder than tool steel and is to be used for aluminum and steel rocket nozzles. The spray gun uses oxygen, acetylene, and nitrogen to obtain the 5500 F temperatures needed to fuse the cermet powder. Another Armour development is a vortex tube for use as a free air temperature indicator for supersonic aircraft. Air enters the tube at an angle, a vortex is created which cools the incoming air to compensate for the aerodynamic heating effect produced by high speed flight. The thermometer is designed for use up to Mach 1.5 and altitudes of from sea level to 60,000 ft; it operates independently of the aircraft velocity and has little effect on performance at altitudes of up to 40,000 ft.

• A silicon carbide coated graphite liner by the Norton Co. for the uncooled sustainer motor on the NIKE has been successfully tested and will permit a 100 per cent increase in burning time. The Norton process is called "Rokide" and allows coats of 5–50 mils to be placed on various materials. Aluminum oxide is used to coat metals and silicon carbide for graphite. The oxide coatings are said to be extremely durable, flexible, and resistant. They are applied in a molten form by a metalizing spray gun. (Photo.)

Norton

Ramjet gets ceramic liner coating

• Operating temperatures can be upped with a new aluminum alloy developed by the Aluminum Corp. of America. Designated as X2219, the heat-treated alloy has a yield strength of 21,000 psi at 500 F and 14,000 psi at 600 F. Alcoa is also working on a new alloy to be used at temperatures of 300–400 F for the skins of supersonic aircraft.

• Flexible hose suitable for use with high strength hydrogen peroxide has been developed by the Compoflex Co., Ltd., of London, England. The new hoses are made of "Molene," a specially compounded polyvinyl chloride, and "Terylene," a Dacron-type material. One type of supported hose is available for suction or delivery, another type is unsupported.

• Accurate measurement of pulsating fluid flow is possible with a new flowmeter developed by the Dynamic Instrument Co., Cambridge, Mass. The flowmeter can be used with corrosive liquids at pressures up to 2000 psi and rates up to 8 gpm. Dynamic frequency is about 2000 cps. (Photo.)

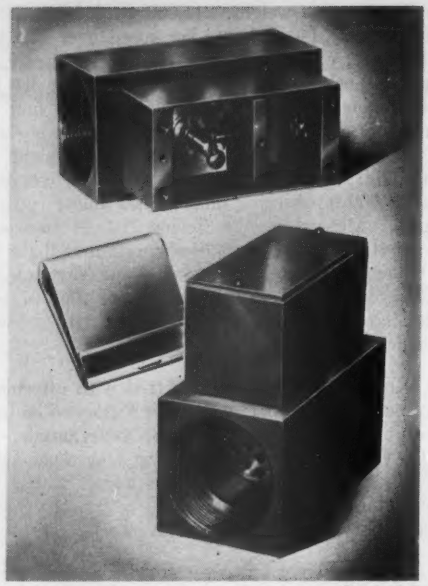

Dynamic Instrument

New dynamic flowmeter

• A new development by Socony Mobil Research Lab., Paulsboro, N. J., may enable jet fuels—similar to JP-5—to withstand high temperatures when the fuels are used as coolants in supersonic aircraft. Temperatures in the 400-500 F range caused gum deposits in filters, nozzles, etc. Pure hydrocarbons were found to be very stable and new cracking processes are to produce the newer, more stable fuels. Additives have also been found effective in reducing filter clogging.

Facilities

THREE new rocket facilities have been in the news. A calibration and test building, costing $1.5 million, at North American's rocket propulsion lab is to be completed on July 20. Fort Crowder, Mo., is to be the location of a new Air Force Rocket Engine Test Facility. Manufacturing buildings will occupy about 200,000 square feet and 500 to 1000 people will be employed there. Aerojet-General Corp. will operate the facility, with construction expected later this year. An auxiliary guided missile base is to be constructed at Cape Canaveral, Fla., and will support long-range tests at Patrick AFB.

• A new ramjet test facility has been completed at the Wright Aeronautical Div., Wood-Ridge, N. J. (Drawing) Construction was begun in 1953 with the total cost near $18 million.

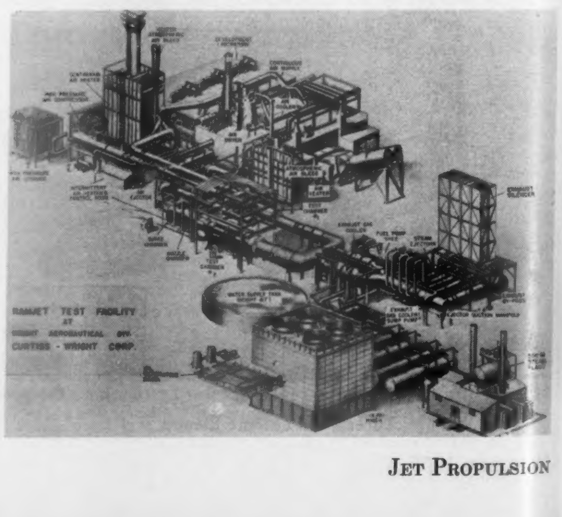

The test section of the new facility is about 14 ft in diameter and is almost 100 ft long. Conditions of from sea level to 50,000 ft can be simulated. Another test section 12 ft in diam and almost 70 ft long has handled supersonic ramjets of up to 50 in. in diam. Steady flow tests of up to one hour can be supplied. For intermittent operations of up to 1 minute, a blowdown system can supply flow rates of up to 700 lb per sec. The test section has a speed range of Mach 1.5-5. Automatic instrumentation is used extensively.

• The new 8-ft supersonic Ames wind tunnel at Moffett Field, Calif., is unique in that data processing is to be speeded by a digital computer. Information will be automatically fed to the computer directly from strain gage balances installed in the test models. The NACA tunnel, which can reach speeds of Mach 3, is powered by electric motors of 216,000 hp.

• Three other wind tunnels are also of interest. Canada is getting a new supersonic wind tunnel at the Uplands Airport near Ottawa. The tunnel has a working section of 4-5 ft, is capable of speeds of up to 3000 mph, and is a part of the Canadian Defense Research Laboratory. Completion of $3.5 million facility is expected in 1958. Another new wind tunnel is being placed into operation by the Armstrong-Whitworth firm at Coventry, England. The British supersonic tunnel is for use at speeds in the Mach 0.3 to 3.0 range. Speeds can be varied by use of nozzle blocks which have been precalibrated. Automatic data-gathering devices are to get extensive use. Technion, the Israel Institute of Technology at Haifa, Israel, is planning a supersonic wind tunnel in the Mach 1.5–4.5 range. Photographic instrumentation is to be used.

Rockets and Guided Missiles

• TALOS is a new supersonic AA missile powered by a McDonnell Aircraft ramjet engine. Bendix is to build the missile at Mishawaka, Ind.

• REGULUS, by Chance Vought, is now being made in three versions. One is a flight test vehicle with wheels which can be landed after a hop and re-used many times. One REGULUS has logged 15 flights. The second version is tactical, without wheels, to carry a warhead. The third is a drone for training in high-speed gunnery. The two latter missiles can be launched from land-based trucks, from carrier decks, guided missile ships, cruisers, and submarines. They are controlled by radio and flown by a mother plane which brings them in. Some are landed by ground crews with the same control equipment.

• The USS *Boston*, formerly a heavy cruiser, has been modified as a guided missile ship. The *Boston* is the sister ship of the *Canberra*, also a guided missile ship. The USS *Mississippi* was the first Navy ship to employ guided missiles when she fired TERRIER AA rockets in fleet operations.

• Two squadrons of the FIREBEE target drones are planned by the Air Force in a training program at Yuma, Ariz. Another new program—using new Q-2A FIREBEES—is to be started at Holloman AFB. Future models will be equipped with firing error indicators, air-to-air radio controls, and smoke-generating equipment. The new drones will also be modified to permit operations at altitudes of less than 500 ft. 130 Q-2A's are being produced by Ryan. 89 drones are to be delivered during the last half of 1955, to be followed by the remaining 41. The Air Force has received 62 XQ-2 FIREBEES, and about 120 test flights have been made.

• In a tactical exercise, an entire squadron of B-61 MATADOR missiles was airlifted from Germany to Tripoli. Firings took place in the Libyan desert in June.

• Unofficial reports indicate that the Northrop SNARK, TM-62, missile has a range of about 5000 mi. SNARK, powered by a turbojet engine of 10,000 lb thrust, cruises at an altitude of 40–45 thousand feet with a speed of about 600 mph. It is said to be launched from a zero-length launcher with RATO and is guided by celestial navigation and autopilot. The missile has a swept vertical tail, is 60 ft long, and has swept-back wings of 40 ft span. Testing is now being made at Cocoa, Fla.

Roundup on RATO

RATO, rocket assisted take-off, was the subject of discussion at a joint ARS-IAS meeting held in New York on January 27, 1955. Many new and interesting facets of this important field of rocket application were touched on. (See listing of papers in JET PROPULSION, January, 1955, p. 45.)

Civilian Rockets

Commercial jet aircraft will do well to consider RATO for civilian applications, suggested R. L. Hirsch of Aerojet-General. Since 1942, over $^1/_4$ million solid propellant units have been used by the armed services. Hirsch believes that airlines will use RATO at high airport elevations, high ambient temperatures, or for short runways to allow normal or near normal payloads. CAA has already certified the 14AS-1000 and the Junior JATO 14KS-250 delivering 1000-lb thrust for 14 sec and 250-lb thrust for 14 sec, respectively. New units will be lighter and may feature increased performance and a smokeless exhaust.

Panagra

DC-4 passenger take-off at LaPaz, Bolivia

American Airlines

American Airlines DC-4 freighter ATO at Mexico City

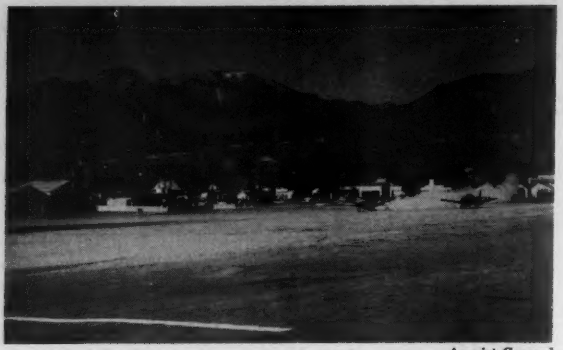

Aerojet-General

Junior JATO 12KS-250B is shown competing with sister Ryan Navion airplane similarly loaded. On the left both have started ground rolls at the same time. At the right the plane with "Junior" has outdistanced the other plane and is airborne in 40° climb. Unboosted plane is still on ground. In tests where the Navion would need 875 ft to clear 50 ft, the use of one such JATO would reduce this distance to 300 ft

Tailor-Made Thrust

By doing some juggling with solid propellant composition and configuration, extremely wide ranges of thrust programs are possible. This makes solid propellants ideal for boosters, stated H. W. Ritchey, Thiokol Chemical Corp. Ritchey differentiates various rocket applications by the velocity of the unit at burnout. For RATO this is 100–400 fps; boosters, 300–1000 fps; single-stage rockets, 600–5000 fps. With a given propellant and nozzle, thrust can be programmed by varying the burning surface. For high thrusts where large burning areas are required, internal burning configurations can be utilized to keep motor walls cool. Grain design thus allows a very flexible choice of thrusts (see photos).

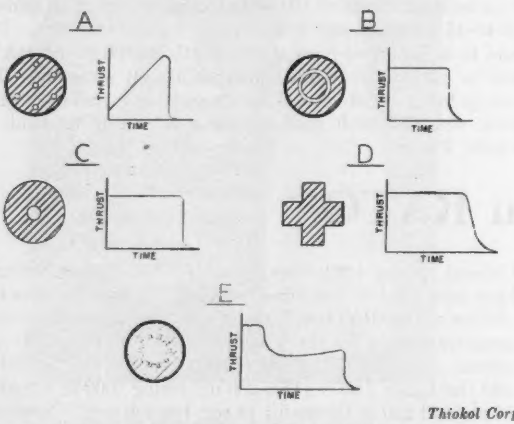

Thiokol Corp.

Grain geometries. A shows progressive burning, multiperforated charge. B is internal-external "iota" grain. C also gives constant thrust if ends are inhibited. The cruciform grain in D is neutral-burning if properly inhibited. Cog-wheel system is shown in E

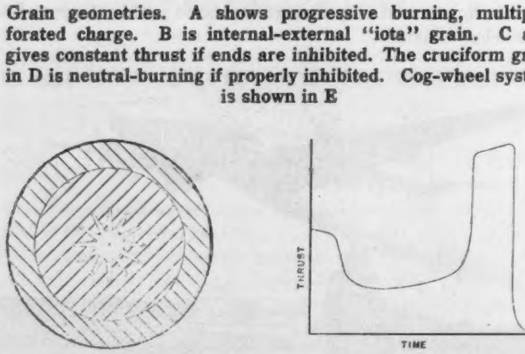

Thiokol Corp.

Thrust programming may be obtained by combining fast and slow burning propellants. Star (slow burning) gives initial thrust and then lower level as an internal burning cylinder. Finally fast burning propellant produces high thrust

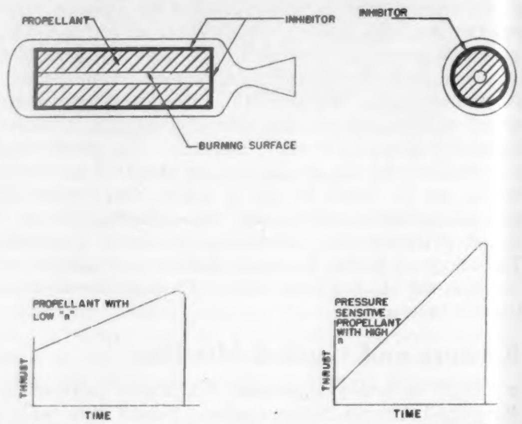

Thiokol Corp.

Internal-burning cylinder charge. Increasing burning area gives progressive thrust, lower left, which may be extremely progressive with a high "n" propellant, lower right

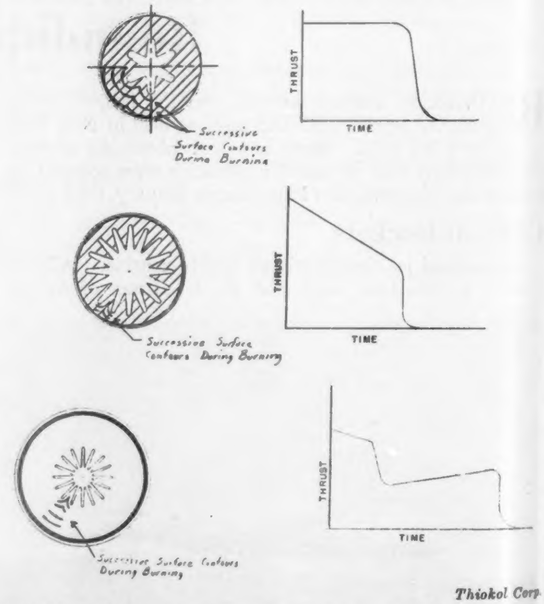

Thiokol Corp.

Variations of star geometry. Top shows neutral burning (constant thrust) internal burning star. Variation of surface area can be kept constant to within 0.3%. Center illustrates degressive thrust. At bottom the star is combined with the cylinder to give a two-stage thrust effect

Space Flight Notes

Kurt R. Stehling, Bell Aircraft Corporation, *Contributor*

Astronautics

THE great excitement which attended the White House announcement of the Earth Satellite Vehicle (ESV) has now subsided. Although much of the planning and background is still obscure, the situation seems to be about as follows:

Although the organization to do the job has not been identified, missile engineers are generally agreed that it can be done within the allowed time. On August 16, at a Hayden Planetarium meeting on the ESV, Homer E. Newell, Jr., Head, Rocket-Sonde Research Branch, Naval Research Laboratory, Washington, D. C., presented a very clear review of the scientific utility of a small ESV. He left no doubt in his listeners' minds that the NRL has thought seriously about an orbital vehicle and would be keenly interested in its construction and flight.

The NRL is, of course, one of the senior agencies in this country in the domain of high altitude rocket research. Dr. Newell's book, "High Altitude Rocket Research" (Academic Press, New York) and Milton W. Rosen's book "The Viking Story" (Harper and Bros., New York) illustrate both the important part which these two scientists have played in the NRL upper altitude program and the great experience which the Laboratory has gathered during several years of tests with V-2, Aerobee, and Viking rockets.

The cost of the program is uncertain, although a figure of $10 million has been mentioned for the satellite alone. No figure has been mentioned for the cost of the carrier rockets. It is not likely that $10 million is to be spent for actual satellite hardware; for comparison, the payloads of the Deacon or Aerobee high altitude rockets cost from a few hundred dollars for the former to a few thousand, at most, for the latter. Of course, the greater required lifetime, durability, and reliability required for the ESV payload will need much expensive development which may soon gobble up a large portion of the $10 million pie.

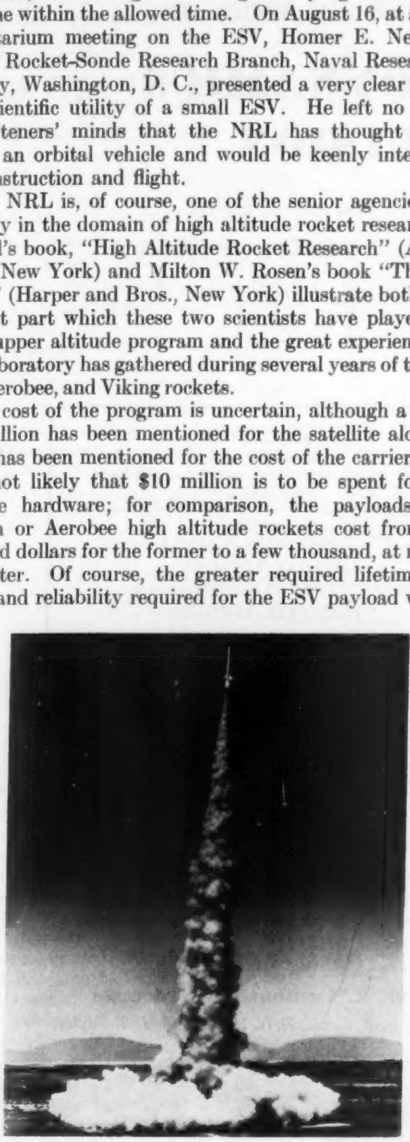

First shot of the Aerobee-Hi hit 125 miles, others 135 miles, and the latest 180 miles

The launching site could well be on a ship, such as the U. S. S. *Norton Sound* which has fired the Viking and Aerobee rockets at sea. This might obviate the danger of an unplanned return in an inhabited region of the second or third stage of the ESV carrier. However, the extensive optical and radar tracking equipment extant at the Army Ordnance White Sands Proving Ground and the associated servicing facilities make this an attractive launching site.

The data received from the ESV will be shared with the 40 countries which participate in the International Geophysical Year program. The Soviet Union is included in this program.

High Altitude

Winzen Research Inc., Minneapolis, on August 5 launched a large balloon carrying a dozen live guinea pigs in a gondola. The balloon reached a record altitude (with this payload) of 100,000 ft. The purpose of the flight was the study of cosmic ray radiation effects upon live animals as part of an Air Force sponsored program. No results have been announced.

A subsequent flight on September 3 with a load of instruments and mice also reached an altitude greater than 100,000 ft. However, a new substitute lightweight timer which would have released the gondola at a given altitude, failed, and the mice apparently were doomed by whatever dooms mice at 100,000 ft.

▶ A series of six balloon flights up to 90,000 ft altitude is planned by two Air Force Officers, Capt. E. G. Sperry and 1st Lt. Henry P. Nielsen. According to *National Geographic Magazine* of August 1955, the purpose of the flights is research on high altitude parachute and bail-out problems.

▶ High altitude rockets will be fired in Northern Ontario and Manitoba next year as part of a general aurora borealis research program. Balloon launched "rockoons," boosted Deacons, and the "Aerobee Hi" will be launched to altitudes of 200 miles. The program is to be jointly conducted by the Signal Corps, Naval Research Laboratory, and the Air Force Cambridge Research Center.

The northern latitudes are very fruitful ones for the study of cosmic rays and such associated phenomena as the aurorae, which may be caused by charged particles entering from outer space. The configuration of the polar magnetic field is favorable for low altitude penetration of the slower, more abundant, charged particles.

DID YOU KNOW?

▶ That the American Rocket Society began in 1930 as the "American Interplanetary Society."

▶ That the present JET PROPULSION journal was named "Astronautics" before World War II.

▶ That Herman Oberth in his book, "Wege Zur Raumschiffahrt," first printed in 1925 in Germany, described the orbits and techniques of satellite vehicles; also the possibilities of particle or photon rockets.

This reviewer will begin a serialized review of Oberth's famous classic (now out of print) in subsequent issues of JET PROPULSION.

EDITOR'S NOTE: This new section of the JOURNAL has been incorporated as a regular monthly feature in response to many requests from ARS members. Mr. Stehling will offer news and comments on space flight and on such related topics as upper atmosphere research, astronomical findings, and aeromedical developments. From time to time, articles and lectures that have appeared elsewhere will be reviewed. Suggestions for subjects worthy of presentation will be welcome.

ARS News

At the Gas Dynamics Symposium, Northwestern University, Evanston, Ill., Aug. 22-24

First Gas Dynamics Symposium Scores Success

About 180 combustion specialists, most of them shown in the above photo, attended the three-day meeting on Aerothermochemistry which marked the First Biennial Gas Dynamics Symposium at Northwestern University, Evanston, Ill., August 22-24. Sponsored by ARS and the Northwestern Technological Institute with the cooperation of the Office of Scientific Research, Air Research and Development Command, the six sessions included 25 papers.

The sessions were opened on August 22 by Northwestern president J. Roscoe Miller and ARS president R. W. Porter and by Symposium Chairman Ali Bulent Cambel.

At a banquet on August 23, H. Guyford Stever, U.S.A.F. Chief Scientist, urged all scientists to individually influence young people to take up careers in technical fields. He stated that more could be done through personal influence than through educational and legislative steps. Introduced at the banquet by toastmaster Edward F. Obert, Northwestern professor of mechanical engineering, were: Cambel, Burgess Jennings, and Paul Klopsteg of the Technological Institute; Martin Summerfield, Editor-in-Chief of Jet Propulsion; Noah S. Davis, vice-president of ARS; James Harford, ARS executive secretary; and Major Robert Crawford of the Office of Scientific Research.

Summary of Technical Sessions

by Alexander Weir, Jr.
University of Michigan

Turbulent Combustion

Martin Summerfield of Princeton University discussed the status of research on turbulent flame propagation. Professor Summerfield presented CH and H_2O traverses of turbulent flames as additional evidence that a "distributed reaction zone" flame model represents a closer approach to an understanding of turbulent flame propagation than theories which attribute the increase of turbulent flame speed to an increase in laminar flame are caused by turbulent wrinkling. During the ensuing discussion, A. C. Scurlock, Atlantic Research Corporation, indicated that the spectral traverses lent credulence to the wrinkled flame theory. In the following paper, John M. Richardson of Ramo-Wooldridge Corporation presented a mathematical theory of turbulent flames. Dr. Richardson's model was a flame of vanishing thickness propagating through a turbulent fluid with a fixed normal velocity with respect to the fluid, i.e., a simplified version of the wrinkled laminar flow model. The burning rates of confined turbulent pentane air and kerosene-air flames were measured by four Johns Hopkins University researchers (J. J. Zelinski, W. T. Baker, L. J. Mathews III, and E. C. Bagnall) and the combustion efficiencies obtained by gas sampling were correlated in an exponential form as a function of pressure, temperature, jet velocity, equivalence ratio, the jet length, the ratio of the total hole area (in the combustion can) to the combustion area, and the hole diameter. I. Kimura and S. Kamagai of the University of Tokyo studied the length of diffusion flames formed by discharging the fuel gas in the center of an annular jet of air. They found that increasing the velocity and eddy diffusivity of the surrounding air jet increased the length of the diffusion flame and that this length could be predicted from the length in quiescent air by a simple relationship.

Flame Stabilization

Several papers were devoted to a study of the recirculation zone behind bluff body flameholders. Edward E. Zukoski and Frank E. Marble of the California Institute of Technology measured the length of this zone by inserting a salt water probe in the flame. Temperatures in this zone were measured by sodium line reversal techniques and found to be ca. 90% of the adiabatic flame temperature, while the residence time of a particle in the zone was estimated to be 2.06×10^{-4} sec. In the discussion which followed, Dr. Zukoski agreed that the sodium line reversal technique measured maximum point temperatures rather than average temperatures through this zone. In the next paper, A. A. Westenberg (with W. G. Berl and J. L. Rice) of Johns Hopkins University presented combustion efficiencies and recirculation zone lengths which were obtained by thermal conductivity measurements of samples downstream of the flameholder. Helium was fed through the porous disk conical flameholder, while confirmation of the zone lengths were obtained by using a salt bead on a wire probe.

Two papers were presented by Marquardt Aircraft Company researchers. John W. Bjerklie stated that flameholder performance was affected by flame speed, drag, fluid dynamics, chemical kinetics, and turbulence generation. Edward P. French presented calculations which indicated that location of the flameholder in the inlet diffuser of a ramjet, while resulting in more pressure loss and higher velocities past the flameholder, would increase the range of a Mach 2 ramjet up to 8% due to the shorter combustion chamber (and hence lighter weight) required.

Detonation and Thermodynamics

All of the symposium papers were not devoted to deflagration. Joseph Rutkowski and James A. Nicholls of the University of Michigan discussed the possibility of obtaining a standing detonation wave. Because of its relatively low detonation Mach number (4.5), the system hydrogen air was proposed. The stagnation conditions thus required (1000 psia and 2800°R) present a difficult heat exchange problem as well as requiring the supersonic mixing of the two reactants after their static temperatures have been lowered by expansion. After the mixing, the detonation wave is to be stabilized on a wedge. Professor Rutkowski presented detonation polar diagrams, similar to shock polars, which indicated that strong and Chapman-Jouget detonations were attainable but not weak detonation waves. In the following discussion, A. Oppenheim of the University of California stated his contention that sonic velocity always occurred behind detonation waves (i.e., the Chapman-Jouget conditions) and the strong detonation waves would not be stable. In a paper on the following day, Boa-Teh Chu of Johns Hopkins University presented an analysis of the vibration of the gaseous column behind a strong detonation wave which indicated that it was closely related to the phenomena associated with spinning detonation. Professor Chu was able to explain the 1936 spinning detonation photograph obtained by Dr. R. P. Fraser of Imperial College, as well as more recent photographs obtained by J. A. Nicholls at the University of Michigan. R. M. Patrick and Arthur Kantrowitz of Cornell University presented a review of work done on strong shock waves in Argon. With gas temperatures up to

30,000°K, obtained from spectral measurements, the equilibrium time is less than 10^{-8} sec. Mr. Patrick then described the effect on the flow by surrounding the shock tube with a strong magnetic field. The use of "magneto hydrodynamics" allowed the computation of the equilibrium time behind the shock.

Several papers on thermodynamics were presented. Shao-Lin Lee (with John F. Lee), North Carolina State College, discussed total entropy production in chemically irreversible processes, while the thermodynamic properties of gases resulting from the combustion of $C_n H_{2n}$-air mixtures were presented by H. N. Powell and S. N. Suciu, of the General Electric Company.

Laminar Flames

The opening paper in a session devoted to laminar flames was by S. S. Penner of the California Institute of Technology. Professor Penner, neglecting thermal diffusion, used the conservation and molecular diffusion equations to relate the flame speed to pressure, i.e., $V_F \sim P^{(N/2)-1}$ where n is the order of the chemical reaction. Thus, for a second order reaction the flame speed is directly proportional to pressure. The introduction of calculational procedures suggested by von Kármán enabled calculation of hydrogen-bromine flame speeds in agreement with the experimental values. E. Mayer and H. Carus of Arde Associates also presented an analysis of flame propagation based on reaction kinetics. Dr. Mayer used the Arrhenius equation, assuming that a propane-air flame was a second order reaction, to check flame speed data of Dr. Friedman (Westinghouse) and Dr. Avery (Johns Hopkins). J. M. Singer, Joseph Grumer, and E. B. Cook of the Bureau of Mines compared flame speed data obtained with slot burners to data obtained using cylindrical bunsen burners. The data agreed more closely with propane-air flames than with methane or ethylene-air flames. In the ensuing discussion, Dr. Singer indicated that flame quenching was insignificant at low pressures, and that data obtained by R. E. Cullen (University of Michigan) which indicated that the presence of a heat sink was deleterious to flame propagation was invalid because of the wrong stiffness factor (= flow pressure/flame pressure) used. Dr. Singer cited the case of a water cooled flameholder in which no change in flame shape could be detected. Dr. A. Weir (University of Michigan) replied that recent spectral traverses of flat propane-air flame indicated that C_2, CH, and OH intensities were proportional to the amount of heat lost from the flame even though no apparent change in flame shape occurred. Dr. Singer indicated that bunsen flames would not be as liable to be affected as flat flames by quenching factors.

In a second paper by Bureau of Mines personnel, John Manton and B. B. Milliken discussed flame speed measurements by spherical bomb techniques, at pressures as low as $^1/_{25}$ atm. Mr. Manton found that the exponent n (in the equation $Su1/Su2 = (P_1/P_2)^N$) varied with burning velocity, and drew the conclusion that all burning velocities must approach a constant value at very low pressures. He

also indicated that mixtures with a positive value of the exponent n were most likely to detonate.

The results of spark ignition experiments were reported by C. F. Mozer and R. K. Sherburne of the New Mexico College of Agriculture and Mechanic Arts. Professor Sherburne distinguished between ignition with and without subsequent flame propagation by means of schlieren photography. The radius of the flame kernal was plotted versus time, and after about 200 microsec, the radius required for subsequent flame propagation was about 0.2 cm. A plot of critical kernel radius versus the ratio of hydrogen atoms to oxygen atoms had a minimum value at an H/O ratio of 1.0, while decreasing the spark plug gap width from 0.020 in. to 0.010 in. resulted in decreasing the critical radius from 0.2 cm to 0.1 cm.

NONSTEADY COMBUSTION

The subject of combustion instability in rocket motors was discussed in two papers. Luigi Crocco and Jerry Grey of Princeton University found that a variable time lag was needed to characterize "screaming" combustion, although a constant time lag concept was adequate for "chugging" motors. Dr. Grey stated that increased stability is obtained for increased values of n in the relation $T P^n$ = const (where T is the time lag and P the pressure). Thus, treating a rocket motor as a quarter wavelength pipe, longer chambers and/or higher chamber pressures result in increased stability. Some very interesting Fastex movies of chugging rocket motors were shown by Adelbert O. Tischler and Theodore Male of the National Advisory Committee for Aeronautics. Dr. Tischler indicated that the combustion time delay increased as the ratio of injector pressure drop to combustion chamber pressure increased, the nonchugging region occurring at the higher values of the latter ratio. The time delay decreased as the frequency of oscillations increased, nonchugging occurring at the longer time delay periods. In the discussion which followed, personnel from Aerojet-General indicated that shock fronted longitudinal waves occurred in their engines as well as the high frequency lateral oscillations considered by Dr. Tischler.

G. H. Markstein and D. Schwartz of Cornell Aeronautical Laboratory, Inc., presented photographs of cellular slot burner flames. Dr. Markstein measured the minimum rather than the average cell width, this width remaining constant for equivalence ratios from 1.25 to 1.45, and increasing at a ratio of 1.75. Dr. Markstein presented graphs of flow rate versus equivalence ratio with the following regions indicated: flashback, unsteady cellular flames, steady cellular flames, and noncellular flames. Dr. M. Uberoi (University of Michigan) disagreed with the quenching theory advanced by Dr. Markstein.

COMBUSTION OF CONDENSED PHASES

A number of papers were presented on liquid fuel combustion. C. C. Miesse of Aerojet-General Corporation found that the Weber number of the liquid, the Reynolds number, the Schmidt number, and the ratio of air kinematic viscosity of

the combustion rate of the droplet are important parameters in droplet studies. R. S. Carr, Jack Lorell, and Henry Wise, of California Institute Technology, applied chemical reaction kinetics to the steady state burning of a droplet to calculate composition and temperature profiles. S. L. Soo and H. K. Ihrig of Princeton University studied a similar problem, omitting the reaction kinetics, but including thermal and molecular diffusion neglected by the previous authors. Professor Soo found that the wet bulb condition was the most significant factor in droplet life. In the final paper of the symposium, G. P. Watchell of the Franklin Institute presented a theory of the spread of flame in a propellant bed. A critical length was found for the propellant bed; for shorter lengths the pressure tends to become uniform throughout the bed, while in longer beds the pressure difference between the middle and the end increase with time.

Webb Succeeds Purdy in Maryland

WILLIAM A. WEBB, project engineer at Aircraft Armaments, Inc., Baltimore, is the new president of the Maryland Section, succeeding William G. Purdy of The Glenn L. Martin Co.

Other officers are A. W. McCourt, Air Arm Division, Westinghouse Electric Corp., vice president; Henry A. Smith, Aircraft Armaments, secretary; Samuel Fradin, Miller Metal Products, treasurer.

Purdy will continue to serve the Section as a director. Other new directors are James Burridge, Martin Co., and Milton Rogers, Aircraft Armaments. Continuing as directors are Ivan Tuhy of Martin and Joel M. Jacobson of Aircraft Armaments.

Installation of officers took place at a June 21 dinner meeting which also included a program presented by a student rocket group called "Rocket Research of Baltimore."

Diamond Heads Indiana Group

NEW officers of the **Indiana** Section include Philip M. Diamond, president; Robert C. Bowlin, vice-president; James A. Bottorff, secretary; and Helmut Wolf, treasurer.

On the Board of Directors are C. F. Warner, David G. Elliott, Alfred R. Graham, Guy F. Cooper, and the above officers. D. E. Robison will serve as faculty adviser to the Section, whose members are principally from the Purdue University Rocket Laboratory in Lafayette.

Southern Ohio Plans Award

BENDIX Aviation Corporation's Hamilton Division will sponsor an award to the **Southern Ohio** Section member presenting the best paper on a subject allied to rocket and jet propulsion at a November meeting.

The award is expected to be clock-pen set with a model rocket adorning it. Chairman of the Award Committee is John T. Marshall, chief engineer of the Hamilton Division.

AMERICAN ROCKET SOCIETY MEMBERSHIP REQUIREMENTS, PROCEDURES, AND BENEFITS

I Interpretation of the ARS By-Laws for Membership

This note is intended to explain the provisions of those By-Laws of the Society which apply to membership. It will also explain the procedures used to admit new members, and to effect transfers in grade for existing members.

Grades of Membership

There are three types of membership open to individuals. We will discuss these, and try to describe the definitions so that future applicants will know into which category they most properly belong.

(1) ***Member***

The By-Laws state: "Members shall consist of engineers and scientists who are actively engaged in the development or application of rocket or jet propulsion, other persons who have been working on the development or application of rocket or jet propulsion for at least four years and who hold or have held responsible positions in these fields, and such persons as may be deemed eligible for this class of membership by the Board of Directors by virtue of their outstanding accomplishments in other fields and their unusual interest in the purposes of the Society."

The phrase "development or application" does not mean that the engineer or scientist need necessarily be directly concerned with actual jet-propulsion-powered vehicles or missiles. His primary field of employment might be, for example, that of a civil engineer laying out a missile test facility or range. What is intended to be meant by the definition is that the engineer or scientist be employed in a job or government service whose over-all scope is one of developing and/or using jet propelled devices.

(2) ***Associate Member***

"Associate members shall consist of persons, other than students, who are actively interested in the development or application of rocket or jet propulsion."

Here the criterion is whether or not the applicant has a strong and sincere interest in the American Rocket Society and its aims. The Society is anxious to maintain and augment its roster of enthusiastic, active members.

(3) ***Student Member***

"Student members shall consist of persons, not less than 17 years of age, whose principal occupation is study at a recognized educational institution or who are serving as enlisted personnel in the Armed Forces of the United States, and who are interested in the development or application of rocket or jet propulsion."

The institution in which the applicant is enrolled should be a fully accredited four-year college, or a recognized junior college whose credits are acceptable at one of the accredited colleges. Military membership is really a separate class of membership. In this way the Society wishes to lessen the financial burden on enlisted men in the Armed Forces. When a student member leaves college and when an enlisted man leaves the service (or becomes an officer) he will automatically become eligible for a higher grade of membership.

II How to Become a Member

1. Application forms may be obtained from either the local section membership committee, local secretary, or the national office.
2. Return the application to either the local section membership committee, or the national office.
3. The form should be filled out carefully and completely. Each reference given is contacted, so they should be able to answer questions about your technical background and abilities.
4. You will be notified of the decision of the National Membership Committee within 6 to 12 weeks.

III How the Society Screens and Evaluates Applicants

1. If the application is submitted through a local section of the Society, their membership committee may carry out an initial screening.
2. Normally, the application reaches the Society office in New York City before any formal screening, even though it may have been forwarded through a local section office. When it is received, the New York office prepares form letters which are sent to each of the references, for their evaluation and comment.
3. When the confidential information forms are returned to the national office, the original application and the information forms are sent to the National Membership Committee for evaluation and final action.
4. Notification of membership and grade is made to both the applicant and his local section office by the national secretary.

IV Transfer of Membership to a Different Grade

There are several possible transfers of membership between the Student, Associate, and Member grades.

1. When a student member leaves college, he automatically becomes eligible for upgrading to either associate or member status, and the national office should be notified.
2. Upon discharge from the service or if he becomes a commissioned officer, the serviceman becomes eligible for upgrading to either associate or member status.
3. Transfers between associate member and member status are infrequent, but do occur.
4. All membership transfers are implemented through the use of a special form, copies of which should be requested from the national office.

G. P. Sutton
1955 Chairman, Membership Committee

SECTION PRESIDENTS

Alabama: Joseph Wiggins, *Thiokol Chem. Corp.;* **Arizona:** Chas. J. Green, *Hughes Aircraft Co.;* **Central Texas:** B. S. Adelman, *Phillips Petroleum Co.;* **Chicago:** V. J. Cushing, *Armour Research Foundation;* **Cleveland-Akron:** W. T. Olson, *NACA;* **Detroit:** Fred Klemach, *Natl. Research & Development Corp.;* **Florida:** R. S. Mitchell, *Pan American World Airways;* **Fort Wayne:** Norman Baker, *Indiana Technical College;* **Indiana:** P. M. Diamond, *Purdue Univ.;* **Maryland:** W. A. Webb, *Aircraft Armaments, Inc.;* **National Capital:** E. C. Page, *Page Communications, Inc.;* **New England:** C. Lincoln Jewett, *Arthur D. Little, Inc.;* **New Mexico-West Texas:** R. C. Sherburne, *New Mexico A & M;* **New York:** C. W. Chillson, *Curtiss-Wright Corp.;* **Niagara Frontier:** T. Zannes, *Bell Aircraft Corp.;* **Northeastern New York:** A. H. Fox, *Union College;* **Northern California:** M. A. Pino, *California Research Corp.;* **Pacific Northwest:** R. M. Bridgforth, *Boeing Airplane Co.;* **Princeton Group:** Irvin Glassman, *Princeton Univ.;* **St. Louis:** Norton B. Moore, *McDonnell Aircraft Corp.;* **Southern California:** C. M. McCloskey, *ONR;* **Southern Ohio:** W. J. Mizen, *Bendix Aviation Corp.;* **Twin Cities:** J. J. Schons, *Univ. of Minnesota.*

Book Reviews

C. F. Warner, Purdue University, *Associate Editor*

Turboblowers, by A. J. Stepanoff, John Wiley and Sons, Inc., New York, 1955, 377 pp. $8.

Reviewed by R. C. Binder
Purdue University

The word "turboblowers" refers to centrifugal and axial flow compressors and fans. This book deals with the hydrodynamic and thermodynamic aspects of turboblower design.

The chapter headings indicate such topics as fluid mechanics, theory of the centrifugal impeller for incompressible flow, vortex theory for incompressible flow, general incompressible characteristics of turbomachinery, hydraulic performance of centrifugal flowers, thermodynamics of blowers, blower casing, leakage, disk friction, and axial thrust, compression with cooling, centrifugal fans, single-stage axial flow fans and blowers, high pressure multistage axial flow compressors, application of blowers, and design of mixed flow impellers.

This book discusses the art of building compressors in the United States and Europe. New methods of attack on turbomachinery problems are outlined. Information which is scattered in different places in the literature is excellently correlated in this book. The design method for axial flow compressors is based on actual fluid deflection and observed pressure and capacity coefficients rather than on lift and drag coefficients. The thermodynamic aspects of gas compression are treated with the concept of "available energy."

This book is well written and clear. Various numerical examples are given which help illustrate the text. The book is an excellent reference and is highly recommended for the engineering student, teacher, and practicing engineer.

Gas Dynamics of Cosmic Clouds, edited by H. C. Van de Hulst and J. M. Burgers, Interscience Publishers, Inc., New York, 1955, 247 pp. $5.75.

Reviewed by S. F. Singer
University of Maryland

The present volume is a report of a symposium held at Cambridge, England, July 1953, and organized by the International Union of Theoretical Applied Mechanics and the International Astronomical Union. The purpose of the symposium was to bring together astrophysicists who are concerned with the properties of interstellar gases in the universe and aerodynamicists who are concerned with more terrestrial problems. The idea was that aerodynamicists who have solved a limited number of problems of continuous media might have something to contribute to astrophysical theory and, perhaps, vice versa. Both aerodynamicists and astrophysicists have come up against the problem of turbulence and have been trying to incorporate it into their theories. In astrophysics there is the additional difficulty of the presence of magnetic fields which enter into the description of the hydrodynamics of the gas, because of the very high conductivity of the ionized interstellar gas. In fact, the importance of the magnetic fields in cosmic physics has given rise to the science of magnetohydrodynamics.

There were some forty contributed papers and discussions at the symposium which appear in the present volume. They are divided into several parts, the first part dealing with the observational data of cosmical gas dynamics, and the second with the physical conditions of the interstellar gas. Then follows a set of papers on shock waves and collision problems, and another set on turbulence and magnetic fields in a compressible gas. Finally there is a series of papers of more cosmological importance concerned with the formation of cosmic clouds and galaxies, and in Part 6 a discussion of accretion problems, i.e., the acquisition of gas by means of gravitational action. The final portion of the program was concerned with gas and dust in the interstellar medium and their relationships. The papers in this volume are addressed mainly to a specialized audience, although there are some which are more of a review character.

Millimicrosecond Pulse Techniques, by I. A. D. Lewis and F. H. Wells, McGraw-Hill Book Co., Inc., New York, 1954, and Pergamon Press Ltds., London, England, 310 pp. $7.50.

Reviewed by F. W. Lehan
Ramo-Wooldridge Corporation

In the early days of radio the use of "wireless telegraphy and telephony" imposed no requirements on the information bandwidth of the input and output circuits other than being reasonably distortion free to an upper frequency of a few thousand cycles per second. Fairly simple engineering techniques were adequate to handle these keying and audio circuits. With the exception of an occasional lumped-constant analysis of a critical circuit, frequency-response and transient problems could be handled by large overdesign.

With the advent of pulse radar and television, the input and output circuits were now required to be quite low in distortion out to several megacycles per second. These requirements together with the components available at the time made close design necessary. Lumped-constant analysis was required for most new circuits and an occasional distributed constant analysis was needed.

Improved components and understanding are making simple overdesign now possible in some video circuits but the nuclear instrumentation field and possible trends in radar and communication are now creating a need for input-output circuit techniques capable of the low-distortion handling of a broad band of frequencies up to a few kilomegacycles per second. This new strain of the "state of the art" calls again for closer design techniques.

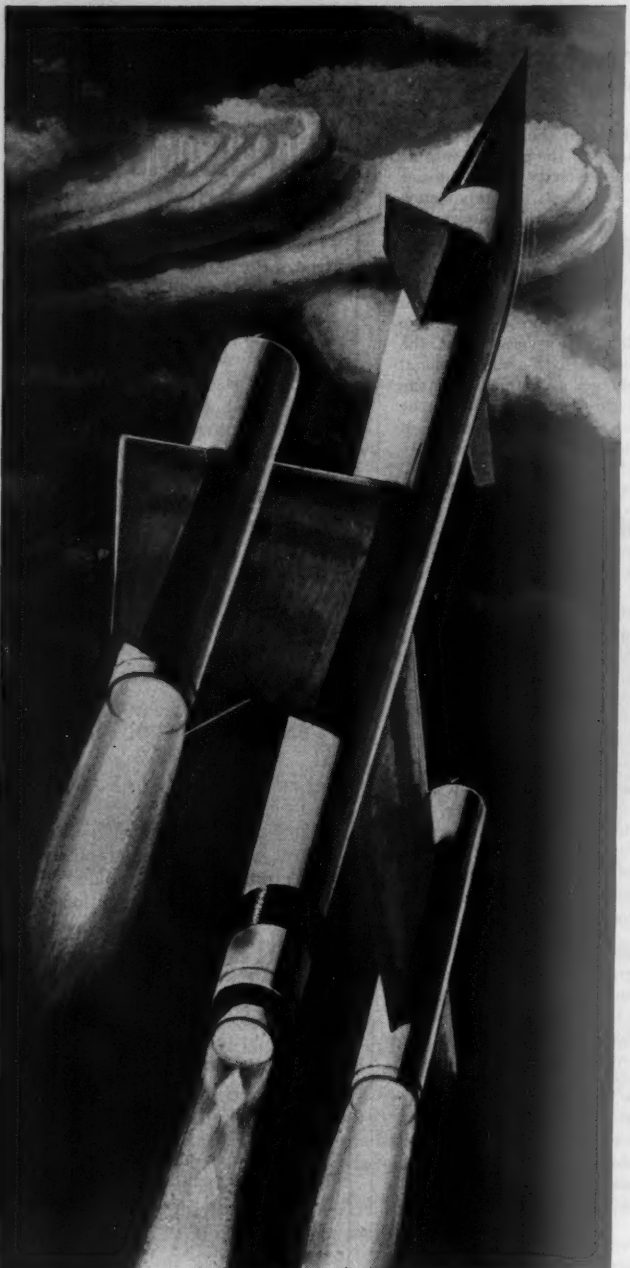

a helping hand UP or OUT

MCDONNELL F-101 VOODOO

Armament Jettisoning Developments by the Explosives Division of the OLIN MATHIESON CHEMICAL CORPORATION Have Proved to be Ideal Solutions to a Variety of Jet Age Problems.

Many tough missile and aircraft problems have yielded to speedy solutions with the specialized aid provided by Olin Explosives Division experts. Recently, new developments by leading aircraft manufacturers have greatly been expedited by the unmatched knowledge and know-how Olin automatically places at the disposal of a manufacturer. If there is a possibility that any of your own problems can be answered through a creative utilization of solid propellants or explosives, a call to East Alton today may well prove an important step to a rapid solution.

OLIN SOLID PROPELLANTS ARE READY FOR USE IN THE FOLLOWING APPLICATIONS

- Missile Propulsion Units, Boosters and Sustainers, ATO Motors
- Solid Propellant Turbo Jet Engine Starter Cartridges
- Gas Generators and Auxiliary Power Units
- Power Packages for External Stores, Canopies and Pilot Seats Forced Ejection Systems
- High Explosives, Ignitors, Fuses, Detonators, Flares, Pyrotechnics
- Explosive Formation of Metal Parts

Olin
TRADE MARK
EXPLOSIVES DIVISION
OLIN MATHIESON CHEMICAL CORPORATION
EAST ALTON, ILLINOIS

Distributed constant analysis must frequently be used and occasional direct recourse to Maxwell's equations in three dimensions is required.

"Millimicrosecond Pulse Techniques" deals with the methods of generating, handling, and measuring kilomegacycle per second "video" signals. It is a fairly short (310 pages) résumé of techniques in this broad new field.

Chap. 1 gives a brief résumé of the related Laplace and Fourier transform methods of analysis. Chap. 2 applies such methods to transmission lines including helical lines and artificial lumped-lines. The Clogston line is briefly mentioned and references given. Chap. 3 discusses transformers, major emphasis being placed on tapered line transformers.

Chap. 4 discusses Pulse generators of the discharge line type and the secondary emission type as well as mentioning a number of other schemes.

Chap. 5 covers straightforward video amplifiers, secondary emission amplifiers, distributed amplifiers with mention only of traveling wave tube. Chap. 6 describes both conventional and special oscilloscope instrumentation techniques. Chap. 7 gives specific nuclear physics application of the preceding chapters. It discusses such items as scintillation counters, spark counters, amplitude discriminators, and scaling and coincidence circuits. Chap. 8 is a collection of miscellaneous applications such as signal generation for radio receiver testing and Kerr cell photography. This chapter does not seem to add much to the book.

A certain amount of data on transmission lines and tubes is included in the appendixes and a long list of references is given for each chapter.

The book is written from the point of view of an English atomic physicist interested in instrumentation. This made its style and phrasing at times seem unusual to an American electronic engineer, but I found the freshness of viewpoint added rather than detracted from the book. The derivations in the book are sketchy but excellent full references are given. It is recommended to those interested in advanced work in radar and communication technique as well as those interested in atomic instrumentation.

The Physics of the Stratosphere, by R. M. Goody, Cambridge University Press, 1954, 175 pp. $5.

Reviewed by S. F. Singer
University of Maryland

This slim volume gives a brief and up-to-date account of the physics of the atmosphere from the weather forming layers up to the base of the ionosphere (250,000 ft.). It discusses the temperature of the stratosphere and the methods which have been used for measuring it. It gives a concise account of winds and turbulence. The treatment is particularly authoritative in the author's own speciality, radiation and its control by radiative atmospheric components such as water vapor, carbon dioxide, and ozone. The subjects discussed in this volume are of considerable importance to high altitude flight both with regard to aerodynamics and heating. This monograph will also be of

value to anyone wishing to get acquainted with the physics of the stratosphere and with the experimental methods used to investigate it.

Physics and Medicine of the Upper Atmosphere, A Study of the Aeropause, edited by Clayton S. White and Otis O. Benson, Jr., The University of New Mexico Press, Albuquerque, 1952, 584 pp. $10.

Reviewed by S. F. Singer
University of Maryland

This book is a likely candidate to become the classic in its field. It deals comprehensively and authoritatively with all aspects of the upper atmosphere as seen from the point of view of the physicist, the engineer, and the biologist.

The book is based on a Symposium on the Physics and Medicine of the Upper Atmosphere held at San Antonio, Texas, in November 1951, sponsored by the Air University School of Aviation Medicine and arranged by the Lovelace Foundation for Medical Education and Research. The papers presented at this Symposium have been expanded by the authors and form chapters in the volume. There are about 30 individual contributions dealing with a great variety of upper atmosphere phenomena. The physical problems discussed include the characteristics of the upper atmosphere, its chemical aspects including the problems of ozone, and chapters on the various radiations and particles from outer space: the solar radiation, cosmic rays, and meteors. The biological problems include radiation effects and other environmental influences on human flight. In addition there are a number of shorter discussion papers dealing with methods and vehicles for research in the high atmosphere and with problems of human travel in the aeropause.

Book Notices

Proceedings of the Second U. S. National Congress of Applied Mechanics, 825 pp., $9. The American Society of Mechanical Engineers. This book contains 95 papers presented at the Congress covering such subjects as elasticity, plasticity, fluid mechanics, vibrations, aerodynamics, heat transfer, and the behavior of materials.

Bibliography of Industrial Radiology 1952–54 (Fifth Supplement to Industrial Radiology), by Herbert R. Isenburger. St. John X-Ray Laboratory, Califon, N. J., 1955, 24 pp., $3. A chronological listing of almost 700 references to periodical articles, books, documents, and patents. English translations of the titles of foreign works are included.

• Announcement has been received that *Astronautica Acta*, official journal of the International Astronautical Federation, published quarterly, is available from booksellers at $9 yearly. Members of the Constituents Federation may obtain the journal at a reduction of 20 per cent through their Societies.

American Mathematical Society's Wave Motion and Vibration Theory, McGraw-Hill Book Co., Inc., New York, 1955, 169 pp., $7. This book, Volume V of a series, contains fifteen papers delivered at the Fifth Symposium on Applied Mathematics of the American Mathematical Society.

New Patents

George F. McLaughlin, *Contributor*

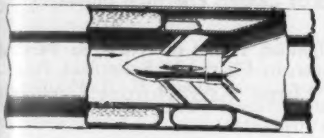

2,715,813

Fuel injector and flameholder (2,715,813). Frederick T. Holmes, Denver, Colo., and Robin E. Taylor, San Francisco, Calif., assignors to the U. S. Navy.

Burner assembly containing concentric manifolds, one containing a pilot fuel and another a supporting medium. Orifices in the manifolds are arranged in proximity to provide commingling jets. Nozzles direct a fuel spray to the pilot flames.

Multiple pressure responsive control device for a variable area nozzle of a jet engine (2,715,311). Richard J. Coar, Hartford Conn., assignor to United Aircraft Corp.

Aircraft jet propulsion system having a variable area propelling nozzle controlled by a valve responsive to the ratio of absolute pressures existing at two spaced points in the gas flow path.

Sintered titanium carbide alloy turbine blade (2,714,245). Claus G. Goetzel, Yonkers, N. Y., assignor to Sintercast Corp.

Composite material shaped blade for jet engine turbines, with porous skeleton body, the trailing edge having increased ductility, improved resistance to thermal and mechanical shock and to bending and fatigue stresses.

Flameholder device for turbojet afterburner (2,714,287). John C. Carr, Norwood, Pa., assignor to Westinghouse Electric Corp.

Device in the combustion gas stream for effecting sufficient stagnancy to retain the flame formation. It is attached so as to permit relative thermal expansion without strain on the casing structure.

Gasoline air-hydropulse (2,714,800). Calvin A. Gongwer, Azusa, Calif., assignor to Aerojet-General Corp.

Jet propulsive device adapted for operation through water. An automatic pressure-operable inlet valve intermittently passes water entering the duct in a downstream direction only. The escape of pressurized gases forces water within the duct toward the exhaust opening.

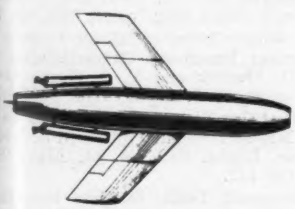

172,170

Pilotless aircraft design (172,170). I. Nevin Palley, Lancaster, Calif., assignor to Chance-Vought Aircraft, Inc.

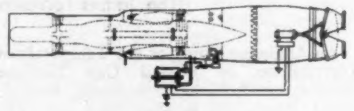

2,714,801

Variable area nozzle for a gas turbine (2,714,801). Peter M. Sarles, Wilton, Conn., assignor to Westinghouse Electric Corp.

Electro-responsive nozzle for the control of the discharge of gases from the afterburner of a power plant. The casing has a reference pressure chamber, and an operating chamber is connected to the turbine discharge passage.

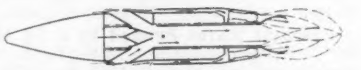

2,714,999

Jet propelled bombing aircraft (2,714,999). Armand J. Thieblot and Rodger W. Davis, Hagerstown, Md., assignors to Fairchild Engine and Airplane Co.

Plurality of combustion gas reaction engines arranged in circular series within the annular space adjacent to the rear end of a circular fuselage. Fuel is contained in the annular space forward of the engines.

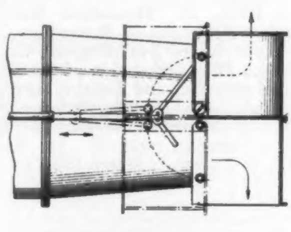

2,715,312

Jet spoiler for gas turbine jet propulsion plant (2,715,312). Eugene Brame, Farnborough, England, assignor to Power Jets (Research and Development) Ltd.

Cylindrical member coaxially disposed around the rear end of the jet pipe, and bisected in an axial plane. The two parts have a rearward common diameter. Two deflectors with concave sides pivot so the jet stream is diverted to either side in proportion to the angular position of the deflectors.

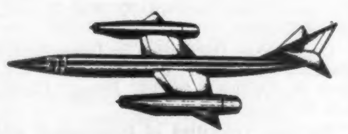

175,342

Airplane design (175,342). Henry B. Gibbons, Alfred L. Jarrett, and Forbes Mann, Dallas, Tex., assignors to Chance-Vought Aircraft, Inc.

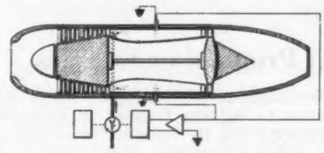

2,715,815

Resonance detector for jet engines (2,715,815). Emil A. Malick and Deslonde R. deBoisblanc, Bartlesville, Okla., assignors to Phillips Petroleum Co.

Detector for reproducing a variable electrical output representative of flame intensity in a reaction motor, and means for sensing periodicity in the variations of electrical output.

Combustion chamber for use with internal combustion turbines (2,715,816). James D. Thorn and Anthony V. G. Jackman, Lincoln, England, assignors to Ruston & Hornsby, Ltd.

A main chamber having an inner cone dividing the inlet into two separate ducts, one in communication with the annular space for delivering primary air, and the other in communication with the main combustion chamber for delivering secondary air. A vane in one duct causes air in one duct to take a predetermined path through the combustion chamber.

Method of making turbine blades (2,716,270). Emil F. Gibian, Cleveland Heights, Ohio, assignor to Thompson Products, Inc.

Jet engine (2,716,329). David R. Lunger, Westfield, Pa.

Fuel supply for ramjet powered helicopters (2,716,459). Ernest W. Toney, Normandy, and Harold H. O. Stroff and Alb C. Ballauer, Ferguson, Mo., assignors to McDonnell Aircraft Corp.

Wing-mounted jet nozzle for aircraft propulsion and sustenation (2,716,528). David M. Hammock, Falls Church, Va.

Continuous flow and internal combustion engines and in particular turbo-jets or turbo-props (2,716,863). Lucien Reingold and Claude Foure, Paris, France, assignors to Office National d'Études et de Recherches Aéronautiques (ONRA).

Controllable jet-driven helicopter rotor (2,717,043). Vittorio Isacco, Paris, France.

Helicopter blades which can be telescoped to storage position and extended to operative position. Jet engines on the blade tips are fed by fuel lines wound on a reel rotably mounted at the root ends of the rotor blades.

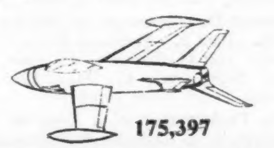

175,397

Airplane design (175,397). Ivan H. Driggs and Frampton E. Ellis, Jr., Montgomery County, Md., and Abraham Hyatt, Washington, D. C.

Editor's Note: The patents listed above were selected from recent issues of the Official Gazette of the U. S. Patent Office. Printed copies of patents may be obtained at a cost of 25 cents each, from the Commissioner of Patents, Washington 25, D. C.

Technical Literature Digest

M. H. Smith, Associate Editor, and M. H. Fisher, Contributor
The James Forrestal Research Center, Princeton University

Jet Propulsion Engines

Investigation of Jet-Engine Noise Reduction by Screens Located Transversely Across the Jet, by Edmund E. Callaghan and Willard D. Coles, *NACA TN* 3452. May 1955, 27 pp.

Criterions for Prediction and Control of Ram Jet Flow Pulsations, by William H. Sterbentz and John C. Evvard, *NACA RM* E51C27, May 1951, 63 pp. (Declassified from Confidential 4/14/55.)

The Control of Turbojet Engines, by Donald F. Winters, *Aeron. Engng. Rev.*, vol. 14, June 1955, pp. 62–65.

Report of The Definitions Panel On The Definitions of the Thrust of a Jet Engine and of the Internal Drag of a Ducted Body, *Gt. Brit. Aeron. Res. Counc. Current Pap.* 190. (Formerly ARC Tech. Rep. 16793), 1955, 25 pp.

Analyzing a Typical Simple-Cycle Turbo-Jet Design and Development Program, by Merrill G. Hinton, Jr. and John M. Wetzler, *Gen. Motors Engng. J.*, vol. 2, May-June 1955, pp. 16–21.

Heat Transfer and Fluid Flow

Analysis of Fully Developed Turbulent Heat Transfer and Flow In An Annulus With Various Eccentricities, by Robert G. Deissler and Maynard F. Taylor, *NACA TN* 3451, May 1955, 42 pp.

Compressor Surge and Stall Propagation, by H. W. Emmons, C. E. Pearson, and H. P. Grant, *Trans. ASME*, vol. 77, May 1955, pp. 455–470.

Pin-Fin Heat-Exchanger Surfaces, by W. M. Kays, *Trans. ASME*, vol. 77, May 1955, pp. 471–483.

The Dynamics of Filled Temperature-Measuring Systems, by Otto Muller-Girard. *Trans. ASME*, vol. 77, May 1955, pp. 591–595.

High Temperature Thermal Conductivity of Gases, by Albert J. Rothman and LeRoy A. Bromley, *Indust. Engng. Chem.*, vol. 47, May 1955, pp. 899–906.

Fluid Mechanics Studies—Isothermal Skin Friction in Flow Through Annular Sections, by R. R. Rothfus, C. C. Monrad, K. G. Sikchi, and W. J. Heideger, *Indust. Engng. Chem.*, vol. 47, May 1955, pp. 913–918.

On the Production of Sound by Jets, by Nigel Thomas, *J. Acoust. Soc. Amer.*, vol. 27, May 1955, pp. 446–448.

S.N.E.C.M.A.'s Aerodynamic Nozzle, *Aeroplane*, vol. 89, July 1, 1955, p. 22.

Recent Developments in Boiling Research. Part 2. Pressure Drop, by W. H. Jens and G. Leppert, *J. Amer. Soc. Naval Engrs.*, vol. 67, May 1955, pp. 437–456.

The Performance of a Type of Swirl Atomizer, by A. Radcliffe, *Proc. Inst. Mech. Engrs.*, vol. 169, 1955, pp. 93–106.

An Analogue Study of the Temperature Distribution in Cooled Gas Turbine Blades, by C. F. Kettleborough, *Brit. J. Appl. Phys.*, vol. 6, May 1955, pp. 174–176.

The Solution of Transient Heat Flow and Heat Transfer Problems by Relaxation, by G. Liebman, *Brit. J. Appl. Phys.*, vol. 6, April 1955, pp. 129–135.

Extension of the Laws of Thermodynamics to Turbulent Systems, by Alfred E. Blackadar, *J. Meteor.*, vol. 12, April 1955, pp. 165–175.

Thermal Convection in a Long Cell Containing a Heat Generating Fluid, by W. Murgatroyd, *Gt. Brit. Atomic Energy Res. Estab.* ED/R 1559, Nov. 18, 1954, 16 pp.

Resonant Waves Emitted by a Jet of Air (in French), by Marie Merle, *Comptes Rendus*, vol. 240, May 23, 1955, pp. 2055–2056.

Entrainment and Turbulence in Open Gas Streams, by R. H. Gough, *Proc. Phys. Soc.*, vol. 68B, April 1, 1955, pp. 234–240.

Mean Temperature Differences in Cross Flow Heat Transfer (in German), by A. F. Fritzsche. *Allgem. Wärmeubertragen; Z. Wärme u. Kältechnik*, vol. 6, no. 1, 1955, p. 4–9.

Transport of Momentum and Energy in a Ducted Jet. I. Experimental Study of a Nonisothermal Jet of Air Discharging into a Duct. II. Theoretical Study of Turbulent Transport of Momentum, Energy and Matter in Ducted Coaxial Streams. III. Correlation of Profiles of Total Momentum and Energy Flux in a Nonisothermal Jet Discharging into a Duct, by L. G. Alexander, Arnold Kivnick, E. W. Comings, and E. D. Henze, *A.I.Ch. E. J.*, vol. 1, March 1955, pp. 55–73.

Combustion

Formation and Combustion of Smoke in Laminar Flames, by Rose L. Schalla, Thomas P. Clark, and Glen E. McDonald, *NACA Rep.* 1186, 1954, 21 pp.

Stability and Burning Velocities of Laminar Carbon Monoxide Air Flames at Pressures Up to 93 Atmospheres, by Rudolph Edse and William A. Strauss, *Wright Air Dev. Cent. TR* 53-214, July 1953, 31 pp.

The Study of Chlorine Atom Reactions in the Gas Phase, by H. O. Pritchard, J. B. Pyke, and A. F. Trotman-Dickenson, *J. Amer. Chem. Soc.* vol. 77, May 5, 1955. pp. 2629–2633.

Organ-Pipe Oscillation in Deep-Ported Burner, by Abbott A. Putnam and William R. Dennis. *Indust. Engng. Chem.*, vol. 47, June 1955, p. 1184.

Burning Velocities of Isopropenyl and Diisopropenyl Acetylene, by Paul Wagner, *J. Amer. Chem. Soc.*, vol. 77, May 5, 1955, pp. 2650–2651.

Ignition Limits of Hydrogen Peroxide Vapor, by Charles N. Satterfield, Peter J. Ceccotti, and Alonzo H. R. Feldbrugge, *Indust. Engng. Chem.*, vol. 47, May 1955, pp. 1040–1043.

Applied Chemical Kinetics. XI. Heterogenous Catalysis, by J. C. Jungers and J. C. Balaceanu. *Inst. Français du Pétrole, Rev. Ann. Combustibles Liq.*, vol. X, Jan. 1955, pp. 30–92.

The Entrainment of Air by Flames, by W. A. Simmonds and M. J. G. Wilson, *Gas Research Board*, London, *Communication* GRB 61, Nov. 1951, 31 pp.

Some Calculations on Ideal Combustion in a Parallel Duct, by A. B. P. Beeton, *Gt. Brit. Nat. Gas Turbine Estab. Mem.* 221, July 1954, 16 pp.

Studies of Flames Burning with Chlorine Trifluoride, by G. Skirrow, R. A. M. Straker, and H. G. Wolfhard, *Gt. Brit. Roy. Aircr. Estab. Rep.* R.P.D. 22, Sept. 1954, 12 pp.

The High Temperature Hydrogen Bromine Reaction, by M. Plooster and David Garvin, *Princeton Univ. Chem. Kinetics Project. TN* 16, April 1955, 68 pp.

Rich Blow-Off Limits of Binary Hydrocarbon Mixtures on a Bunsen Burner Shielded with Inert Gas, by Philip F. Kurz, *Battelle Mem. Inst. TR* 15036-25, April 29, 1955, 11 pp.

Preflame Oxidation and Detonation of Cyclopentane and 2,2,4-Trimethylpentane, by B. J. Reitzer and G. G. Lamb, *Indust. Engng. Chem.*, vol. 47, June 1955, pp. 1239–1243.

Wave Action in Gases: the Attenuation and Reflection of Compression Waves Propagated in Pipes, by G. F. Mucklow and A. J. Wilson, *Proc. Instn. Mech. Engrs.*, vol. 169, 1955, pp. 69–82.

Approximate Theories for the Propagation of Flames, by Morton Mitchner. *Harvard Univ. Combustion Aerodyn. Project. Interim TR* 12, Feb. 1955, 37 pp.

Instrumentation and Experimental Techniques

Heat-Loss Characteristics of Hot-Wire Anemometers at Various Densities in Transonic and Supersonic Flow, by W. G. Spangenberg, *NACA TN* 3381, May 1955, 82 pp.

Measurement of Rapidly Fluctuating Pressures, by E. J. Diehl and H. Visser, *Internat. Shipb. Prog.*, vol. 1, 1954, pp. 1–7.

A Wider Choice of Missile Control Instrument Functional Characteristics, by B. C. Muzzey and V. J. Sims, *Aeron. Engng. Rev.*, vol. 14, May 1955, pp. 73–76.

What Can Electronic Simulators do for the Missile Designer? by Floyd E. Nixon, *Aeron. Engng. Rev.* vol. 14, May 1955, pp. 109–112.

Ultrasonic Tester for Jato Propellant, *Electrocircuits, Inc. Rep.* 18, March 20–June 20, 1954, 7 pp.

Editor's Note: This collection of references is not intended to be comprehensive, but is rather a selection of the most significant and stimulating papers which have come to the attention of the contributors. The readers will understand that a considerable body of literature is unavailable because of security restrictions. We invite contributions to this department of references which have not come to our attention, as well as comment on how the department may better serve its function of providing leads to the jet propulsion applications of many diverse fields of knowledge.

A Double-Beam Method of Spectral Selection with Flames, by C. T. J. Alkemade and J. M. W. Milatz, *Appl. Sci. Res.*, vol. B4, no. 4, 1955, pp. 289–299.

Research on Direct Measurement of Rocket Exhaust Velocities, by R. Edse and L. E. Bollinger, *Ohio State Univ. Res. Found. Quart. Prog. Rep.* Sept. 1–Nov. 30, 1953, 21 pp.

Fuels, Propellants, and Materials

The Storage and Handling of Liquid Propellants for Rockets and Guided Missiles, by W. P. Henderson, *Army Chem. Corps Tech. Command*, CRLR 343, May 11, 1954, 72 pp.

High Temperature Ceramic Coatings, Ceramic and Metal Ceramic Bodies, *Illinois Univer. Dept. Ceramic Engng. Prog. Rep.*, Dec. 27, 1954–Mar. 26, 1955, 16 pp.

Thermodynamic Properties of Ethylene (in German), by F. Cramer, *Chemische Technik*, vol. 7, Feb. 1955, pp. 68–82.

The Heats of Combustion and Formation of Boron Carbide, by D. Smith, A. S. Dworkin, and E. R. Van Artsdalen. *J. Amer. Chem. Soc.*, vol. 77, May 5, 1955, pp. 2654–2656.

Rocket Engines and Propellants, by A. V. Cleaver, *J. Brit. Interplan. Soc.*, vol. 14, May-June 1955, pp. 154–158.

Using Hydrogen Peroxide, by A. V. Cleaver, *J. Brit. Interplan. Soc.*, vol. 14, May-June 1955, pp. 159–164.

Liquid Oxygen as a Rocket Propellant, by S. Allen, *J. Brit. Interplan. Soc.*, Vol. 14, May-June 1955, pp. 165–168.

Specific Heats and Entropies of Hydrocarbons and of Some Combustible Liquids (in French), by M. Aubert, *France. Ministère de l'Air Pub. Sci. Tech.* no. 297, 1955, 202 pp.

Hydrazine from Semicarbazide Solvolysis, by George W. Watt and Joseph D. Crisp, *Indust. Engng. Chem.*, vol. 47, June 1955, pp. 1206–1208.

Viscosity and Density of the Nitric Acid-Nitrogen Dioxide-Water System, by D. M. Mason, Ira Petker, and S. P. Vango, *J. Phys. Chem.*, vol. 59, June 1955, pp. 511–514.

Heats of Solution of Nitrogen Dioxide in the Nitric Acid-Nitrogen Dioxide System at 0°, by Keith Booman, G. W. Elverum, Jr., and D. M. Mason, *J. Phys. Chem.*, vol. 59, June 1955, pp. 516–519.

A Survey of High Temperature Materials for High Speed Aircraft, *SAE J.*, vol. 63, July 1955, pp. 31–38.

Space Flight, Astrophysics, and Aerophysics

The Orbit Lifetimes of the Two New Earth Satellites, by H. B. Ketchum, *J. Space Flight*, vol. 7, May 1955, pp. 1–7.

The Forbidden Line of Atomic Nitrogen, by René Bernard (transl. by Evro Layton, from *J. Physique Radium*, vol. 7, 1938, pp. 157–158), *Amer. Meteorological Soc.*, April 22, 1954, 3 pp.

A New Method of Investigating the Ion Spectrum in the Atmosphere, by E. K. Fedorov (transl. by John G. Estam, from *Doklady Akad. Nauk, SSSR*, vol. 82, 1952, p. 717–718), *Amer. Meteorological Soc.*, June 24, 1954, 4 pp.

Astronautical Activities in Germany, by H. H. Koelle, *J. Brit. Interplan. Soc.* vol. 14, May-June 1955, pp. 121–133.

Recent Research On the Moon II, by H. Percy Wilkins, *J. Brit. Interplan. Soc.*, vol. 14, May-June 1955, pp. 133–136.

The Law of Space, by C. E. S. Horsford, *J. Brit. Interplan. Soc.*, vol. 14, May-June 1955, pp. 144–150.

Balloon-Launching an Earth Satellite Rocket, by Kurt Stehling, *Aviation Age*, vol. 24, July 1955, pp. 16–25.

The Temperature of the Upper Layers of the Atmospheres (Up to 120 KM)—The Sodium Layer and the Noctilucent Clouds, by I. A. Khvostikov (trans. by David Kraus, *Akad Nauk, SSSR*, Chap. 9, Section 16, pp. 457–462 (1948), *Amer. Meteorological Soc.*, May 27, 1954, 6 pp.

Extra-Terrestrial Observations—Their Purpose and Location, by C. A. Cross, *Brit. Interplan. Soc.*, vol. 14, May-June 1955, pp. 137–143.

Atomic Energy

Liquid Hydrogen Bubble Chambers, by Harry Cline Dittler and Thomas Frank Gerecke, *Atomic Energy Comm.* UCRL-2985, May 10, 1955, 67 pp.

A Reactor Control System Utilizing Boron Trifluoride Gas, by W. E. Cawley, *Atomic Energy Comm.* HW-34476, Jan. 18, 1955, 20 pp.

Can Nuclear Energy Drive Interplanetary Rockets? by Clifford Mannal, *Gen. Elect. Rev.*, vol. 58, May 1955, pp. 48–49, 51–52.

Reactor Vessels, by B. A. Mong. *Nucleonics*, vol. 13, June 1955, pp. 66–69.

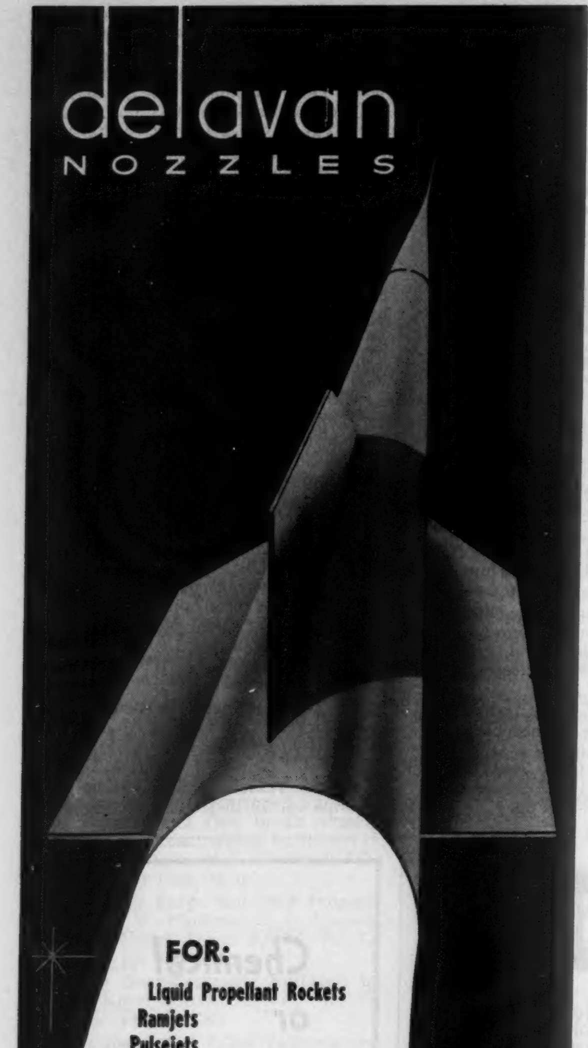

Index to Advertisers